UNIVERSITÀ DEGLI STUDI DI TRIESTE
GRADUATE SCHOOL OF NANOTECHNOLOGY
XXIX CYCLE – 2014-2016

Doctoral Thesis on:

Development of microarrays for proteic and genetic screening with an Electrochemical and Electrochemiluminescence-based transduction scheme

By
ALESSANDRA ZANUT
Matr.N. PHD0600007

Under the supervision of
Dr. MASSIMO TORMEN

UNIVERSITÀ DEGLI STUDI DI TRIESTE

XXIX CICLO DEL DOTTORATO DI RICERCA IN

NANOTECNOLOGIE

Development of microarrays for proteic and genetic screening with an Electrochemical and Electrochemiluminescence-based transduction scheme

Settore scientifico-disciplinare: **FIS/03**

DOTTORANDA
ZANUT ALESSANDRA

COORDINATORE
PROF. LUCIA PASQUATO

SUPERVISORE DI TESI
DR. MASSIMO TORMEN

ANNO ACCADEMICO 2015/2016

Institutions

Università degli Studi di Trieste
Piazzale Europa, 1
34127 Trieste, Italy
www.units.it

Graduate School of Nanotechnology
c/o Dipartimento di Fisica
Università di Trieste
Via A.Valerio, 2
34127 Trieste, Italy
www.nanotech.units.it

CNR - Istituto Officina dei Materiali
Laboratorio TASC
Area Science Park - Basovizza
Edificio MM<
S.S. 14, km 163.5
34149 Trieste, Italy

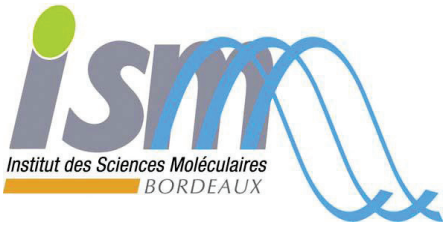

ISM – Institut des Sciences Moléculaires
Group NanoSystèmes Analytiques
ENSCBP, Building A, 1st floor
16 Avenue Pey Berland
33607 Pessac, France

Contents

Contents

Abstract

Considering the increasing need for sensing elements that is emerging in different fields and applications, particularly in relation to the Internet of Things, electrochemical sensors and biosensors, also for their exceptional attributes, such as being easy-to-operate, economical, sensitive, portable, are candidates to become essential pillars in future scenarios and to play a significant role biomedical and environmental monitoring.

Electrochemical and electrochemiluminescent sensors, are devices capable of detecting molecules and biomolecules in solutions and determining the concentration through direct electrical measurements, arising from the change in the redox state of the analyte, and monitored through classical electroanalytical techniques. Remarkably, recent achievements in nanoscience and nanotechnology, have demonstrated the potential for improving greatly both the sensitivity and selectivity of electrochemical sensors and biosensors. In fact, an electrochemical sensor can be miniaturized to a size less than one micrometer or to small-size arrays of nano-electrodes, offering advantages in terms of increased sensitivity and compactness (NEA). The attractiveness of such nanostructured systems resides also in the possibility to immobilized biomolecules on the dielectric surface surrounding each nanoelectrode, instead of on the electrode itself. Therefore, in NEAs, where the electrochemical properties of the electrode and the physical-chemical properties of the dielectric surface may be optimized independently, it may result easier to combine the highly specific molecular recognition mechanisms with high sensitivity (low detection limits).

The aim of this work is the development of nanostructured electrochemical and electrochemiluminescence-based sensors for the detection of biomolecules, such as DNA and proteins.

The fabrication of arrays of nanoelectrodes was performed by deposition of a thin film of polycarbonate (PC) as insulator on a layer of Boron Doped Diamond (BDD) or Glassy Carbon (GC). NEAs were obtained by creating an array of nanoholes in the

Abstract

polymeric film using two different nanofabrication techniques: electron beam lithography (EBL) and nanoimprint lithography (NIL). These approaches lead to the formation of recessed nanoelectrodes. Particulary, the optimization of the parameters to fabricate NEAs by nanoimprint lithography (NIL) has allowed to reduce time and manufacturing costs.

Initially, the sensors were tested for the detection of HPV (Human Papilloma Virus) DNA sequences. Later we focused on the optimization of the protocol for the detection of proteins by enzyme immuno-assay with the enzyme Horse Radish Peroxidase (HRP), using Gliadin and Tumor necrosis factor (TNF-α) as target. The process of bio-recognition and detection was carried out by cyclic voltammetry and consists of an immuno-indirect scheme. This method allows to detect a concentration of 0.1 nM for Gliadin fragment and the experiments performed indicate the possibility to further low this limit.

Nanoelectrode arrays are opening new applicative prospects to the development of highly sensitive, selective and miniaturized biosensing devices. Definitely, nanofabrication techniques such as electron-beam or nanoimprinting lithography, allow the preparation of highly ordered arrays with perfectly controlled geometries. The smart use of the morphological characteristics and the composite structure of our sensor allow to maximize their biorecognition performances. In fact, we demonstrate the possibility to efficiently immobilize biomolecules, on the relatively large surface of the PC of our NEAs in order to develop sensitive electrochemical biosensors. However, further studies should be performed in order to understand the mechanism of functionalization with biomolecules and the amount of immobilized molecules on the surface of the PC.

Finally, the electrochemiluminescence (ECL) properties of NEA for bioanalytical applications were investigate. ECL measuraments on our NEAs were performed at the Institut des Sciences Molèculaires University of Bordeaux (Group of Nanosystèmes Analitique) using electrochemiluminescence (ECL). In these sensors the transduction scheme involves a secondary antibody labbeled with Biotin, that

Abstract

provides a strong interaction with the complex streptavidin- $Ru(bpy)_3^{2+}$. The ECL signal obtained in the presence of the co-reactant tripropylamine (TPrA) was recorded using both a CCD camera and a photomultiplier tube. Furthemore, additional sensors have been prepared using GC as conductive material and PC as insulating layer. The surface of the PC was patterned with different geometries in order to evaluate the diffusion of the electrochemiluminescence signal obtained from $Ru(bpy)_3^{2+}$ immobilized on the surface, in between the different shapes of the electrode.

List of Abbreviations

NEA …… Nano Electrode Array
NEE …… Nano Electrode Esemble
EBL …… Electron Beam Lithography
NIL …… Nano Imprint Lithography
RIE …… Reactive Ion Etching
ICP …… Inductively Coupled Plasma
SEM …… Scanning Electron Microscope
ECL …… ElectroChemiLuminescence
CCD …… Charge Coupled Device
EM-CCD …… Electron Multiplying Charge Coupled Device
RT …… Room Temperature
CV …… Cyclic voltammetry
GC …… Glassy Carbon
BDD …… Boron Doped Diamond
PC …… Poly-Carbonate
PMMA …… Poly (methilmethacrylate)
HPV …… Human Papilloma Virus
GOx …… Glucose Oxidase
HRP…… … Horse Radish Peroxidase
PBS …… Phosphate Buffered Saline
OTS …… Octadecyl Trichloro Silane
EDC …… N-ethyl-N'-(3-dimethylaminopropyl)carbodiimide hydrochloride
Sulfo-NHS …… N-hydroxysulfosuccinimide sodium salt
BSA …… Bovine Serum Albumin
FA+ …… (Ferrocenyl methyl) trimethyl ammonium cation
$Ru(bipy)_3^{2+}$ …… Ruthenium (II) tris(bipyridine)
TrPA (or TPA) …… TriPropylAmine
DBAE …… DiButhil Amino Ethanol

Introduction

1.1 Biosensors

The term “biosensor” refers to analytical devices involving biological sensing element with a wide range of applications, such as drug discovery, diagnosis, biomedicine, food safety and processing, environmental monitoring, defense, and security.[1]

The first biosensor was introduced by Leland C. Clark at the New York Academy of Sciences Symposium in 1962 to measure glucose in biological samples exploiting the strategy of electrochemical detection of oxygen or Hydrogen peroxide using immobilized glucose oxidase electrode[2].

Initially, the field was largely focused on immobilizing enzymes onto electrodes. Gradually, the field expanded to include other biorecognition elements such as antibodies, cells, and nucleic acids, and the early term ‘‘enzyme electrode’’ was replaced by ‘‘biosensor’’. Since then, incredible progress has been made both in technology and applications of biosensors with innovative approaches involving electrochemistry, nanotechnology and bioelectronics.

The selection of receptors for biosensor development, and the use of different transduction techniques and fast screening strategies are extremely important for applications of biosensors in food, and environmental safety and monitoring.[3]

Depending on the type of signal transduction, biosensors can be differentiated in optical, bioluminescent, electrochemical, piezoelectric and calorimetric (Figure 1).

Below we will focus on the salient aspects of electrochemical sensors.

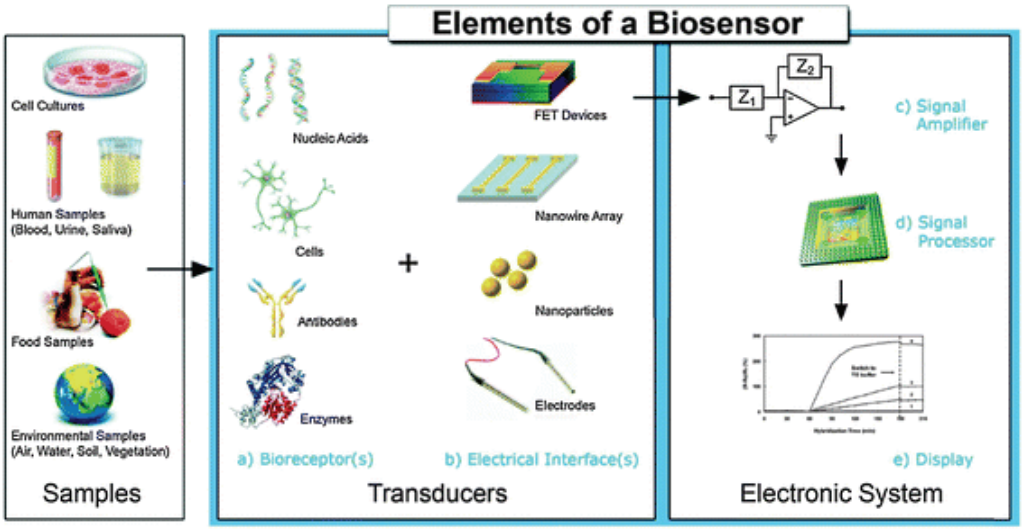

Fig. 1.1. *Elements and selected components of a typical biosensor.*[4]

1.1.2 Electrochemical Biosensors

Among the various kinds of biosensors, electrochemical biosensors are the class of the most widespread, numerous and successfully commercialized devices of biomolecular electronics.[1]

Due to the possibility of being miniaturized, to operate in turbid media (unlike optical ones), to have short response time (unlike bioluminescent ones), to reach low detection limits and to be produced at low cost, electrochemical biosensors are widely used for monitoring the products of industrial bioprocesses (aminoacids, yeast, lactic acid, ethanol, etc.), pollutants in the environment (pesticides, fertilizers, estrogenic substances, CO, CO2, etc...), relevant substances in clinical diagnostics (glucose, alcohol, DNA, hormones, etc...) and in the forensic field (cocaine, anthrax, nerve agents, etc...).[5]

An electrochemical biosensor produces an electrical signal proportional to the concentration of a single analyte or group of analytes. Electrochemical biosensors may

be classified according to the type of electrochemical measurement (conductometric, potentiometric and amperometric) or depending on the nature of the biological recognition process: biocatalytic devices (for example based on enzymes as immobilize biocomponent) and affinity sensors (based on antibodies, membrane receptors, or nucleic acids)[6].

Biocatalytic devices are mainly based on the interaction of an enzymatic layer with a suitable sensing device, like an appropriate electrode. These types of devices combine the specificity of the catalytic protein for its substrate with the sensitivity of the transducer. The process follows, in the majority of the cases, the Michaelis-Menten kinetic model and it can be studied by following the measured kinetic signal[7].

Another biosensing strategy exploits the interaction between a recognition molecule and its specific target to produce a detectable signal. In these sensors, called affinity electrochemical biosensors, the recognition event is strongly influenced by the characteristics (e.g., shape and size) of the interacting biomolecules and high specificity and affinity are required to ensure a strong and stable interaction[8].

Sensing element and target can interact by several kinds of affinity systems, such as antibody-antigen complexes or the formation of the DNA double helix by hybridization between a probe and its complementary target. This interaction can be detected by direct electrochemistry, or by detecting the electrochemical signal of a suitable electroactive or redox enzyme label[7,9].

In the latter case, the enzymatic label is typically bound to the analyte, exploiting its electrocatalytic properties to detect the formation of the probe-analyte complex. The electrocatalytic signal of the label will be indeed detected only when the biorecognition event (the binding between the probe and the enzyme-labelled analyte) has been successful. In this case, the characteristics of the affinity biosensor intersect with those of an electrocatalytic sensor[10].

Several electrochemical techniques (potentiometric, amperometric, and conductimetric) can be applied for analytical purposes; however, amperometric detection systems have been demonstrated to be the most suitable means for electrochemical biosensor

construction due to their high sensitivity, low cost and the possibility of instrument miniaturization.

In amperometric detection the electrical current resulting from oxidation or reduction reactions is measured at a fixed (potentiostatic technique) or variable (voltammetric technique) potential. Classically, it involves a three-electrode system, although this is often reduced in practice to two electrodes in many devices. By applying a certain potential between the working and the reference electrode, the species of interest is either oxidised or reduced at the working electrode causing a transfer of electrons which ultimately results in a measurable current that is directly proportional to the concentration of the electroactive species at the electrode surface over a wide dynamic range.

1.1.2.1 Electrochemical Immunosensor

In recent years, electrochemical immunosensors have become widely used in different sectors such as agriculture, food and medical applications, quality control, environmental and industrial surveillance as well as point-of-care devices.

Biosensors generally involve biological recognition components such as enzymes, nucleic acids, antibodies, animal or vegetable tissues in intimate contact with an appropriate transducer[3]. When the molecular recognition elements are antibodies or antibody fragments specific for particular analytes (antigens) to form a stable complex, the device is called immunosensor. Depending on the method of signal transduction, immunosensors may be divided into four basic groups: electrochemical, optical, piezoelectric and thermometric[11]. The transducers chosen are directly related to the labelling, enzymatic or not, performed on the antigen or on the antibody.

Most of the developed immunosensors are based either on a competitive or sandwich assay, when applied to the detection of low (i.e. herbicides, toxins) and high (proteins,

cells) molecular weight molecules, respectively[12]. In order to develop a competitive immunosensors, two approaches can be followed: a first one in which immobilized antigens (Ag) compete with free antigens for labelled free antibodies (Ab)(Fig. 1.2a) or a second one in which immobilized antibodies react with the free antigens in competition with labelled Ag (Fig. 1.2b). Both these approaches are defined as direct competitive immunoassay.[3]

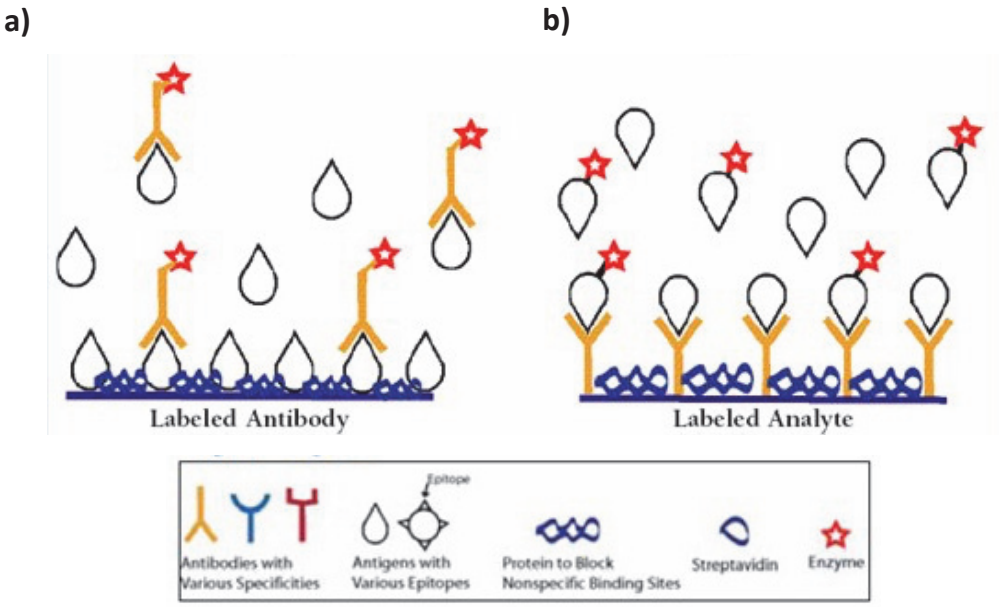

Fig. 1.2. *Schematic representation of direct competitive* ***(a)*** *and indirect competitive strategy* ***(b)****.*

The second format is denoted as indirect competitive immunoassay and avoids all problems related to antibody immobilization (loss of affinity or correct orientation of the antibody), and is also used when enzyme conjugated primary antibodies are not available for the selected analyte. In this case an anti-IgG enzyme labeled (secondary antibody) is used as label after binding with the Fc region of the primary antibody[3]. In a sandwich assay, after interaction between immobilized antibodies and free antigens, labelled antibodies, directed toward a second binding site of the antigen) are added; at this point, the Ag is "sandwiched" between two antibodies.

Immunosensor signals are conventionally obtained using labels such as enzymes,

electroactive molecules, redox complexes, and metal ions (Figure 1.3), despite of the fact that the majority of amperometric immunoassays are based on the use of specific enzyme/substrate couples. This is due to the fact that enzyme labels provide great signal amplification and also a large number of antibodies–enzyme or antigen–enzyme conjugates are commercially available.

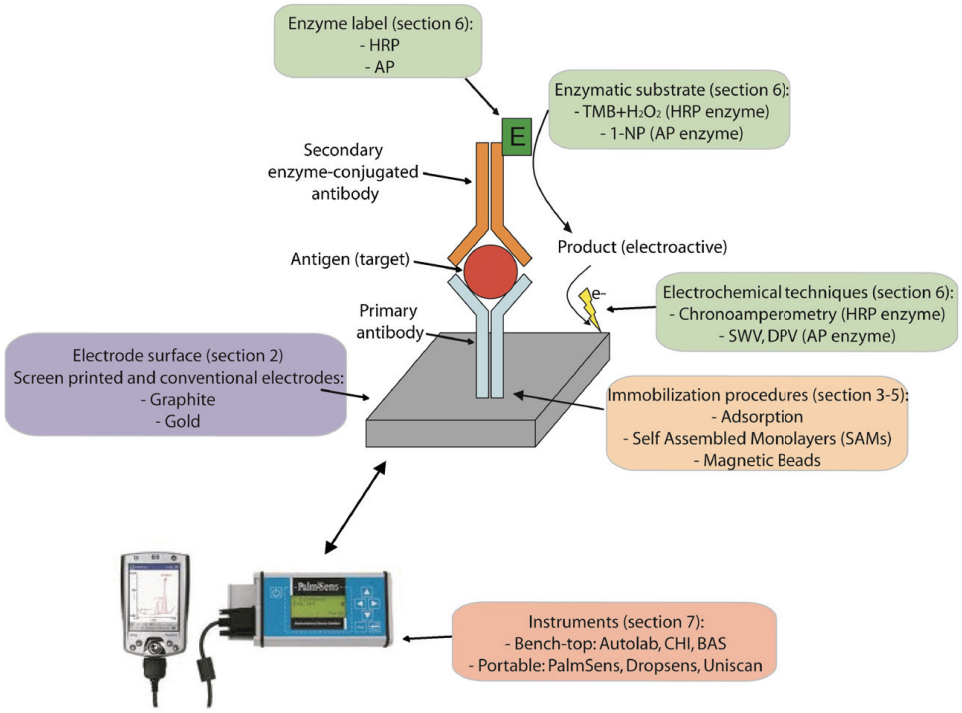

Fig. 1.3: *General overview of the main components of an electrochemical immunosensor*[3].

1.1.2.2 Electrochemical DNA-based biosensors

DNA features a unique complementary between the base pairs adenine/thymine and cytosine/guanine, that has been the basis for genetic analysis over the last few decades. The foundation of DNA-based detection systems lies in the ability of a single stranded DNA (ssDNA), to hybridize to its complementary strand in a sample. There is a great

potential for simple, cheap, rapid, and quantitative detection of specific genes. Areas of application include clinical, veterinary, medico-legal, environmental, and the food industry[13].

In electrochemical DNA biosensors, a single-chain of DNA is immobilized onto an electrically active surface (electrode), and then, changes in electrical parameters (e.g., current, potential, conductance, impedance and capacitance) caused by the hybridization reaction are measured (Figure 1.4).

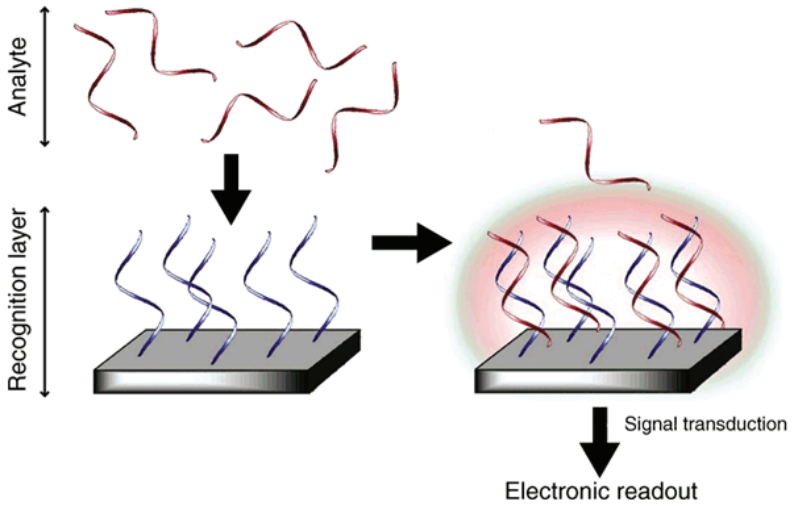

***Fig. 1.4**: General DNA biosensor design. Target DNA is captured by the recognition layer, and the resulting hybridization signal is transduced into a usable electronic signal for display and analysis.*[13]

Sensitive electrochemical signaling strategies based on the direct or catalyzed oxidation of DNA bases, as well as the redox reactions of reporter molecules or enzymes recruited to the electrode surface by specific DNA probe-target interaction have been all demonstrated.

Transduction of the hybridization event can be divided into two broad classes of approaches where a redox active species or an enzyme is used as a label and those where changes in the DNA interface are monitored electrochemically without the use of any labels.

For many years the electrochemistry of nucleic acids was studied at mercury electrodes, but in more recent years the purine bases of DNA have been electrochemically tested

using carbon, gold, indium tin oxide (ITO) and polymer coated electrodes[14].

Recent design employs physical separation techniques to remove the sources of background interference, for example by the immobilization of capturing probe DNA onto magnetic beads[15,16].

Methods to indirectly oxidize target DNA through the use of electro-chemical mediators have also been explored. An especially attractive approach uses poly-pyridyl complexes of Ru(II) and Os(II) to mediate the electrochemical oxidation of guanine.[17,18]

The formation of the double helix structure can also be detected following the electrochemistry of specific intercalating molecules, which interact with the "π-stacking" formed by the DNA-base pairs in the DNA duplex[19].

The target sequence can also be labelled with redox-active molecules, such as enzymes, that allow the indirect detection of the hybridization event by the introduction of an electroactive mediator in solution.

Enzymatic labels are commonly used to generate electrical signals for detection of DNA hybridization. The enzyme, previously bound to the DNA probe, triggers the catalysis of a redox reaction and generates an electrochemical change due to the hybridization event. Lumley–Woodyear et al. monitored the duplex formation with a carbon fiber transducer, using a horseradish peroxidase-labelled DNA-target[20]. The resulting electro-reduction of H_2O_2 was followed by amperometry, with single base-pair resolution.

In addition, the use of nanoscale materials, namely nanoparticles nanotubes and nanowires, has recently facilitated the development of ultrasensitive electrochemical biosensors, that are characterized by high surface area, optimal electrochemical properties and, in many cases, biocompatibility[21].

1.2 ELECTROCHEMILUMINESCENCE (ECL)

Electrogenerated Chemiluminescence (ECL) is an electrochemical process, where light emission is initiated by an electron-transfer reaction occurring at an electrode surface[22,23,24]. ECL is by essence a Chemiluminescence reaction (CL), triggered by electrochemical methods[25]. This technique represents a marriage between electrochemistry and spectroscopy. The smart combination of two analytical methods offers to ECL unique superiorities over other optical sensing methods.

ECL allows simultaneous measurements of two experimental parameters, the light intensity and the Faradaic current, as function of the potential, which facilitates the investigation of light emission mechanism and enables the ECL and electrochemical detections, simultaneously. Due to these properties, ECL has become an important detection method in analytical chemistry.

In classical photoluminescence methods, the absorption of a photon causes a transition from electronic ground state S0 to various vibrational levels in electronic S1 excited state (Figure 1.5). Once a molecule arrives at the lowest vibrational level of an exited singlet state, it can do a number of things, one of which is to return to the ground state S0 by photon emission.

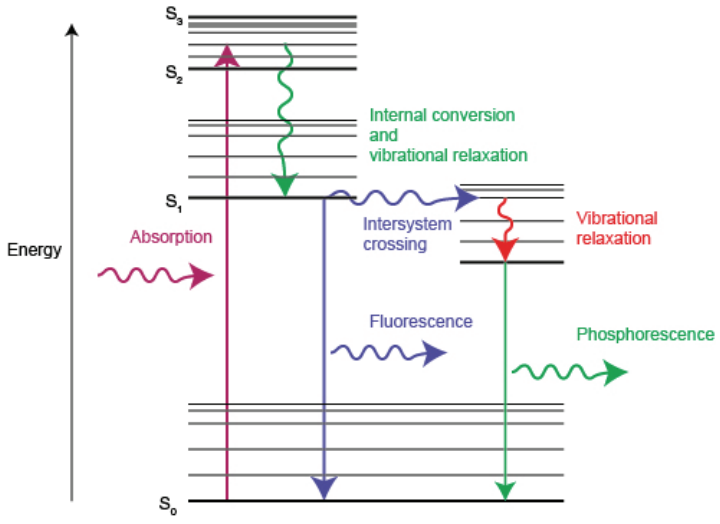

Fig. 1.5: *Partial energy diagram for a photoluminescence system (Jablonski diagram).*

This process is called fluorescence. The lifetime of an excited singlet state is approximately 10^{-9} to 10^{-7} sec and, therefore, the decay time of fluorescence is of the same order of magnitude. On the other side, it is also possible an inter-system crossing (vibrational coupling) between the excited singlet state S1 and the triplet state T1 followed by decay to S0 and consequent photon emission. This process is called phosphorescence. The lifetime of a triplet state is 10^{-2} to 10 sec, so phosphorescence usually last longer with respect to fluorescence emission.

The ECL emission results from the same excited states as photoluminescence but compared to these methods, in which the excited state is generated by light irradiation, the ECL excited state is generated by an electrochemical reaction. As it does not require a light source, it simplifies the detection apparatus and most importantly invalidates background signals from scattered light and luminescent impurities, thus providing improved sensitivity[22,26,27]. This fact, coupled with the possibility to place the optical detectors very close to the electrode surface, allows accurate spatial and temporal control over the reaction. By controlling its initiation, light emission can be delayed until events such as immune or enzyme-catalyzed reactions have taken place.
ECL processes have been established for many different molecules by several different mechanisms, it can occur by annihilation or by the use of a coreactant[23].

1.2.1 Co-reactant pathway

The co-reactant route is an electrochemical (E) step followed by a chemical (C) one, which can be considered as an EC process. The co-reactant is a deliberately introduced specie that, upon its oxidation or reduction, reacts with ECL luminophores to produce the excited state. Co-reactant induced ECL is more suitable for work not only in aqueous media but also in physiological conditions (pH ~ 7.4).

Thus co-reactant ECL technology is an essential part of all commercially available ECL

analytical instrumentations.

The most known and commonly used ECL system is constituted by ruthenium tris-bypiridine salts ($Ru(bpy)_3^{2+}$) as electroactive light emitting probe and tri-n-propylamine (TrPA) as coreactant.

According to literature, the mechanistic routes of the ECL reaction mechanism of dissolved $Ru(bpy)_3^{2+}$ species with TPrA have been established. ECL is produced upon concomitant electro-oxidation of $Ru(bpy)_3^{2+}$ and TPrA (Schemes 1 and 2)[25,28].

Scheme 1:

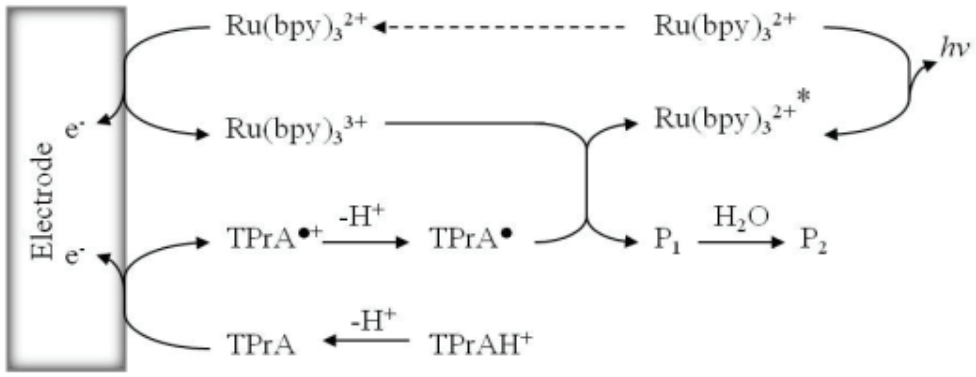

Scheme 2:

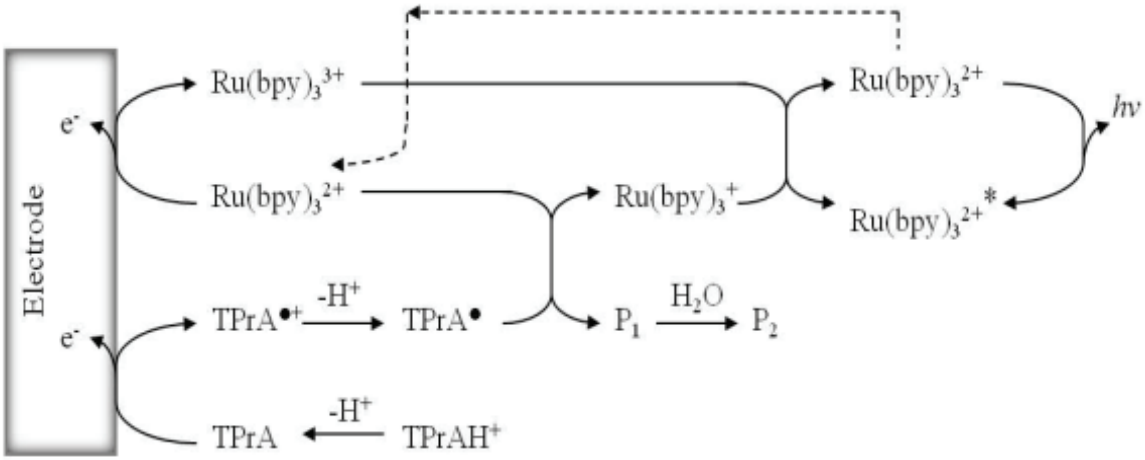

It has been reported that TPrA can be oxidized directly at the electrode surface, but also via catalytic homogeneous reaction with $Ru(bpy)_3^{3+}$ (Scheme 3)[29]:

Scheme 3:

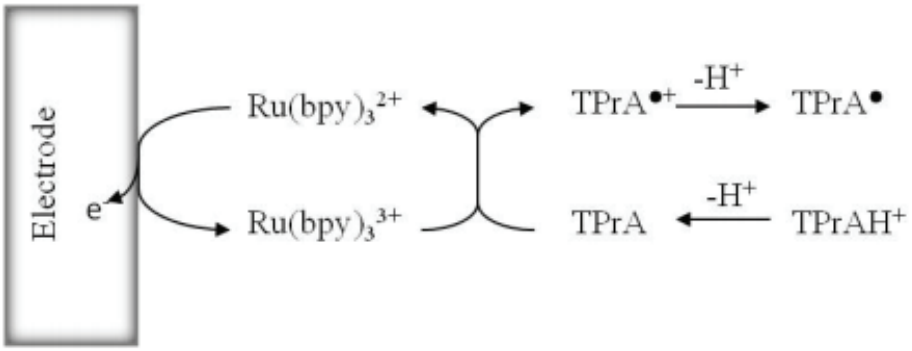

It should be noted that, although TPrA can also be oxidized by $Ru(bpy)_3^{3+}$, this oxidation reaction occurs only when $Ru(bpy)_3^{2+}$ concentration is high enough. *Miao* and *Bard* reported a "revisited" route where ECL emission is completely independent of direct oxidation of $Ru(bpy)_3^{2+}$ at the electrode surface and involves cation radical $TPrA^{\bullet+}$[28].

The mechanism is based on the assumption that $TPrA^{\bullet+}$ through a very reactive intermediate, has a life-time long enough to react itself before it undergoes deprotonation (Scheme 4).

Scheme 4:

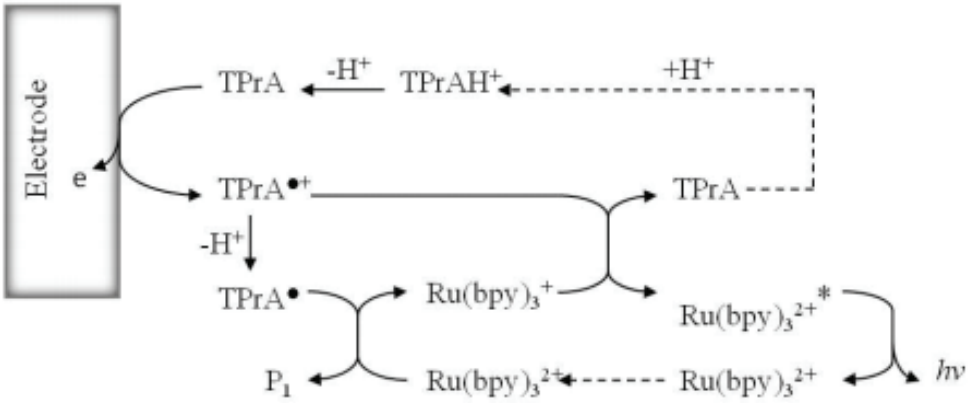

1.2.2 ECL applications in assays and commercialized systems

Because of very high sensitivity, good selectivity, insensitivity to matrix effects and high dynamic range ECL is a robust detection methodology. It is widely used in clinical diagnostics, environmental assay such as food and water testing and biowarfare agent detection. Due to high ECL efficiency, the majority of ECL detection systems involve the $Ru(bpy)_3^{2+}$ luminophore or its derivatives and TPrA or other related amines as co-reactant[30]. The analytical application is based on the fact that ECL intensity is proportional to the concentration of the ECL luminophore or of concentration of co-reactant, depending on the case. If ECL experiments are carried out in the presence of high and constant concentration of co-reactant, the ECL intensity will linearly depend on the concentration of ECL emitter in a wide dynamic range.

The most common and most important commercial applications of ECL are in diagnostic assays. Immunoassays based on ECL detection have several advantages over other techniques. No radioactive isotopes are used, thus reducing the problems of sample storage, handling and disposal. Since each label can emit several photons per measurement cycle and the linear dynamic range extends over 6 or more orders of magnitude, the detection levels are extremely low. Also, their small size allows multiple labelling of the same molecule without affecting the immunoreactivity or hybridization of the probes.

A large number of biomolecules such as proteins, DNAs and peptides have no co-reactant functionalities or they can give very poor ECL signal. Thus, their ECL detections are mainly carried out with solid phase ECL assay formats in which biomolecules linked with ECL labels, usually $Ru(bpy)_3^{2+}$ or its derivates, are immobilized on a solid substrate and ECL is generated in the presence of a co-reactant, typically TPrA.

Many works have been done and many commercial systems have been developed for immunoassay and DNA detection. Sensitive and selective detection of DNA hybridization has a great importance in genetic disease screening. An ultrasensitive DNA hybridization detection method based on ECL using polystyrene microspheres/beads (PSB) as the

carrier of the ECL label tris(2,2'-bipyridyl)ruthenium(II) tetrakis (pentafluorophenyl)borate (Ru(bpy)3-[B(C6F5)4]2) has been reported (Figure 1.6)[31,32].

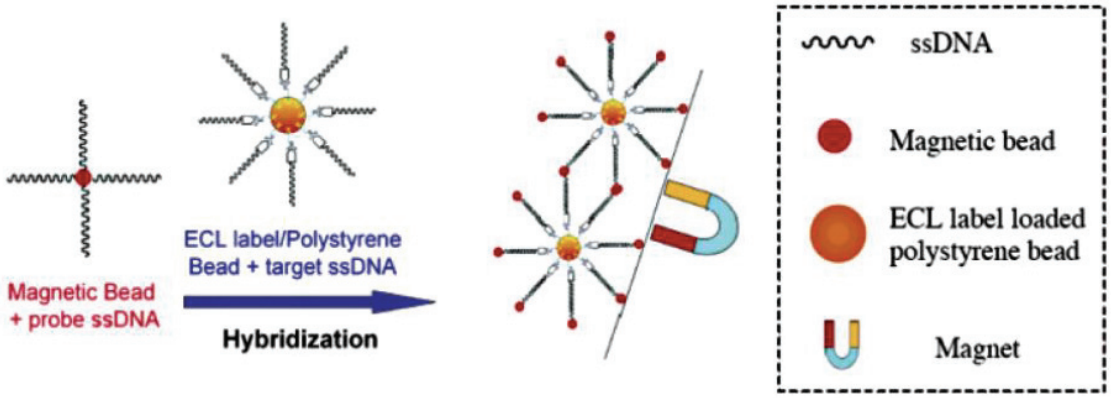

Fig. 1.6: *Schematic diagram of DNA hybridization on a polystyrene bead as the ECL label carrier and a magnetic bead for the separation of analyte-contained ECL label/polystyrene beads.*[33]

The ECL system can also be used for protein detection. For example, anti-C-reactive protein (CRP), an acute-phase protein found in the human serum, can be determined by a sandwich-type immunoassay which uses ECL as a readout mechanism. Biotinylated CRP species were attached to the surface of streptavidin-coated magnetic beads (MB) and Avidin-coated polystyrene microspheres/beads (PSB) entrapping a large number of ECL labels ($Ru(bpy)_3$-$[B(C_6F_5)_4]_2$) to form anti-CRP↔MB and Ru(II)-PSB/Avidin↔anti-CRP to form a sandwich type binding in the presence of analyte CRP.[34]

The sandwich format is widely used in immunoassays based on recognition properties and antibody/antigen binding. A bead-based platform that exploits ECL to detect three antigens simultaneously has been reported.[35] Microspheres with different antibodies and the bead-based assays were prepared by incubating the array first in a sample containing the antigen and then in a solution of biotinylated detection antibody that was finally attached to streptavidin-modified $Ru(bpy)_3^{2+}$ as an ECL label. The ECL response of the beads on the platform was recorded with a CCD camera.

The ECL imaging can be even developed for single cell analysis. Recently, the

development of a new transparent electrochemical cell for imaging suitable for single cell analysis has been reported.[36] For the above reasons we put our efforts in exploring the possibility to combine sensors based on nanoelectrode arrays (NEA) or ensemble (NEE) with detection schemes based on ECL methods.[37]

1.3 Nanoelectrodes Array (NEAs)

Nanoelectrodes may be defined as electrodes having at least one dimension (called critical dimension) in the nanometer range. On the other hand, a microelectrode or ultramicroelectrode may be viewed as any electrode smaller than the scale of the diffusion layer, which can be achieved in an experiment. When the electrode's critical dimension becomes comparable to the electrical double layer thickness or to the molecular size, the experimental behaviour starts to deviate from extrapolations of behaviour of larger electrodes[38].

Microelectrodes offer different benefits over conventionally sized macroelectrodes in electrochemical experiments, such as the possibility of use in very small sample volumes or in vivo measurements, the faster response time, extremely efficient mass transport (due to the strong concentration gradients pointing towards the electrode) and smaller double layer capacitance[10].

When electrodes decrease in size, radial (three-dimensional) diffusion becomes dominant and results in faster mass transport that enables measurement of kinetics by steady-state experiments rather than by transient techniques[39].

By decreasing electrode size from micrometer to nanometer scale, the study of faster electrochemical and chemical reactions becomes possible. This is because at very high rates of mass transport, the electron transfer process is less limited by the mass transport of reactant to the electrode surface[40]. Moreover, the dominance of radial diffusion decreases charging currents and so deleterious effects of solution resistance.

Since, the main disadvantage of using individual nanoscale electrodes is the extremely small current that can be achieved with them, the development of Ensemble (random distributed) or Arrays (arranged in an ordered manner with a controlled inter-electrode spacing) of nanoelectrodes (NEE or NEA) operating in parallel has attract a great deal of interest.

1.3.1 Electrochemistry at nanoelectrodes

From a voltammetric point of view, NEAs can be considered as an array of extremely small ultramicroelectrodes separated by an electrical insulator interposed between them. An ultramicroelectrode is considered as an electrode with at least one dimension comparable or lower than the thickness of the diffusion layer (typically < 25 μm)[41]. At such small dimensions, edge effects from the electrode become relevant and diffusion from the bulk solution to the electrode surface is described in terms of radial geometry instead of the simpler linear geometry used for larger electrodes (> 100 μm).[42]

In fact, due to their small size, nanoelectrodes exhibit a fast (three-dimensional) diffusion field and produce steady-state voltammograms (i.e. sigmoidal shape). The voltammogram shape is independent of the nanoelectrode geometry.

Generally, the nanoelectrodes critical parameter (i.e. radius of the disc) is extracted by applying a suitable model for the steady-state current. Figure 1.6 illustrates the possible diffusion modes and the corresponding steady-state current (limiting current) equations for hemisphere, inlaid disc and recessed disc electrodes geometries.[43]

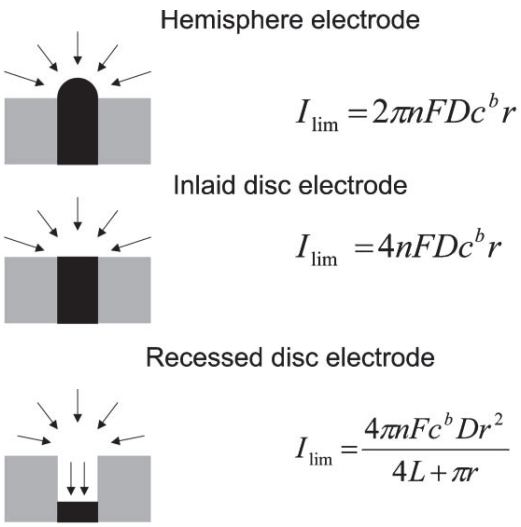

Fig. 1.6: *Nanoelectrodes geometries: hemispherical electrode, inlaid disc electrode and recessed disc electrode; diffusion modes and the equations for the corresponding steady-state limiting currents:* ***n*** *is the number of electrons involved in the electrode reaction,* ***F*** *is the Faraday constant,* ***D*** *is the diffusion coefficient of the electroactive species,* ***c*** *is concentration,* ***r*** *is the electrode radius and* ***L*** *is the recession depth of the electrode.*

By decreasing the electrode size from micrometer to nanometer scale, the study of faster electrochemical and chemical reactions is possible. This is because at very high rates of mass transport, the electron transfer rate is not limited by the mass transport of the reactant to the electrode surface.[44,45] The main disadvantage of using individual nanoscale electrodes is the extremely small current that can be achieved with them. For this reason, the development of ensemble of nanoelectrodes operating in parallel has attracted a great deal of interest. Even better performances are available when this ensemble is arranged in an ordered manner with a controlled inter-electrode spacing, more precisely with arrays.

Moreover, NEA can exhibit different diffusion regimes. According to the model proposed by Guo and Lindner[39], diffusion regimes occurring to an array of

microelectrodes can be divided into five categories (Figure 1.7) depending on the scan rate or the reciprocal distance among nanoelectrodes:

(I) planar diffusion to each microelectrode;

(II) mixed diffusion to each microelectrode (transition between planar and hemispherical diffusion);

(III) hemispherical diffusion;

(IV) diffusion mixed (planar/hemispherical) with onset of overlap of diffusion layers;

(V) planar diffusion over the entire array.

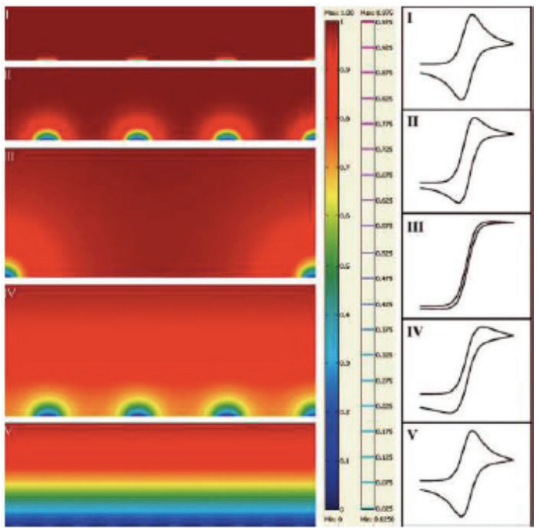

Fig 1.7: *Simulated concentration profiles, with isoconcentration contour lines, over an ultramicroelectrode array representing the five main categories of diffusion modes (forms I to V). In the scale bar next to the figure, the red color represents the bulk concentration and the blue color represents zero concentration. The second scale bar represents a relative concentration scale for the contour lines. Typical cyclic voltammograms obtained for each diffusion regime are shown on the right, as proposed by Guo and Linder*[39].

As mentioned before, the characteristic of the time-dependent diffusion profile of NEEs/NEAs depends primarily on the relative inter-electrode spacing, *d/r* (where *d* is the

centre-to-centre distance between nanoelectrodes and *r* is their mean radius), as well as the scan rate, which determines the time-constant of the experiment.

In the case of widely spaced electrodes (with a large *d/r* ratio) or at high scan rates, diffusion of the electroactive species to each individual electrode remains independent from all others and linear diffusion predominates at each nanoelectrode (case I, peak-shaped voltammograms)[46]. This is the regime that gives the highest Faradaic current, therefore this is the regime of choice for obtaining the maximum improvement of detection limits when there are no constraints in increasing the distance between the nanoelectrodes.

When the radial diffusion-boundary layers totally overlap, i.e. when the diffusion hemisphere is larger than the mean hemidistance among the nanoelectrodes, ensemble or array behave as a whole macroelectrode with regard to the Faradic current (total overlap, peak shape voltammograms, case V). Therefore, the diffusion-controlled current will be proportional to the geometric area, of the ensemble or array (i.e. active electrode surface as well as inter-electrode insulation). The background or charging current instead is proportional only to the active area of the electrode elements, in contrast to the conventional electrodes (CE)[47,48].

1.4 Micro-fabrication techniques

1.4.1 Introduction and preliminary concepts

Nanofabrication commonly refers to any technique used to fabricate miniature components and devices with sub-100 nm scale features, which are playing an increasing role in science and technology. Many opportunities derive from the ability to fabricate new types of micro- or nanostructures or to reconstitute existing structures in down-sized versions. The most obvious examples are in the electronics field but microstructures also provide the opportunity to study basic scientific phenomena that occur at small dimensions.[49]

Although micro-fabrication has its basis in microelectronics and most research in micro-fabrication has been focused on microelectronic devices[50], applications in other areas are rapidly emerging. These include systems for micro-analysis[51,52,53,54], micro volume reactors[55,56], combinatorial synthesis[57], MicroElectroMechanical Systems (MEMS)[58,59] and micro-optical components[60,61]. A wide range of micro-fabrication techniques has been developed to produce miniature components and devices with sub-micrometer-scale resolution but the main "standard" lithographic techniques are photolithography, Electron Beam Lithography (EBL) and Ion Beam Lithography (IBL).

These techniques generally consist of three successive steps (Figure 1.8):

- Coating a substrate with irradiation-sensitive polymer layer (resist),
- Exposing the resist with light, electron or ion beams,
- Developing the resist image with a suitable chemical.

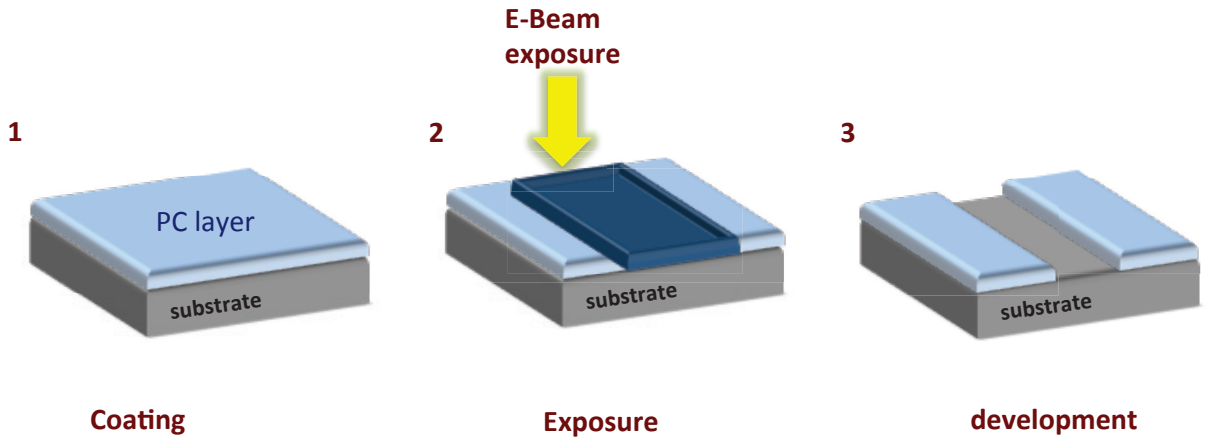

Fig. 1.8: *Representation of the main lithographic steps.*

Exposures can be done either by scanning a focused beam pixel by pixel according to a pre-defined pattern, or by exposing through a mask for parallel replication. The absorption of light or inelastic scattering of particles can affect the chemical structure of the resist, leading to a change of their solubility in suitable solvents. The response of the resist to the exposure can be either positive or negative, depending on whether the

exposed or unexposed portions will be removed from the substrate after development. In the case of positive resist the effect of the exposure is the cutting of polymeric chains in smaller molecular weight fragments that are then dissolved in an appropriate developer. In case of negative resist the exposure causes instead the cross-linking of the polymer. Serial beam scanning is used for mask fabrication and single component fabrication, but it does not supply adequate throughput for manufacturing. Industrial techniques must be fast, reliable and cost-effective. Therefore, in contrast to "conventional" techniques, a number of new and nonconventional lithographic techniques have been developed which are low cost and much more accessible, such as nanoimprint lithography, soft-lithography, near field optical lithography and a number of proximity probe techniques.[62] In the following paragraph the fabrication techniques used in this work (Electron Beam Lithography and thermal Nanoimprint Lithography) will be briefly described.

1.4.2 Electron Beam Direct Writing

Electron Beam Lithography (EBL) is used for primary patterning directly from a computer-designed pattern. It has been mainly used for patterning masks and reticules in the semiconductor industry and it has been developed according to the scaling up of circuit integration and the miniaturization of patterns. Electron Beam direct writing plays an important role in developing advanced devices because it offers high resolutions and short turn-around time, though its patterning speed has not been high enough for mass production use.[63]

Patterning using an electron beam (EB) goes back to the early 1960's.[64] At that time, the systems were essentially modified electron microscopes that used Gaussian beams (also called point beams) in which the beam was converging to the smallest possible spot. The patterns were directly written on substrates/films without using masks. The resolution was already under 1 μm, and the applications to the fabrication of circuits began soon.

A typical EBL system consists essentially of a column, an electron optics for shaping and deflecting in controlled manner the electron beam, a sample stage and an electronic control system. The column, the electron optics system and stage is maintained in high vacuum to ensure scattering-free electron trajectories.

The column (Figure 1.9) includes principally an electron source, magnetic lenses, a beam blanker and a mechanism for deflecting the beam. The electron source can be either a thermo-ionic emitter or a thermal field emission.

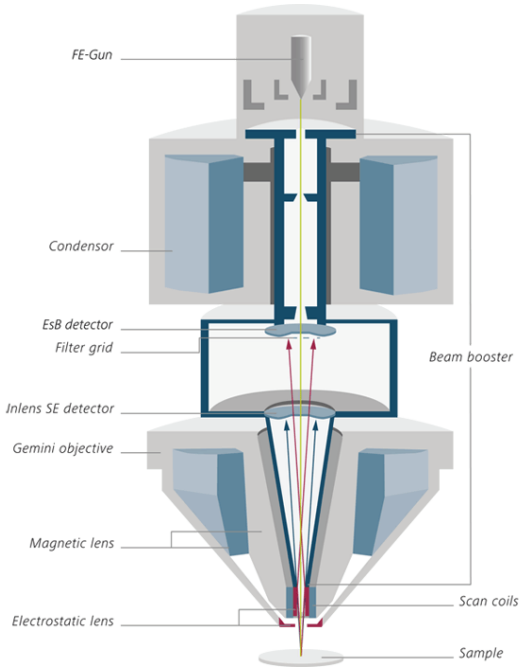

Fig. 1.9 *Cross section of the GEMINI® electron optical column.*

Depending on the design, e-beam energy varies in the range of 1-200 keV with a spot size down a few nanometers. The beam current and the scanning field size are determined according to the experimental requirements. The resolution of e-beam lithography depends on the beam size and on several factors related to the electron-solid interaction.[65]

In a resist, electrons undergo small angle forward scattering and some back scattering event coming from the substrate. The forward scattering tends to broaden the initial

beam diameter, whereas the back-scattering can spread over a large volume (proximity effects). During this process, the electrons are continuously slowing down, providing a cascade of secondary electrons which are responsible for resist reactions, as polymerization, polymer cross-linking or chain scission.

In addition to the characteristics of the electron beam, the success of lithography depends also on the choice of the resist, the subsequent development and postprocessing. It is desirable to use resist and developers that have highly non linear response to exposure dose. Indeed, very important resist propriety for high resolution lithography is the contrast. The contrast of a resist (γ) is defined as the slope of the sensitivity curve on a semi-log scale and it is calculated according to the following equation:

$$\gamma = \left[\log 10 \left(\frac{Do}{D1}\right)\right]^{-1}$$

where *D0* is the critical dose necessary to completely open the structures, and *D1* is the dose at which the developer first begins to attack the irradiated film.

A high contrast (positive) resist permits a very little change in thickness in the under-exposed regions and it permits a completely removal of the resist in regions dosed above a threshold value. In other words, it generally allows to obtain sharp edges and higher resolutions. In addition, the contrast between developed/undeveloped areas can be improved by selecting an appropriate developer.[66]

1.4.3 Nanoimprint Lithography

Nanoimprint lithography is one of the most promising low-cost, high-throughput technologies for manufacturing nanostructures.

In the imprint, a mould with nanostructures on its surface is used to deform a thin resist film (or an active material) deposited on a substrate. In the pattern-transfer, an anisotropic etching process, such as reactive ion etching (RIE) or induced coupled

plasma (ICP) is used to remove the residual resist in compressed areas, transferring the thickness contrast pattern created by the imprint into the entire resist.

The resist can be either a thermoplastic, UV or thermally curable polymer or other deformable materials. For a thermoplastic resist, the resist is heated above its glass transition temperature (Tg) during imprint, where the resist becomes viscous liquid and the mould is pressed into the resist.[67] Then the resist is cooled below its Tg before being separated from the mould. For an UV or thermally curable polymer, a monomer mix, often as a liquid thin film on a substrate, is imprinted by a mould and then cured by UV light radiation or thermal heating to form polymers (due to polymerization and cross-linking) before being separated from the mould.

In essence, the process consists of pressing the stamp using a pressure in the range of about 50–100 bar, against a thin polymer film.[68] This takes place when the polymer is held at 90–100 °C above its Tg, in a time scale of a few minutes, during which the polymer can flow to fill in the volume delimited by the surface topology of the stamp.

The stamp is detached from the printed substrate after cooling both the stamp and substrate: this ensures that the polymer maintains its shape after the release of the mould. This takes place in a cycle involving time, temperature and pressure. In Figure 1.9, the schematic of the NIL process is shown, as well as a characteristic temperature and pressure cycle[69].

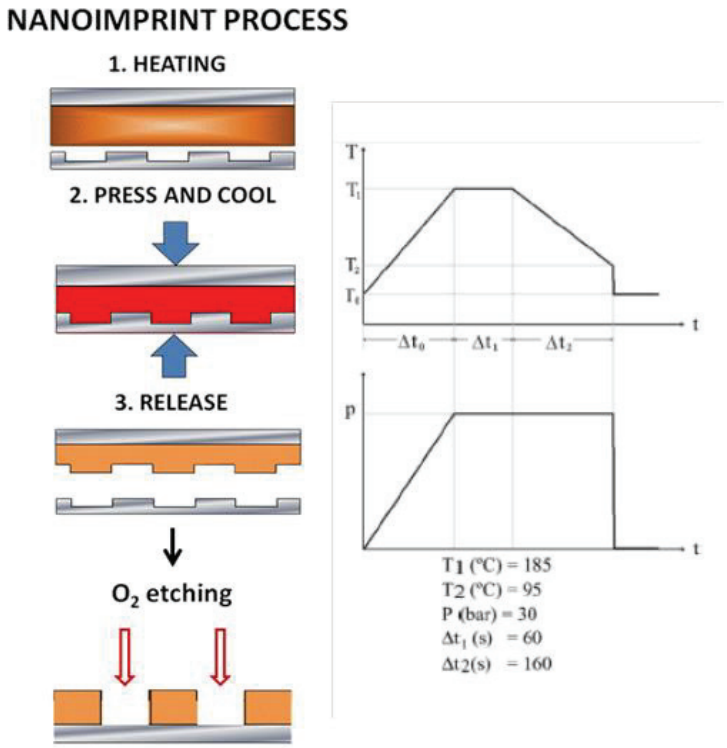

Fig. 1.9: *Schematics of the nanoimprint lithography process (left) and of the temperature– pressure temporal* sequence (right). The inset shows typical process parameters.

To summarize, three basic components are required to nanoimprint a surface. These are:

(i) a stamp with suitable feature sizes fabricated by, for example, electron beam lithography and dry etching, if features below 200 nm are needed, or by optical lithography for micrometer-scale features;

(ii) the material to be printed, usually a layer of polymer of a few hundred nanometers' thickness with suitable glass transition temperature Tg and molecular weight, spun on a substrate;

(iii) the equipment for printing with adequate control of temperature, pressure and control of parallelism of the stamp and substrate.

The minimal requirements for thermal-NIL process are:[70]

i) the Young modulus of the resist has to be much smaller than that of the mould during the imprinting;

ii) the minimal pressure required to perform the imprint should be higher than the shear modulus of the polymer;

iii) the highest temperature reached during the imprinting cycle should be sufficient to reduce the viscosity of the polymer at a value at which the NIL process could take place within a practical time frame; a typical value of viscosity reached during the nanoimprint step is 10^4-10^5 Pa*s.

These conditions can be satisfied not only by dielectric thermoplastic polymers but also in some cases, by conjugated polymers and small organic semiconducting molecules.

References:

1. Vigneshvar, S., Sudhakumari, C. C., Senthilkumaran, B. & Prakash, H. Recent Advances in Biosensor Technology for Potential Applications - An Overview. *Front. Bioeng. Biotechnol.* **4,** 11 (2016).
2. Clark, L. C. & Lyons, C. Electrode systems for continuous monitoring in cardiovascular surgery. *Ann. N. Y. Acad. Sci.* **102,** 29–45 (1962).
3. Ricci, F., Adornetto, G. & Palleschi, G. A review of experimental aspects of electrochemical immunosensors. *Electrochim. Acta* **84,** 74–83 (2012).
4. Kirsch, J., Siltanen, C., Zhou, Q., Revzin, A. & Simonian, A. Biosensor technology: recent advances in threat agent detection and medicine. *Chem. Soc. Rev.* **42,** 8733 (2013).
5. Thévenot, D. R., Toth, K., Durst, R. A. & Wilson, G. S. Electrochemical biosensors: Recommended definitions and classification. *Biosens. Bioelectron.* **16,** 121–131 (2001).
6. Ronkainen, N. J., Halsall, H. B. & Heineman, W. R. Electrochemical biosensors. *Chem. Soc. Rev.* **39,** 1747 (2010).
7. Barlett P.N., T. C. S. *Biosensor*. (Oxford Press. University, 2004).
8. Joseph, W. *Analytical Electrochemistry*. (2006). doi:10.1002/0471790303
9. Yakovleva J., E. J. *Bioelectrochemistry Bioelectrochemistry Fundamentals , Experimental Techniques and Applications*. *Experimental Techniques* (Wiley-VCH, 2008).
10. Virgilio, F., Prasciolu, M., Ugo, P. & Tormen, M. Development of electrochemical biosensors by e-beam lithography for medical diagnostics. *Microelectron. Eng.* **111,** 320–324 (2013).
11. Luppa, P. B., Sokoll, L. J. & Chan, D. W. Immunosensors—principles and applications to clinical chemistry. *Clin. Chim. Acta* **314,** 1–26 (2001).
12. Marquette, C. A. & Blum, L. J. State of the art and recent advances in immunoanalytical systems. *Biosens. Bioelectron.* **21,** 1424–1433 (2006).
13. Drummond, T. G. *et al.* Electrochemical DNA sensors. *Nat. Biotechnol.* **21,** 1192–9 (2003).
14. Singhal, P. & Kuhr, W. G. Ultrasensitive Voltammetric Detection of Underivatized Oligonucleotides and DNA. *Anal. Chem.* **69,** 4828–4832 (1997).
15. Wang, J., Kawde, A.-N., Musameh, M. & Rivas, G. Dual enzyme electrochemical coding for detecting DNA hybridization. *Analyst* **127,** 1279–1282 (2002).
16. Hasoň, S., Pivoňková, H., Vetterl, V. & Fojta, M. Label-free sequence-specific DNA sensing using copper-enhanced anodic stripping of purine bases at boron-doped diamond electrodes. *Anal. Chem.* **80,** 2391–2399 (2008).
17. Yang, I. V. & Thorp, H. H. Modification of indium tin oxide electrodes with repeat polynucleotides:

Electrochemical detection of trinucleotide repeat expansion. *Anal. Chem.* **73,** 5316–5322 (2001).

18. Armistead, P. M. & Thorp, H. H. Electrochemical detection of gene expression in tumor samples: Overexpression of Rak nuclear tyrosine kinase. *Bioconjug. Chem.* **13,** 172–176 (2002).
19. Aleksić, M. M. & Kapetanović, V. An overview of the optical and electrochemical methods for detection of DNA - Drug interactions. *Acta Chimica Slovenica* **61,** 555–573 (2014).
20. De Lumley-Woodyear, T., Campbell, C. N. & Heller, A. Direct enzyme-amplified electrical recognition of a 30-base model oligonucleotide. *J. Am. Chem. Soc.* **118,** 5504–5505 (1996).
21. Zhu, C., Yang, G., Li, H., Du, D. & Lin, Y. Electrochemical Sensors and Biosensors Based on Nanomaterials and Nanostructures. (2015).
22. Miao, W. Electrogenerated chemiluminescence and its biorelated applications. *Chemical Reviews* **108,** 2506–2553 (2008).
23. Richter, M. M. Electrochemiluminescence (ECL). (2004).
24. Bard, J. A. Electrogenerated Chemiluminescence. **195,** 414–419 (2004).
25. Leland, J. K. & Powell, M. Electrogenerated Chemiluminescence: An Oxidative-Reduction Type ECL Reaction Sequence Using Tripropyl Amine. *J. Electrochem. Soc.* **137,** 3127 (1990).
26. Bertoncello, P. & Forster, R. J. Nanostructured materials for electrochemiluminescence (ECL)-based detection methods: Recent advances and future perspectives. *Biosens. Bioelectron.* **24,** 3191–3200 (2009).
27. Martin, A. F. & Nieman, T. A. Glucose quantitation using an immobilized glucose dehydrogenase enzyme reactor and a tris(2,2-bipyridyl) ruthenium(II) chemiluminescent sensor. *Anal. Chim. Acta* **281,** 475–481 (1993).
28. Miao, W., Choi, J. P. & Bard, A. J. Electrogenerated chemiluminescence 69: The Tris(2,2???-bipyridine)ruthenium(II), (Ru(bpy)32+)/tri-n-propylamine (TPrA) system revisited - A new route involving TPrA.+ cation radicals. *J. Am. Chem. Soc.* **124,** 14478–14485 (2002).
29. Zu, Y. & Bard, A. J. Dependence of Light Emission of the Tris (2 , 2 ′) bipyridylruthenium (II)/ Tripropylamine System on Electrode Surface Hydrophobicity. *Society* **73,** 3960–3964 (2001).
30. Yuan, Y., Han, S., Hu, L., Parveen, S. & Xu, G. Coreactants of tris(2,2???-bipyridyl)ruthenium(II) Electrogenerated Chemiluminescence. in *Electrochimica Acta* **82,** 484–492 (2012).
31. Bard A.J., Debad J.D., Leland J.K., Sigal G.B., Wilbur J.L., W. J. N. *Encyclopedia of Analytical Chemistry*. (2000).
32. Kenten, J. H. *et al.* Improved electrochemiluminescent label for DNA probe assays: Rapid quantitative assays of HIV-1 polymerase chain reaction products. *Clin. Chem.* **38,** 873–879 (1992).
33. Miao, W. & Bard, A. J. Electrogenerated chemiluminescence. 77. DNA hybridization detection at high amplification with [Ru(bpy)3]2+-containing microspheres. *Anal. Chem.* **76,** 5379–5386 (2004).
34. Miao, W. & Bard, A. J. Electrogenerated chemiluminescence. 80. C-reactive protein determination

at high amplification with [Ru(bpy)3]2+-containing microspheres. *Anal. Chem.* **76,** 7109–7113 (2005).

35. Deiss, F. *et al.* Multiplexed sandwich immunoassays using electrochemiluminescence imaging resolved at the single bead level. *J. Am. Chem. Soc.* **131,** 6088–6089 (2009).
36. Dolci, L. S., Zanarini, S., Della Ciana, L., Paolucci, F. & Roda, A. Development of a new device for ultrasensitive electrochemiluminescence microscopy imaging. *Anal. Chem.* **81,** 6234–6241 (2009).
37. Sentic, M. *et al.* Microscopic imaging and tuning of electrogenerated chemiluminescence with boron-doped diamond nanoelectrode arrays. *Analytical and Bioanalytical Chemistry* 1–10 (2016).
38. Hye Jin Lee, Beriet, C., Ferrigno, R. & Girault, H. H. Cyclic voltammetry at a regular microdisc electrode array. *J. Electroanal. Chem.* **502,** 138–145 (2001).
39. Guo, J. & Lindner, E. Cyclic voltammograms at coplanar and shallow recessed microdisk electrode arrays: Guidelines for design and experiment. *Anal. Chem.* **81,** 130–138 (2009).
40. Mirkin, M. V. & Bard, A. J. Multidimensional integral equations. Part 1. A new approach to solving microelectrode diffusion problems. *J. Electroanal. Chem.* **323,** 1–27 (1992).
41. Bard, A. J. & Faulkner. *Electrochemical Methods*. *Annual Review of Materials Science* **30,** (2000).
42. Silvestrini, M., Dottorato, C. & Ugo, P. P. Advances in the Use of Nanoelectrode Ensembles in Analytical Chemistry and Molecular Diagnostics. (2011).
43. Arrigan, D. W. M. Nanoelectrodes, nanoelectrode arrays and their applications. *Analyst* **129,** 1157–1165 (2004).
44. Penner, R. M., Heben, M. J., Longin, T. L. & Lewis, N. S. Fabrication and Use of Nanometer-Sized Electrodes in Electrochemistry. *Science (80-.).* **250,** 1118–1121 (1990).
45. Mirkin, M. V, Fan, F.-R. F. & Bard, A. J. Scanning electrochemical Part 13. Evaluation microelectrodes microscopy size of the tip shapes of nanometer. *J. Electroanal. Chem.* **328,** 47–62 (1992).
46. Sandison, M. E. & Cooper, J. M. Nanofabrication of electrode arrays by electron-beam and nanoimprint lithographies. *Lab Chip* **6,** 1020–1025 (2006).
47. Ugo, P., Moretto, L. M. & Vezzà, F. Ionomer-coated electrodes and nanoelectrode ensembles as electrochemical environmental sensors: Recent advances and prospects. *ChemPhysChem* **3,** 917–925 (2002).
48. Ugo, P., Moretto, L. M., Bellomi, S., Menon, V. P. & Martin, C. R. Ion-exchange voltammetry at polymer film-coated nanoelectrode ensembles. *Anal. Chem.* **68,** 4160–4165 (1996).
49. Heitmann, D. & Kotthaus, J. P. The Spectroscopy of Quantum Dot Arrays. *Phys. Today* **46,** 56 (1993).
50. Wayne M. Moreau. *Semiconductor Lithography: Principles, Practices, and Materials*. (Springer Science & Business Media, 1988). doi:10.1007/978-1-4613-0885-0

51. Mitri, E. *et al.* Highly IR-transparent microfluidic chip with surface-modified BaF 2 optical windows for Infrared Microspectroscopy of living cells. *Microelectron. Eng.* **107,** 6–9 (2013).
52. Jacobson, S. C., Hergenroder, R., Koutny, L. B., Warmack, R. J. & Ramsey, J. M. Effects of Injection Schemes and Column Geometry on the Performance of Microchip Electrophoresis Devices. *Anal. Chem.* **66,** 1107–1113 (1994).
53. Bratten, C. D. ., Cobbold, P. H. & Cooper, J. M. Micromachining sensors for electrochemical measurement in subnanoliter volumes. *Anal. Chem* **69,** 253–258 (1997).
54. Clark, R. a., Hietpas, P. B. & Ewing, A. G. Electrochemical Analysis in Picoliter Microvials. *Anal. Chem.* **69,** 259–263 (1997).
55. Ananchenko, G. S., Bagryanskaya, E. G., Tarasov, V. F., Sagdeev, R. Z. & Paul, H. A 31P-SNP study of the photolysis of (2,4,6-trimethylbenzoyl)diphenylphosphine oxide in micelles of different sizes. *Chem. Phys. Lett.* **255,** 267–273 (1996).
56. Song, M. I. *et al.* Multisample Analysis Using An Array of Microreactors for An Alternating-Current Field-Enhanced Latex Immunoassay. *Anal. Chem.* **66,** 778–781 (1994).
57. Briceño, G., Chang, H., Sun, X., Schultz, P. G. & Xiang, X.-D. A Class of Cobalt Oxide Magnetoresistance Materials Discovered with Combinatorial Synthesis. *Science (80-.).* **270,** 273–275 (1995).
58. Kovacs, G. T. A., Petersen, K. & Albin, M. Peer Reviewed: Silicon Micromachining: Sensors to Systems. *Anal. Chem.* **68,** 407A–412A (1996).
59. MacDonald, N. C. SCREAM MicroElectroMechanical Systems. *Microelectron. Eng.* **32,** 49–73 (1996).
60. Lee S. S., L. Y. Lin, and M. C. W. Surface-micromachined free-space micro-optical systems containing three-dimensional micrograting*s*. *Appl. Phys. Lett.* **67,**
61. Wu, M. C., Lin, L. Y., Lee, S. S. & King, C. R. Integrated devices make an optical bench on a chip. *Laser Focus world* **32,** 64–68 (1996).
62. Commission, E. *The Technology Roadmap for Nanoelectronics*. (1999).
63. WILKINSON, C. *Nanofabrication Fundamentals and Applications*. *Microelectronic Engineering* **6,** (1987).
64. Mollenstedt R., S. G. Proceedings of 3rd Symposium on Electron Beam Technology. **340,** (1961).
65. McCord M.A., R. M. J. *Handbook of Microlithography, Microfabrication and Microsystems*. (1997).
66. Tobing L.Y.M., T. L. and Z. D. H. *Nanotechnology 24*. (2013).
67. Pianigiani, M. *et al.* Effect of nanoimprint on the elastic modulus of PMMA: Comparison between standard and ultrafast thermal NIL. *Microelectron. Eng.* **155,** 85–91 (2016).
68. E., S. Influence of nanostructured heterojunctions on the electrical proprierties of photovoltaics cells. (2010).

69. Sotomayor Torres, C. M. *et al.* Nanoimprint lithography: an alternative nanofabrication approach. *Mater. Sci. Eng. C* **23,** 23–31 (2003).

70. Guo, L. J. Nanoimprint lithography: Methods and material requirements. *Adv. Mater.* **19,** 495–513 (2007).

Materials

2.1 Materials

Phosphate buffered saline solution (PBS) 0.01 M pH 7.4 was prepared by the following recipe:

Na2HPO4= 2.76 g

NaH2PO4= 0.35 g

NaCl = 9.0 g

dissolved in 1000 mL distilled water and adjusted pH to 7.2.

HEPES Buffer 0.1 M was prepared by dilution of HEPES buffer 1 M purchased from Sigma-Aldrich.

Other chemicals were purchase from Sigma–Aldrich, unless otherwise stated, and they were used as received. Purified water was obtained by a Milli-RO plus Milli-Q (Millipore) system.

- **Fabrication**

Polycarbonate solutions were obtained by dissolution of solid Bisphenol-A based Polycarbonate Makrolon (Bayer Sheet Europe) in cyclopentanone (Sigma- Aldrich).

Si ‹100› substrates coated with a 400 nm thick layer of BDD (Adamant Technologies SA) and Glassy Carbon Plates 100 x 100 x 1 mm (Tokai Carbon Italia S.r.l), were used as conductive layer for NEAs fabrication.

Resist SU-8 25, SU-8 3000 and SU-8 3005 were purchase from MicroChem Inc. MA, USA and Resist MR I 7010 from micro resist technology GmbH.

- **Electrochemical Measurements**

The salt (ferrocenylmethyl)trimethylammonium hexafluorophosphate ($FA^+PF_6^-$) used as redox probe and mediator for electrochemical measurements was prepared by metathesis of the (ferrocenylmethyl)trimethylammonium iodide (Alfa Aesar) with potassium hexafluorophosphate 99% (Alfa Aesar) and obtained from the Laboratory of Sensors for Electroanalysis, University Ca' Foscari of Venice.

Methylene Blue solution 0.01 mM was prepared by diluition in PBS 0.01M of Methylene Blue powder purchase from A.C.E.F s.p.a.

- **Sensors Functionalization and immunological detection**

HPV16 probe with amino modification, hybridization and washing solutions (HYB-1 and CON-D1 respectively) were purchased from AB Analitica SRL (Padua-Italy). HPV 16 complementary sequence modified with biotin was from TAG Copenhagen A/S.
Gliadin protein fragments (19 kDa), Mouse monoclonal Anti-Gliadin antibody and Goat Anti-Mouse IgG modified with biotin, were purchase from Abcam®. Horseradish Peroxidase (HRP) labelled Goat anti-mouse IgG secondary antibody (Human Serum Adsorbed) was from KLP® and recombinant Human Tumor Necrosis Factor – α (TNF-α) was from Life Technologies.
Bis(2,2'-bipyridine)-4'-methyl-4-carboxybipyridine-ruthenium N-succinimidyl ester bis(hexafluorophosphate) and streptavidin from Streptomyces avidinii, were purchased from Sigma. Slide-A-Lyzer Dialysis Cassettes were from Thermo Scientific.

2.2 Characterization of Materials for NEAs fabrication

2.2.1 Fabrication of Glassy Carbon from SU-8 negative resist pyrolisis

Among the various carbon allotropes, glassy carbon (GC) are widely investigated for electrochemical applications. Glassy Carbon is made by heat treating various polymers that own in their microstructure a combination of graphitic and amorphous zones. In fact, by heating the polymer under pressure in an inert atmosphere to 1000- 3000 ° C, the heteroatoms are evaporated until only carbon remains. The C- C bonds in the polymer backbone do not break at these temperatures, so the carbon can form graphitic planes of only limited size.[1] Moreover, the graphitic content of glassy carbon can be altered by tuning pyrolysis conditions and other fabrication parameters[2]. In this way, GC should ensure a reduction in costs, in order to obtain a wide diffusion and use of the sensor.

For the purpose, different SU-8 resist were tested (SU-8 3005, SU-8 3000, SU-8 25) finding in SU-8 25 the best conditions.

The wafers were dehydrated for 30 minutes at 120◦C right before the application of the photoresist. SU-8 25 photoresist was dropped manually on SiO_2 wafers and spin-coated according to manufacturer's Specifications (MicroChem Data Sheet) to achieve the desired thicknesses. The conditions used are summarized in table 1.

Resist	SU-8 25 negative resist
Spin speed	1500 rpm (30µm thickness)
Soft bake	65°C for 1 min 95°C for 10 min Colling down at 40°C
UV Exposure	350 nm for 1 min
Post- exposure bake	65°C for 1 min 95°C for 5 min

Table 2.1: *Summary of the conditions used for the photoresist layer preparation for pyrolysis process.*

To improve the resist wetting and adhesion, some SiO_2 substrates were pre-treated with HMDS adhesion promoter by spin-coating procedure at 2000 rpm and bake at 115°C for 1 minute.

The thus prepared samples were carbonized using a 3-step pyrolysis process in an open ended quartz-tube furnace: first they were heated under N2 (flow rate: 2000 sccm) at 300◦C for 60 minutes. The temperature was ramped up at a rate of 10◦C/min to the final pyrolysis temperature of 800◦C. Samples were kept at the final pyrolysis temperature for 60 minutes before cooling down.

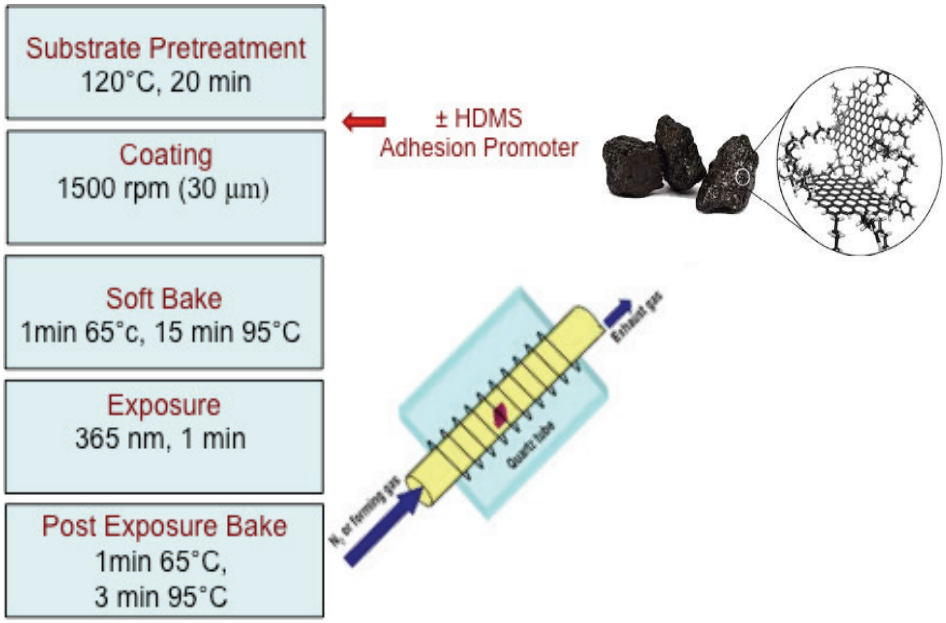

Fig. 2.1: *Schematic rappresentazion of the fabrication process to produce Glassy Carbon starting from SU-8 photoresist.*

In order to clean the surface of the samples from any organic residues due to the pyrolytic process, the samples were treated with Reactive Ion Etching (RIE) using Argon (20 sccm for 30 seconds) and Oxygen (30 sccm for 60 seconds). RIE uses chemically reactive plasma, generated under low pressure (vacuum) by an electromagnetic field, to remove material deposited on wafers.. High-energy ions from the plasma attack the wafer surface and react with it.

Figure 2.2 shows the contact angle of SiO_2 substrates covered with SU-25 before and after the pyrolization process using the condition described above:

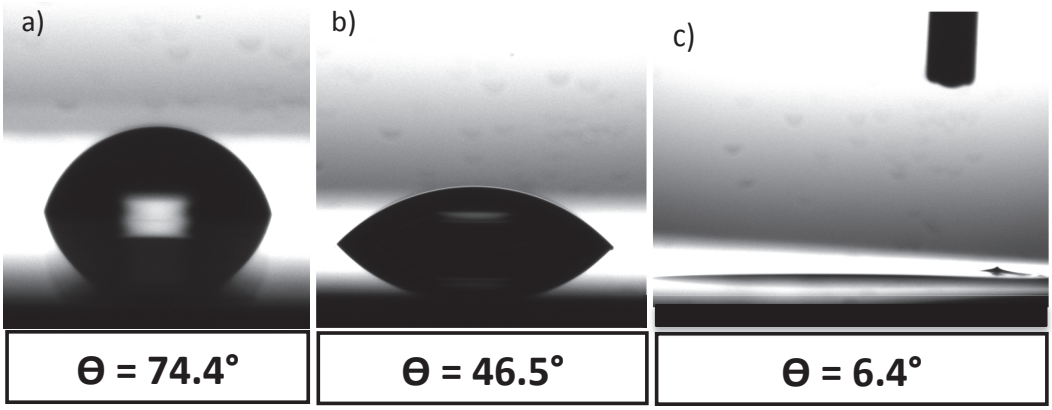

Fig. 2.2: *Water contact angles pictures recorded with a Krüss GmbH instrument:* ***(a)*** *refer to bare SiO_2* ***(b)*** *SU-8 25 spin coated on SiO_2 before pyrolysis (c) SU-8 25 deposited on SiO_2 after pyrolysis; water wetting layer is 0°.*

It can be cleary noticed that the pyrolized surface has a high wettability (contact angle = 0°) compared to the not pyrolized one as expected for glassy surfaces.

2.2.1.1 Electrochemical Characterization

Electrochemical measurements on pyrolized SU-8 were carried out at room temperature in a three-electrode cell with a platinum coil counter electrode and an Ag/AgCl (KCl satured) reference electrode, connected to a CHI Model 660B potentiostat (CHIIJ Cambria Scientific, UK).

Characterization were performed by measuring the potential window (Fig 2.3) of the obtained samples in PBS 0.01M and NaNO3 1M as supporting electrolyte and with cyclic voltammetry at different scan rates using (ferrocenyl methyl) trimethyl ammonium hexafluorophosphate (FA^+PF^6) 0.5 M as reversible redox probe.

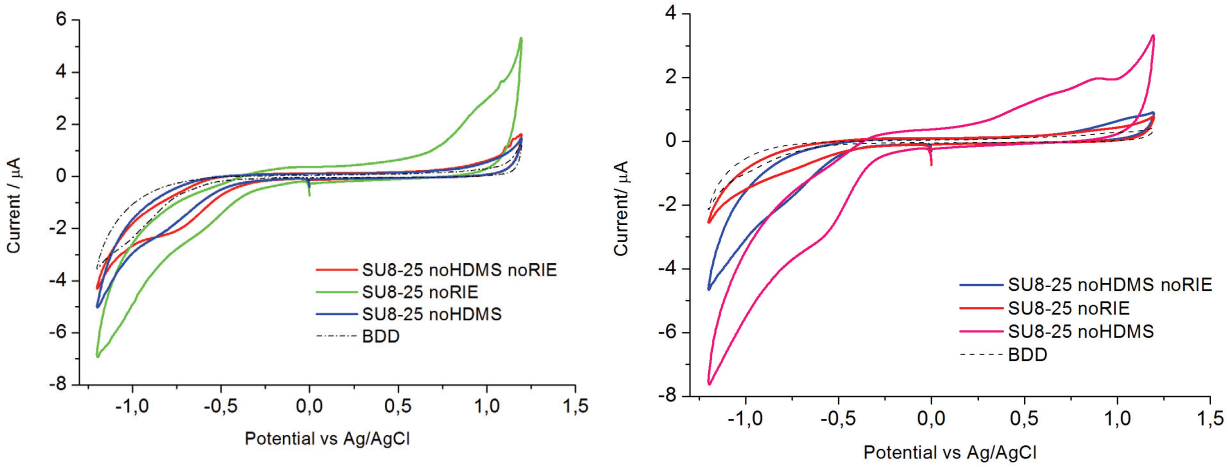

Fig. 2.3: *Potential windows of pyrolized SU-8 treated or not with HDMS and RIE in* ***(left)*** *0.01 PBS buffer and* ***(right)*** *0.1M NaNO3 solution. Scan rate 50 mv/s.*

Comparing the potential windows of BDD and SU-8, treated with different conditions, it can be seen that the overall accessible potential window is similar (2V approximately) in both solutions. However, the background current of the pyrolized SU-8 treated with HMDS and RIE is considerably higher with respect to the not treated ones.

Cyclic voltamograms recorded in $FA^+PF_6^-$ (Fig 2.4) doesn't show any variation in the electrochemical behavior of the pyrolized SU-8 in the presence of HDMS adhesion layer and after RIE treatment.

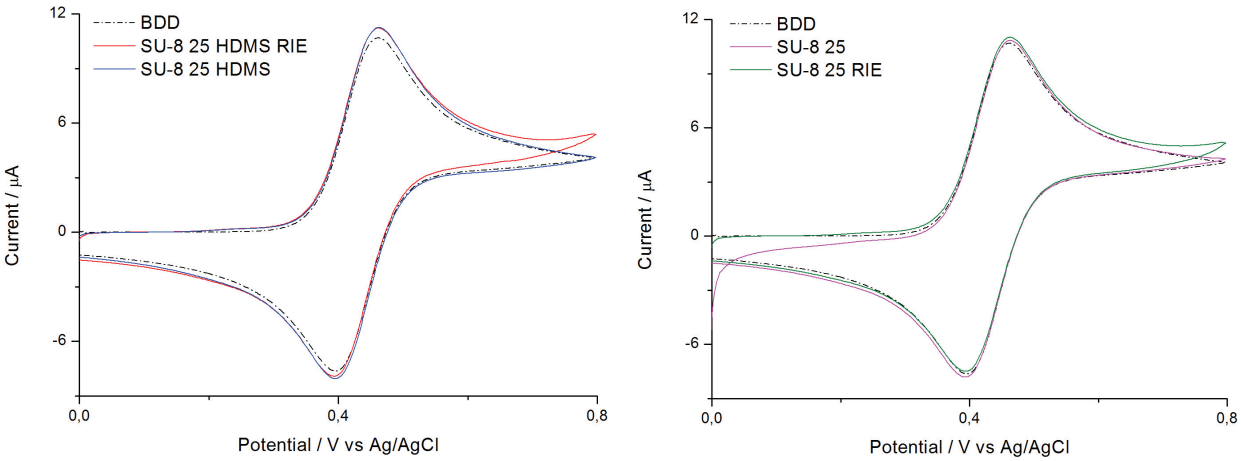

Fig. 2.4: *Cyclic Voltammogram recorded in $FA^+PF_6^-$ 0.5 M of pyrolized SU-8 treated with* ***(left)*** *HDMS and RIE and* ***(right)*** *only RIE. Scan rate 50 mv/s.*

2.2.2 Polycarbonate

Polycarbonate materials can be divided in two structural classes: aliphatics, which are not widely used as thermoplastics, generally being applied as comonomers, and aromatics, which are notable engineered thermoplastics. 4,4' isopropyliden diphenol polycarbonate or poly (bisphenol A carbonate) (BPAPC) is the most common aromatic polycarbonate and it is also the most important and widely used.

BPAC present characteristics that leads to properties as optical clarity and high elastic elongation, impact strength, toughness, shear resistance and heat deflection temperature[3]. This material is not a common resist for lithographic processes, but it was chosen for NEAs fabrication considering that this polymer was successfully used to produce Nanoelectrodes Ensembles (NEEs) based on track etched membranes[4,5]. In particular, this polymer shows satisfactory properties of chemical stability in common electrochemical solutions employed in voltammetric measurements and the possibility of biochemical functionalization[6].

2.2.2.1 Spin-coating - Film Deposition

During spin-coating process, the polymer is applied by dropping its solution on a wafer or a part of it. The wafer is then rotated on a spinning wheel at high speed so that centrifugal forces push the excess solution over the edge of the wafer, while a residue on the wafer remains due to surface tension. Different thickness can be obtained depending on viscosity of polymer solution and spinning speed. Usually this process is followed by thermal curing of the sample to facilitate the evaporation of residual solvent and to obtain a dry film. Schematic description of the process is reported in figure 2.5.

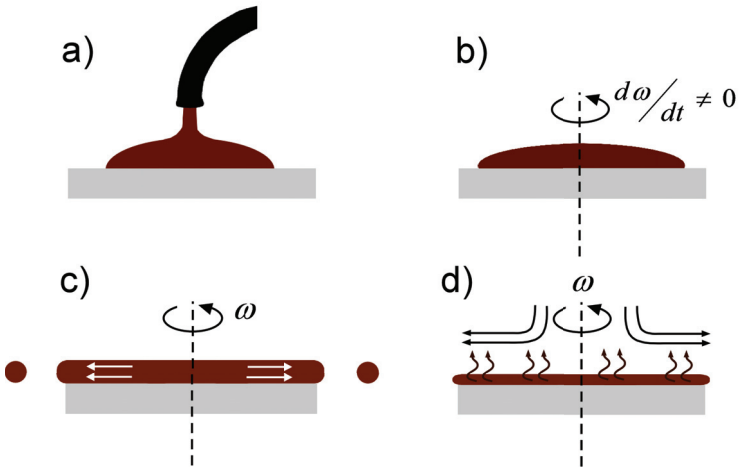

Fig. 2.5: *Spin coating process: (a) resist dropping on the substrate, (b,c) high speed spinning, (d) thermal curing for solvent removal.*

To evaluate the thickness of deposited polycarbonate film, different speeds of spin coating on Glassy Carbon plate were tested and different concentration of polycarbonate solutions (3% and 4%) were used. Obtained spin coating curves are reported in figure 2.6:

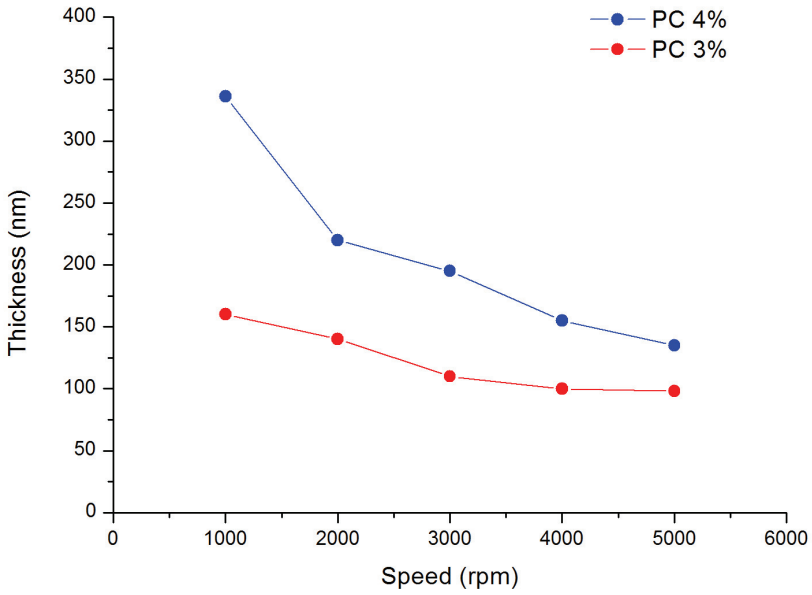

Fig. 2.6: *Spin-coating curves for polycarbonate solutions at different concentration*

References:

1. McCreery, R. L. Advanced carbon electrode materials for molecular electrochemistry. *Chemical Reviews* **108,** 2646–2687 (2008).
2. Mardegan, A. *et al.* Optimization of Carbon Electrodes Derived from Epoxy-based Photoresist. *J. Electrochem. Soc.* **160,** B132–B137 (2013).
3. Delpech, M. C., Coutinho, F. M. B. & Habibe, M. E. S. Viscometry study of ethylene-cyclic olefin copolymers. *Polym. Test.* **21,** 411–415 (2002).
4. Ugo, P., Moretto, L. M., Bellomi, S., Menon, V. P. & Martin, C. R. Ion-exchange voltammetry at polymer film-coated nanoelectrode ensembles. *Anal. Chem.* **68,** 4160–4165 (1996).
5. Habtamu, H. B. *et al.* A Sensitive Electrochemiluminescence Immunosensor for Celiac Disease Diagnosis Based on Nanoelectrode Ensembles. *Anal. Chem.* **87,** 12080–12087 (2015).
6. Virgilio, F., Prasciolu, M., Ugo, P. & Tormen, M. Development of electrochemical biosensors by e-beam lithography for medical diagnostics. *Microelectron. Eng.* **111,** 320–324 (2013).

Nanoelectrode Arrays Fabrication

3.1 Electron Beam Lithography

This section treats very shortly the topic of nanoelectrodes array fabrication by electron beam lithography. Part of the process development was done within previous Ph.D. programs and only minor aspects of the process were modified in order to adapt it to a different underlying macro-electrode (glassy carbon, GC, instead of boron doped diamond, BDD).

The first exposure tests were made to reproduce on GC substrate the lithographic results obtained by Virgilio et al. on polycarbonate deposited on BDD .

The conditions used are summarized in table 3.1.

Resist	PC 3%
Spin Speed	2000 rpm
Bake	170 °C for 5 minutes
Dose Range	50 ÷ 10000 μC/cm2
Developer	NaOH 5M
Temperature	35°C

Table 3.1: *Summary of the conditions used for the EBL writing process. The typical pattern is an array of holes in a rectangular field of 300 μm x 300 μm. The thickness of PC layer was 100 nm.*

After development, the samples were treated in oxygen plasma in order to remove polycarbonate residues at the bottom of nanoelectrodes, and lowering the resistance to electron transfer.

O_2 plasma parameters are reported in table 3.2:

ICP parameters	
Process	O_2 Strip
O_2	40 sccm
Pressure	4 mT
Coil	200 W
Platen	10 W
Bias	30 V

Table 3.2: *Induced Coupled Plasma parameters used for removal of polymer residues from bottom of nanoelectrodes.*

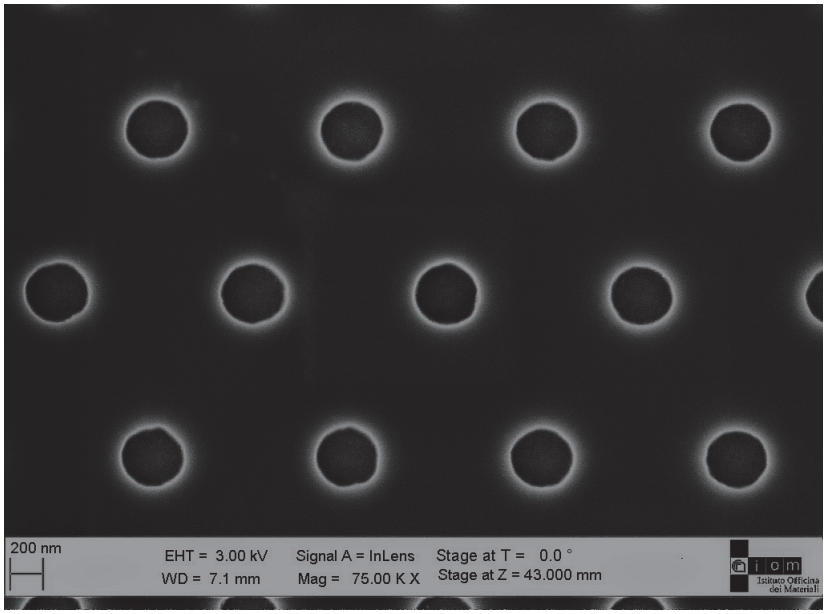

Fig. 3.1: *SEM micrograph of nanoelectrode array pattern on PC 3% deposited on GC obtained by EBL. (r= 250 nm, period = 1200 nm and recession depth 100 nm);*

3.2 Nanoimprint Lithography

In order to reduce time and manufacturing costs, a second technology, Nanoimprint Lithography (NIL), was employed. The parameters for the patterning process based on NIL have been optimized during this Ph.D. work. Nanoimprint lithography was performed with a master obtained by replication of a commercial silicon stamp and

consisting of a square array of holes (instead of hexagonal arrays obtained by EBL). In this case the polycarbonate surface is patterned with nano-electrodes, by displacing the polymer from the area of the stamp pillars during the NIL thermomechanical cycle.

Clearly, NEAs of different size, interelectrode size and field size can be obtained by changing the stamp and by slightly changing, where necessary, the NIL process paramenters. This will allow to optimize the performances of the sensor in future.

The master for NEAs fabrication by NIL, was obtained according to the following procedure:

- First, a Si ‹100› substrate was spin coated with mr-I 7010E (microresist GmbH) at 2000 rpm and then it was annealed at 140 ^{o}C for 2 minutes. A film of 115 nm was obtained using these parameters.
- Then, a commercial master (AMO Gmb) consisting of holes of 800nm period, 400nm diameter and a depth of 400nm, was replicated by Thermal NIL process using press with heating plates. The conditions used are summarized in table 3.3.

Imprinting Temp.	100°C
Pressure	10 MPa
Time	15 min.
Release Temp.	35°C

Table 3.3: *Summary of the conditions used for master replication using Thermal NIL process.*

- After that, induced coupled plasma (ICP) process was used to transfer the pillars pattern on silicon (Fig. 3.2). The process consist of a O_2 Plasma treatment to remove residual layer, then a Fluorine based

plasma for silicon etching and finally a plasma ashing to remove resist mask. ICP parameters are summarized in table 3.4.

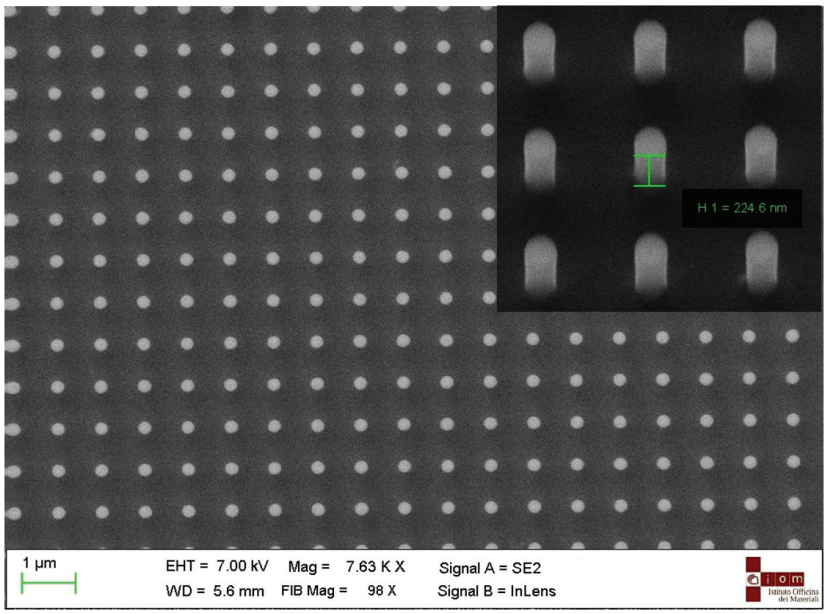

Fig. 3.2: *SEM micrograph of silicon pillars after ICP dry etching.*

	O_2 Plasma	Fluorine based Plasma	Plasma ashing
Coil Power	200 W	400 W	800 W
Platen Power	10 W	20 W	20 W
Flow	O_2 40 sccm	SF_6 30 sccm C_4F_8 60 sccm Ar 10 sccm	O_2 50 sccm
Pressure	4 mT	8 mT	20 mT
BIAS	35 V	95 V	45 V
Time	15 sec.	1 min. 50 sec.	5 min.

Table 3.4: *ICP parameters for pattern transfer dry etching process with fluorine based plasma.*

- The final step in the stamp preparation consisted of applying a low surface energy coating (anti-sticking layer) to reduce the stamp's surface energy promoting the demoulding of the stamp from the sample without pattern damage. In fact, a critical issue in nanoimprint lithography is the separation of the stamp from the imprinted polymer because of the adhesive force between the two surfaces; the high density of nanoscale structures on stamp surface increases the total area of contact, leading to stronger adhesion.

  The anti-adhesive coating has to be chemically inert and hydrophobic, but at the same time it has to allow the filling of the mould cavities when the polymer is in its viscous state. Trichlorosilanes with different carbon chain lengths are commonly used thanks to their property of forming self-assembled monolayers with very low surface energy, and for being rather inert and stable and highly resistant against temperature and pressure cycle. They support multiple long embossing sequences with temperature cycles to ~200 ^{o}C.

  The low surface energy layer on stamp surfaces improves imprint qualities and also it increases the stamp lifetime significantly by preventing or reducing surface contamination. The antisticking layer was formed on prepared stamp for NEAs (after O_2 plasma treatment that leads to the formation of -OH groups on its surface), by deposition of trichloro(octadecyl)silane in vapour phase, i.e. by applying a moderate vacuum of a few mbar in a vacuum chamber containing a drop of silane solution.

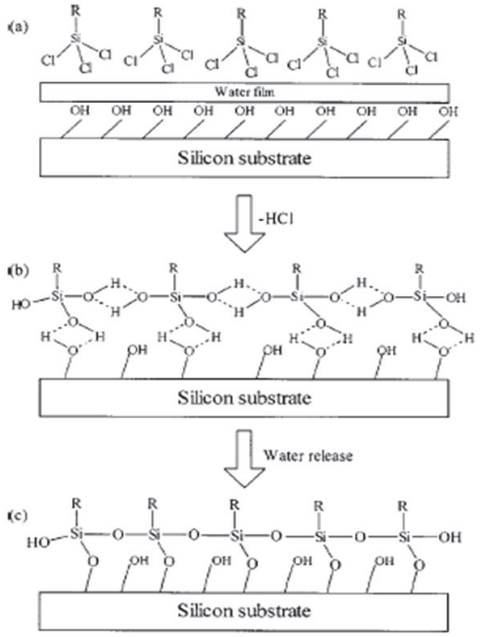

Fig. 3.3: *Reaction between the silane head group and the silicon surface.*

Using the obtained mould, NEAs have been fabricated by Nanoimprint Lithography using the parameters reported in table 3.5.

After the imprinting, the samples were treated with were treated with oxygen plasma (see table 3.2) in order to remove the residual layer from the bottom of nanoelectrodes. A SEM image of imprinted NEA is reported in figure

Substrate	GC plate
Resist	PC 4% @ 2000 rpm
Bake	180°C for 30 min.
Thickness	220 nm
Imprinting Temp.	180°C
Pressure	10 MPa
Time	8 min.
Release Temp.	80°C

Table 3.5: *Nanoimprint Lithography Parameters for NEAs fabrication.*

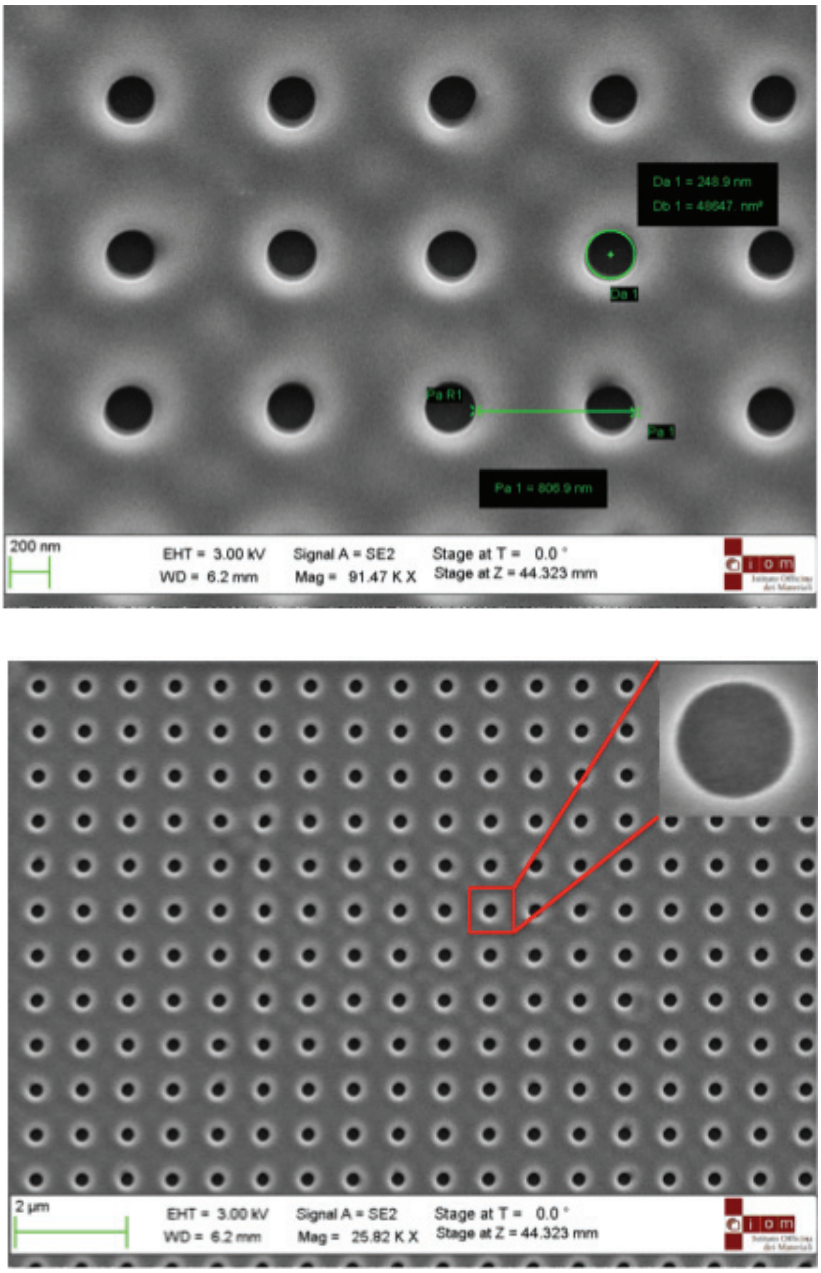

Fig. 3.4: *SEM images of nanoelectrode array pattern on PC deposited on BDD obtained by NIL.*

3.2.1 Electrochemical characterization

Electrochemical measurements on NEAs were carried out at room temperature in a three-electrode cell with a platinum coil counter electrode and an Ag/AgCl (KCl satured) reference electrode, connected to a Palmsens potentiostat, using Methylene Blue as reversible redox probe and PBS 0.01M as supporting electrolyte.

Cyclic Voltammograms in figure 3.5 demonstrate that the NEAs are electroactive and no residuals of PC are present on the surface of the electrodes, while its peak-shape, indicates that under these conditions the diffusion regime is total overlapping. Note that the current obtained from NEA manufactured by NIL is higher compared to the one measured from NEA fabricated with EBL. This fact is due simply to the fact that by NIL the entire PC surface was patterned and the electrode area was restricted subsequently to a disk of 3 mm in diameter, while NEA manufactured with EBL were patterned with nanolelectrodes only in a square field of 300 µm.

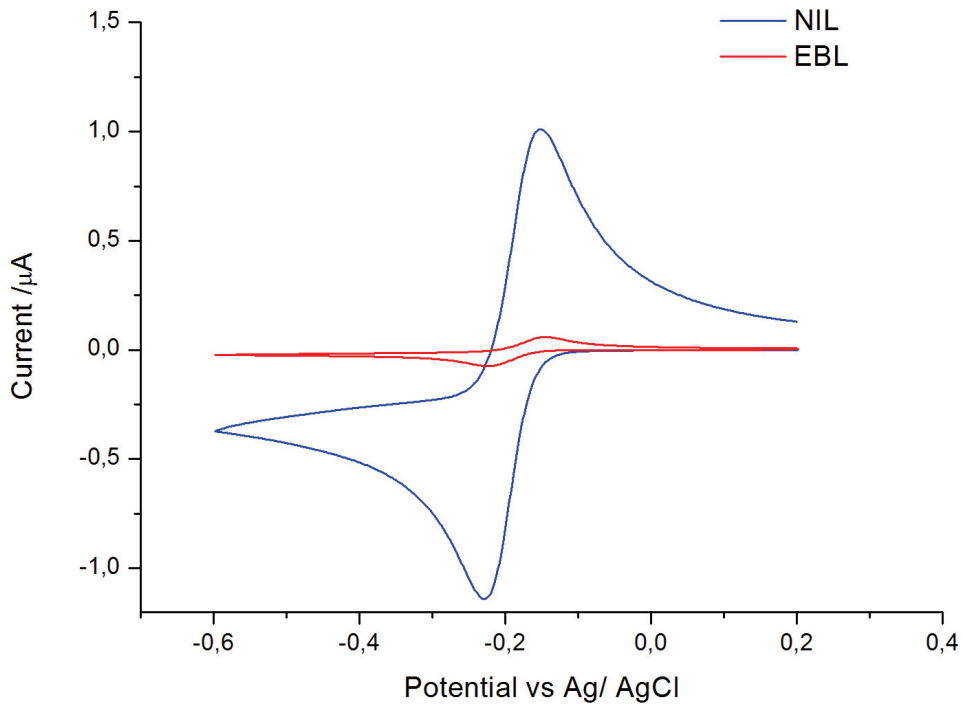

Fig 3.5: *Cyclic voltammograms recorded in 0.1 mM MB of the bare NEA fabricated by Nanoimprint Lithography with GC macroelectrodes. Scan rate 50 mV/s, supporting electrolyte 0.01 mM PBS, pH 7.2.*

In conclusion, the developed processes for the fabrication of NEAs have reached a stage in which they can be manufactured reliably and reproducibly. Therefore, this process might be object of further industrial development towards some market applications.

Surface Functionalization

4.1 Functionalization of PC surface of NEAs

4.1.1 Functionalization with DNA probes

Carboxylic groups present on the surface of PC as terminal were exploited for the immobilization of the single-stranded DNA strands (HPV 16) using a carbodiimide/succinimide strategy (Fig. 4.1). EDC reacts with carboxylic acid groups to form an active O-acylisourea intermediate that is easily displaced by nucleophilic attack from primary amino groups in the reaction mixture. The primary amine forms an amide bond with the original carboxyl group, and an EDC by-product is released as a soluble urea derivative. Since O-acylisourea intermediate is unstable in aqueous solutions, the addition of the succinimide derivative stabilizes the intermediate ester obtained by reaction between EDC and carboxylate groups, thus increasing the efficiency of the coupling reaction with the amino-ssDNA[1].

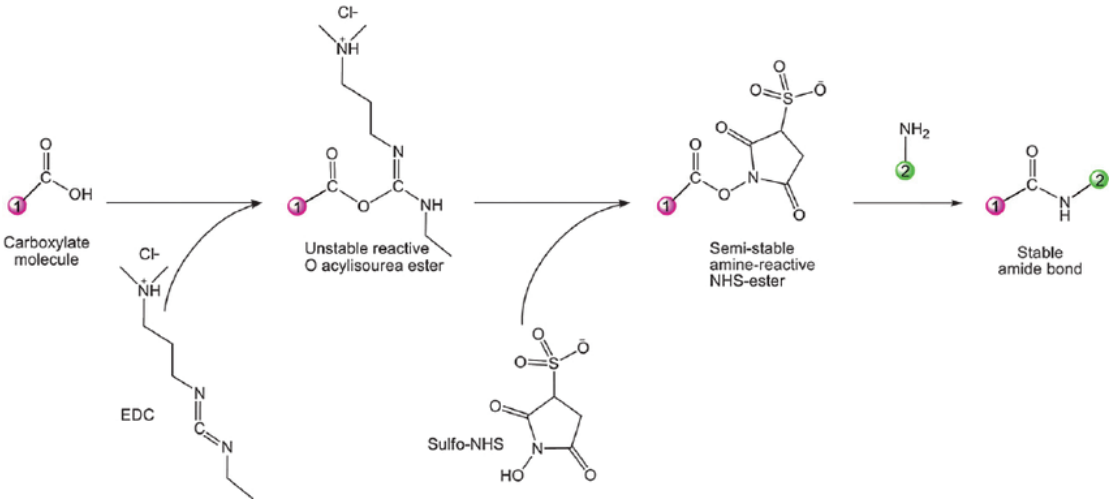

Fig. 4.1: *Reaction scheme for the -COOH surface groups chemical activation.*

Before proceeding with the immobilization of the oligonucleotide probes, the carboxylic groups are activated by immersion of NEAs into a 0.1 M HEPES buffer solution (pH 7.5) containing 2 mM EDC [N-ethyl-N'-(3-dimethylaminopropyl) carbodiimide hydrochloride] and 0.75 mM sulfo-NHS [N-hydroxysulfosuccinimide sodium salt]. The samples are incubated for 1 hour under shaking (at RT). The functionalization is done transferring the electrodes into a 0.1 M HEPES buffer

solution (pH 7.5) containing 250 pmol of HPV-16 (*Human Papilloma Virus 16*) strands and incubating the system for 2 h at 37° C.

Papillomaviruses are small, non-enveloped, double-stranded DNA viruses that infect mucosal and cutaneous epithelia in a wide variety of higher vertebrates in a species-specific manner and induce cellular proliferation.[2] Over 120 human papillomaviruses (HPVs) types have been identified and are referred to by number, some types (HPV-16, 18, 31, 45) can lead to cancers of genitals.[3]

In order to deactivate unreacted carboxylic groups, a blocking treatment is performed, immersing the electrode in ethanolamine 20 mM in 0.01 M PBS solution (pH 7.4) for 30 min at RT, under shaking. Ethanolamine is used to deactivate the remaining NHS-activated carboxylic groups onto the polymeric membrane. After the blocking step with ethanolamine, the NEAs are washed with PBS buffer. The specific DNA probe molecule is then linked to the surface. 10 µL of 2.5 pmol/µL HPV-16 complementary target solution biotin modified (in HYB-1 solution) were spotted on the capture DNA surface. The system is then covered and incubated for 1 hour at 42°C.

The detection scheme chosen for electrochemical detection of hybridization (Fig. 4.2) is based on enzymatic labels. As reported in the picture, in addition to an immobilized enzyme, this type of scheme involves the presence of its substrate and a mediator that promotes electron transfer between the active site of the protein and the electrodic surface.

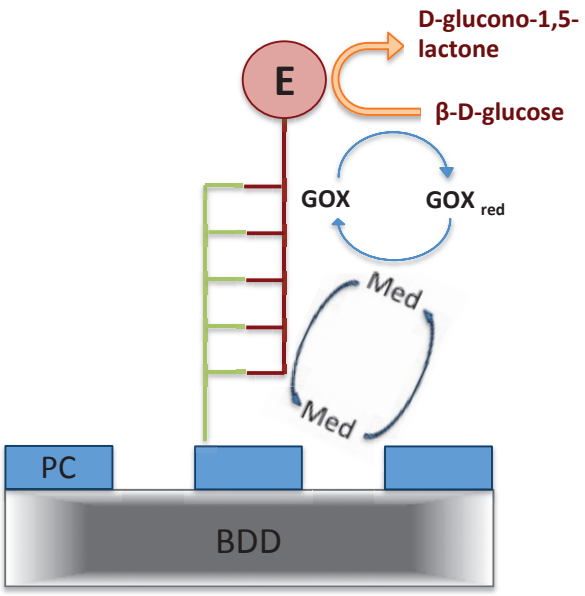

Fig. 4.2: *Schematic picture of enzymatic detection of DNA hybridization.*

In the specific case, glucose oxidase was used, with glucose and (ferrocenylmethyl)trimethylammonium hexafluorophosphate ($FA^+PF_6^-$) as mediator. The resulting dsDNA-modified NEAs were rinsed five times in 0.01 M PBS and after that 10 µL of 2.5 pmol/µL avidine-GOx solution was spotted on the surface and incubated for 2 h at room temperature.

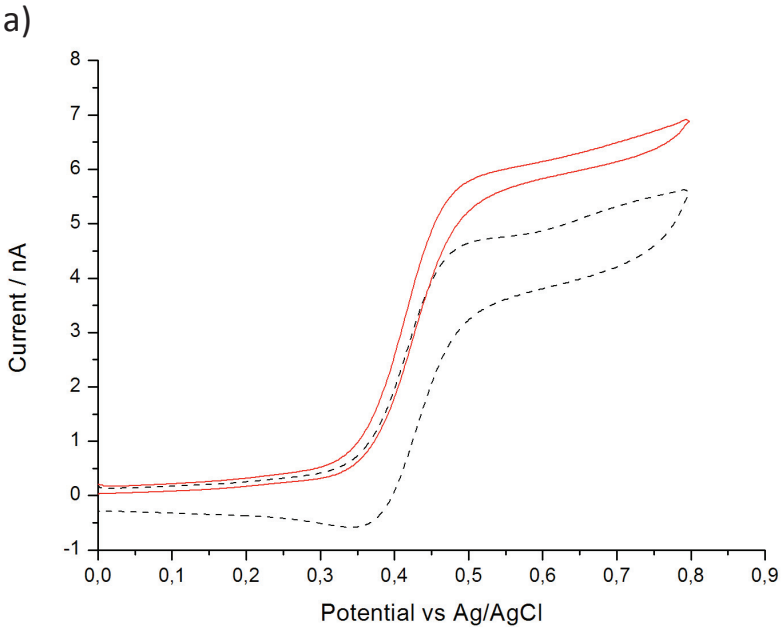

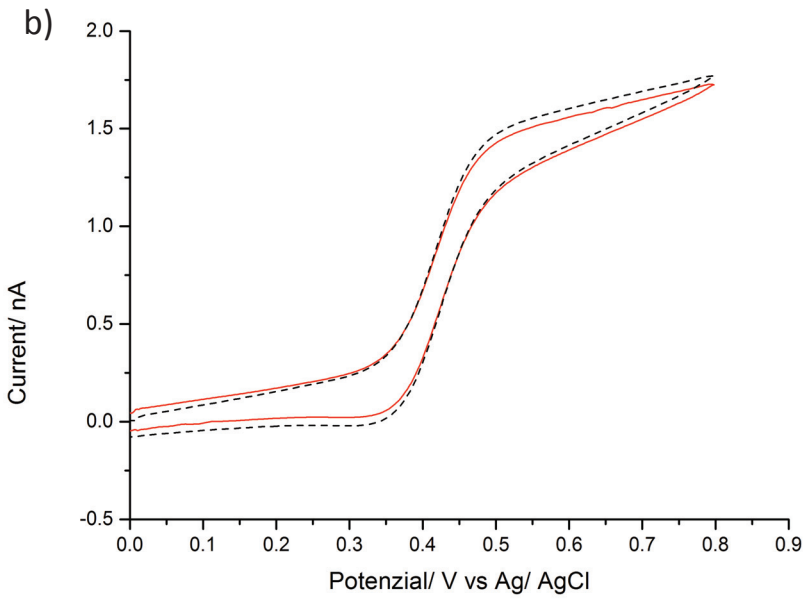

***Fig 4.3**: Cyclic voltammograms of **(a)** the DNA sensor **(b)** the DNA sensor hybridized with a step with Gliadin (negative control) CVs recorded in 10^{-4} M $FA^+PF_6^-$ dissolved in PBS 0.01 M before (dashed curve) and after (red curve) the addiction of 50mM glucose solution (scan rate 10 mV/s in deaerate solution).*

The voltamograms reported in figure 4.3 show the behaviour of the NEA functionalized with HPV-16 fragment and hybridized with its complementary target (Positive control, Fig. 4.3a) or with a random non-complementary target (negative control, Fig. 4.3b) both labeled with Biotin. In the positive control, after the addition of 50 mM glucose, the oxidation peak slightly increases while the reduction peak almost disappears while no changes occurs in the negative control. In fact, in the presence of both the enzyme and the enzymatic substrate, the mediator is chemically reduced at the electrode/solution interface by reaction with the enzyme to be oxidized again directly at the electrode surface. The above described voltammetric evidences show a change in the catalytic current even if the signal obtained is weaker than that expected. However, the negative control doesn't show any catalytic current variation, therefore it can be deduced that the functionalization with HPV-16 fragment sequences and the subsequent hybridization with specific complementary sequences, has been successful.

4.1.2 Functionalization with Gliadin Protein Fragments

Gliadin is a class of proteins that represent the soluble component of gluten, present in wheat and several other cereals and is the main cause of the autoimmune reaction that occur in coeliac patients. Since the only method to treat coeliac disease known until now is a life long gluten-free diet[4], it is essential to have a device easy to use, reliable, inexpensive and fast for Gliadin detection and control in gluten free foods.

NEAs have been functionalized by dropping on the active area of the NEA 10 µl of 10 µg/ml Gliadin fragments (Abcam®) in 0.01M Phosphate Buffer (pH 7.2) and incubating for 2 h at 25°C. Figure 4.4 shows the active area of the sensor with Gliadin fragments immobilized on it. Images were taken by Atomic Force Microscopy.

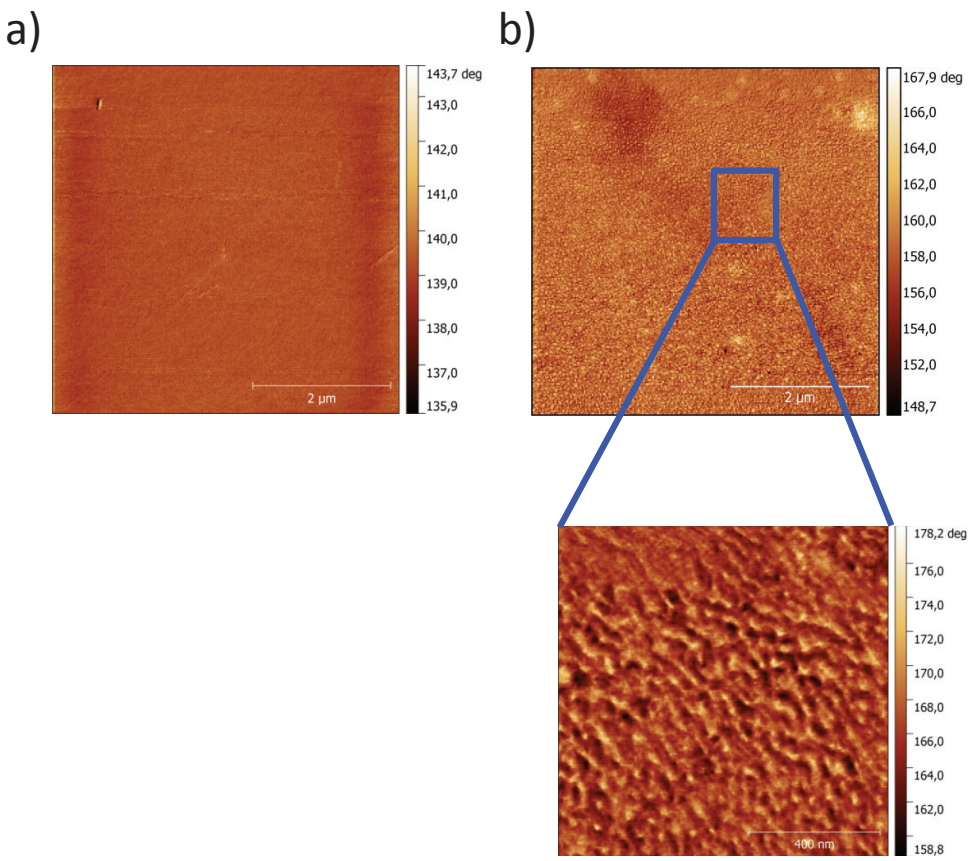

Fig 4.4: *Atomic Force Microscopy images of (a) bare PC surface (b) PC surface functionalized with Gliadin;*

Prior to the immobilization of the antigen probes on the polycarbonate surface, NEAs were treated with a 5M NaOH solution and then rinsed with milliQ water. We found this step essential to the activation of the PC surface of NEAs and efficient functionalization with Gliadin proteins. In fact, according to the chemical literature NaOH treatment leads to the deprotonation of hydroxyl and carboxylic groups, making the surface more hydrophilic (Fig. 4.5)

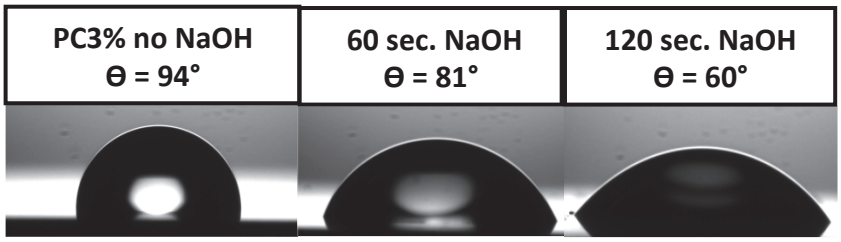

Fig. 4.5: *Water contact angles pictures recorded with a Krüss GmbH instrument.*

The functionalized NEA was incubated with 10 µL of 10 µg/ml solution of anti-Gliadin in 0.01 PBS (pH 7.2) at 25°C for 60 min. The NEA was subsequently blocked with 1% BSA for 30 min and then the captured primary antibody was coupled with 10 µL of 10 µg/ml solution of Goat anti-mouse IgG secondary antibody for 60 min at 25°C.

All incubations were followed by a thorough rinsing in buffer solution in all procedures, wet filter paper was introduced in the incubation container to keep a humid environment.

Cyclic voltammograms were recorded between + 0.2 V and - 0.6 V in a solution of methylene blue 0.1 mM in PBS 0.01 M. The mediator shuttle the electrons between the surface of each nanoelectrodes and the enzyme (HRP) at the end of the biomolecules chains resulting from the sequence biorecognition events and anchored to the dielectric surface surrounding the nanoelectrodes. HRP is reduced by the mediator and oxidized by H_2O_2 (Fig. 4.6).

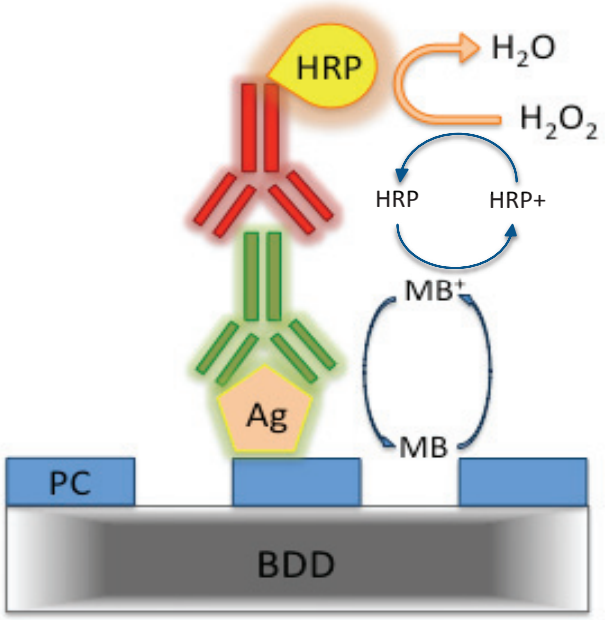

Fig. 4.6: *Scheme of the NEA immunosensor: the PC surface is exploited to immobilize the capture protein, Gliadin. The assay is performed by incubating it with a sample containing the target (i.e. anti-Gliadin antibody) and with a secondary antibody labeled with HRP enzyme;*

In order to determine the right amount of the substrate for the enzyme, we assessed the behaviour of the sensor after the sequence of bio-recognition events before and after adding different concentration (*5 μM - 19 μM*) of the specific substrate H_2O_2 (Fig. 4.7).

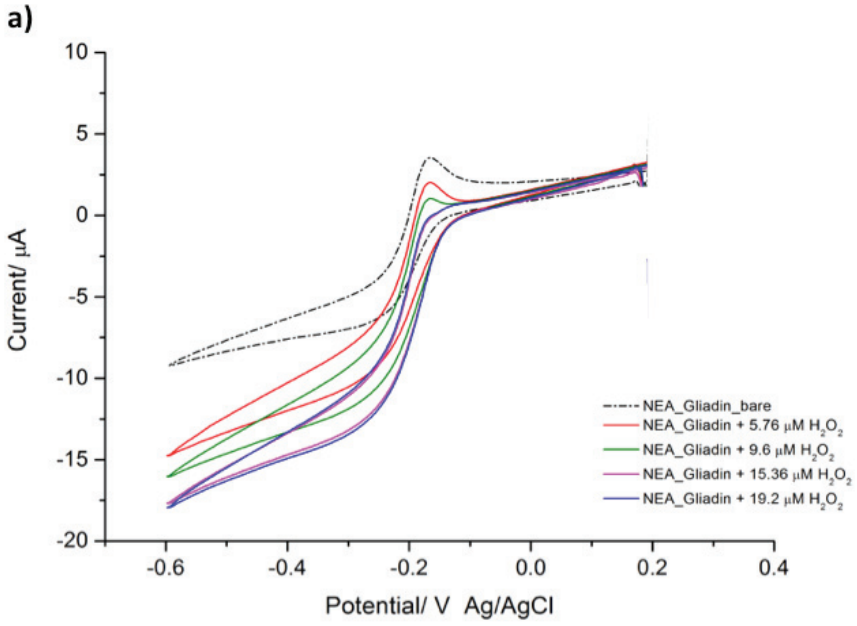

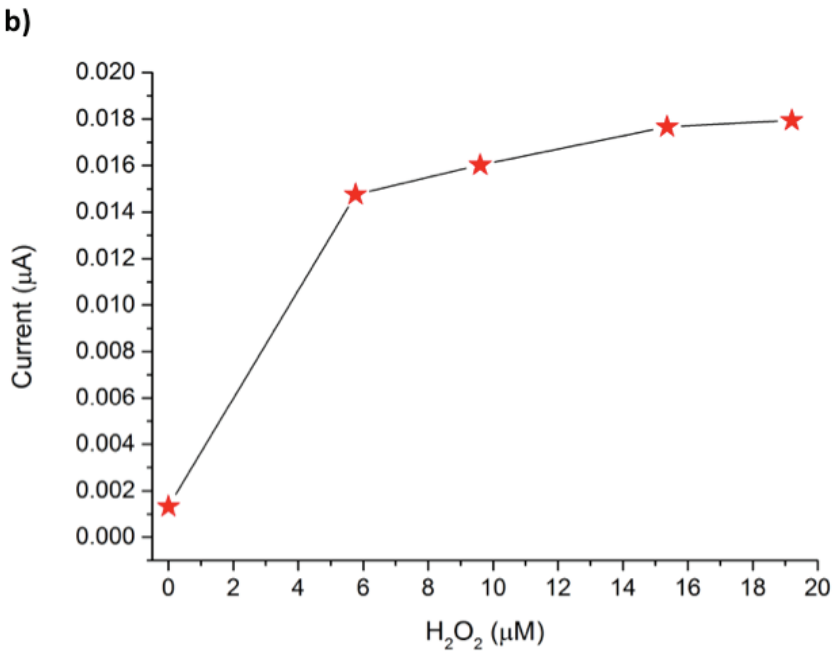

***Fig 4.7**: **a)** Cyclic voltammograms of the immunosensor in the presence of different concentration of H_2O_2 (5 μM - 19 μM) and **b)** anodic peak current as function of H_2O_2 concentration both recorded in 0.1 mM MB. Scan rate 50 mV/s, supporting electrolyte 0.01 mM PBS, pH 7.2,*

Figure 4.7 shows the cyclic voltammograms recorded at 50 mV/s with a NEA functionalized with Gliadin in 0.01M PBS, pH 7.2, containing 0.1 mM Methylene Blue, in the absence (dashed line) and presence (full lines) of different concentrations of H_2O_2 substrate added to the electrolyte.

After adding the substrate to the solution, an evident change in the voltammetric pattern is detected at the functionalized NEA: the reduction peak of the mediator Methylene Blue increases while the reoxidation peak almost disappears indicating the effective immobilization of Gliadin on the PC of the NEA and subsequent reactions with primary and secondary antibodies (Fig. 4.8a).

To observe absence of nonspecific adsorption of the primary and secondary antibodies on the PC surface, the procedure was repeated without the functionalization step with Gliadin but with the incubation with the primary and secondary antibodies. It is worth pointing out that, no catalytic current was observed after addition of 1.2 mM H_2O_2 (Fig. 4.8b) suggesting that there are not non-specific bonds between the activated surface of the PC and the antibodies.

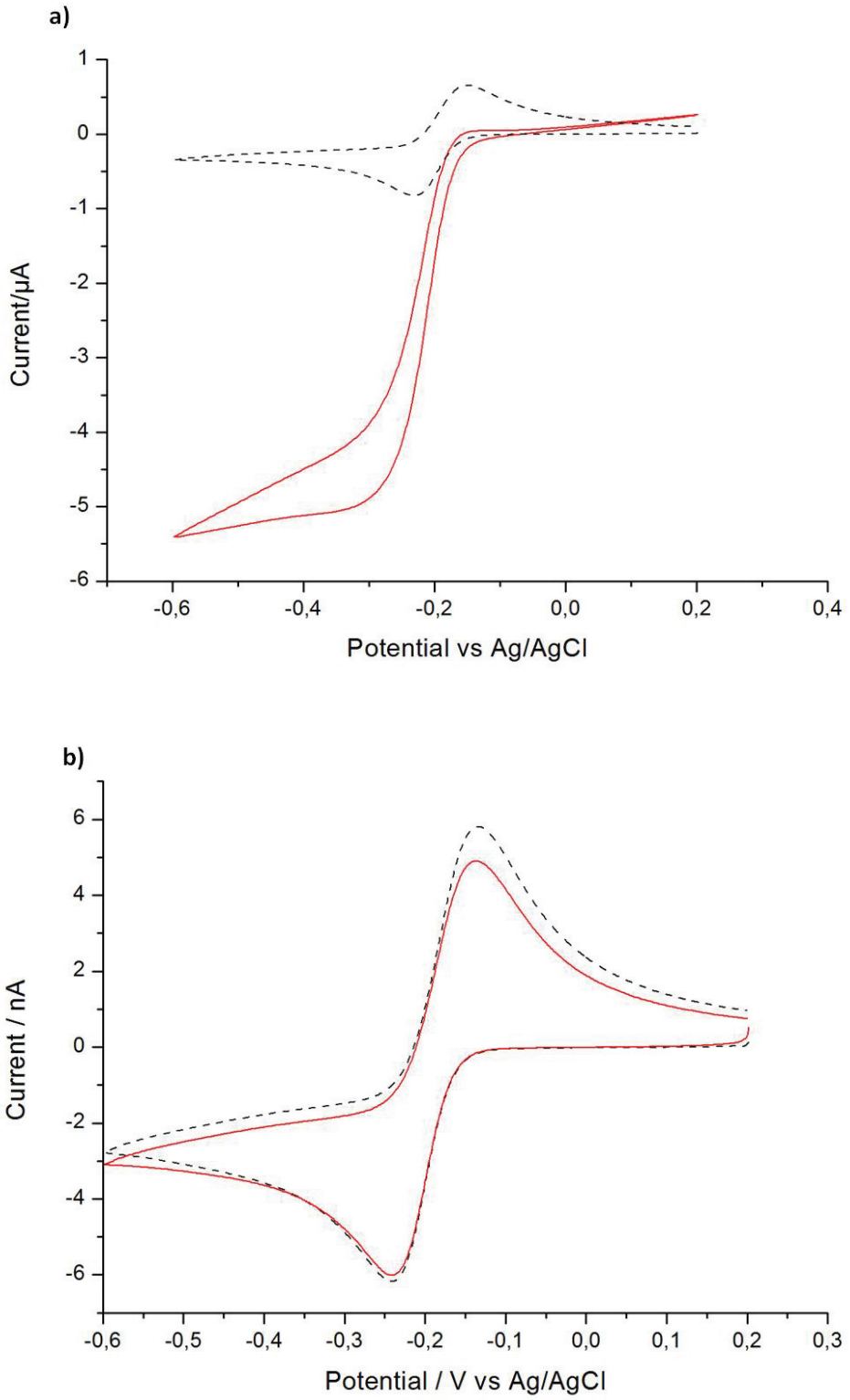

Fig 4.8: *Cyclic voltammograms of* ***(a)*** *the immunosensor* ***(b)*** *the immunosensor without the incubation step with Gliadin (negative control) both recorded in the absence (dashed line) and presence of H_2O_2 1.2 mM. Scan rate 50 mV/s, supporting electrolyte 0.01 mM PBS, pH 7.2.*

Cyclic voltammograms were recorded on the same NEA immunosensors with the previous condition, in the absence and presence of H_2O_2 after 24h and 1 week from the fuctionalization. The sensor was stored at 8°C during the time between the functionalization and voltammetric measurements.

Figure 4.9 shows that the voltammetric signal decrease as a function of time but it is still detectable after 1 week from the functionalization, corroborating the strategy used for the functionalization of the PC surfaces of the NEA.

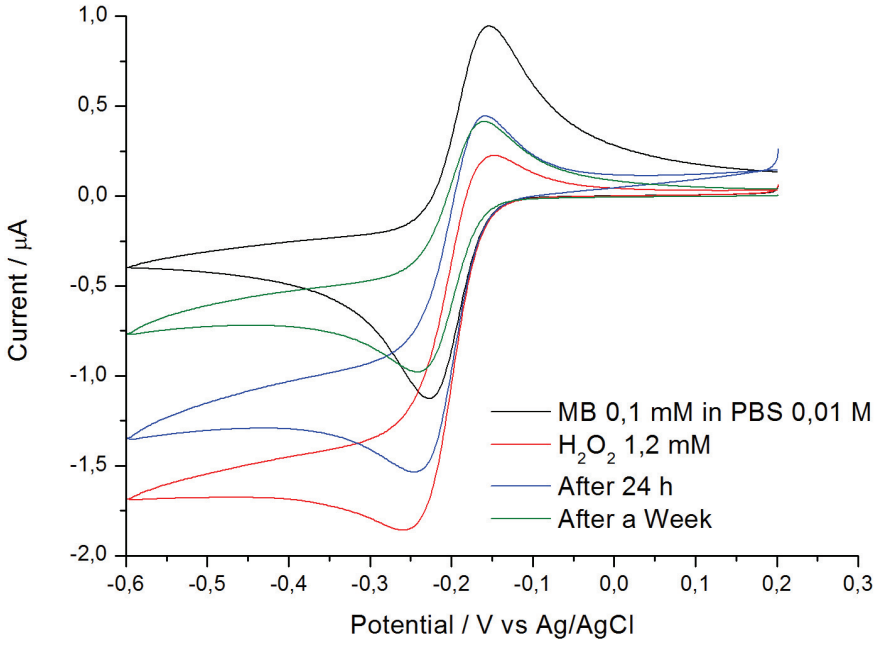

***Fig 4.9**: Cyclic voltammograms of the immunosensor recorded in 0.1 mM MB in the presence of 1.2 mM H_2O_2 (red curve) after 24h (blue curve) and after 1 week (green curve) from the fuctionalization. Scan rate 50 mV/s, supporting electrolyte 0.01 mM PBS, pH 7.2.*

In addition, decreasing concentrations of Gliadin (1-3-10 µl) were tested (Fig. 4.10) obtaining a good signal with concetration of Gliadin of 0.1 nM.

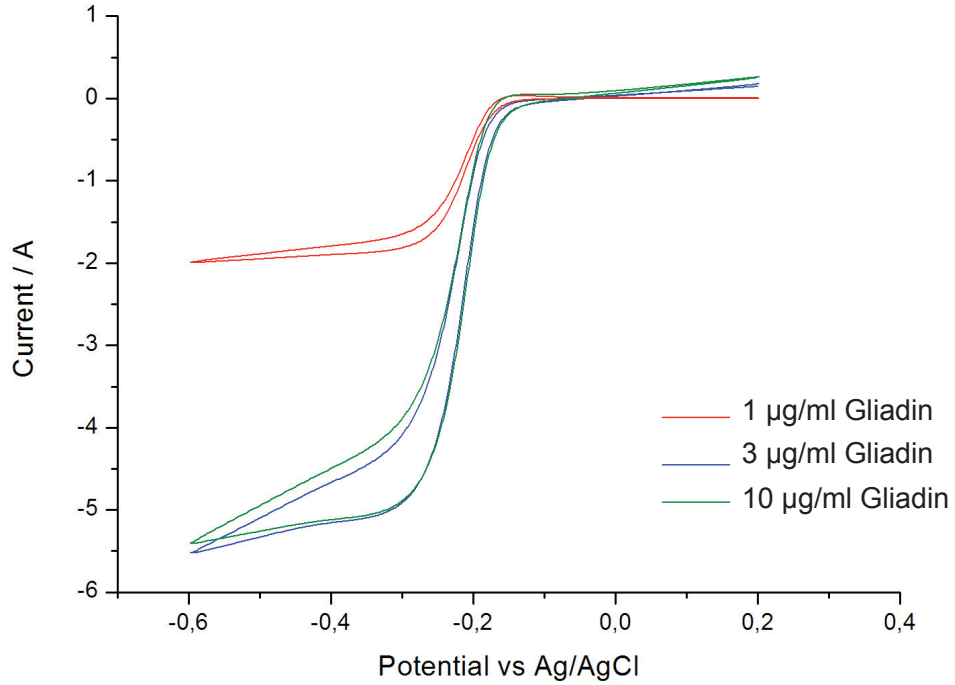

Fig 4.10: *Cyclic voltammograms of the immunosensor recorded in 0.1 mM MB in the absence and presence of decreasing concentrations of Gliadin (1,3,10 µg/ml). Scan rate 50 mV/s, supporting electrolyte 0.01 M PBS (pH 7.2).*

4.1.3 Functionalization with Tumor Necrosis Factor

This project is part of a collaboration with the Department of Pharmacogenetic (University of Trieste) aimed at finding new strategies for diagnostic, therapeutic and clinical care in Infectious and immunological diseases. Anti-tumor necrosis factor (TNF) agents, in particular infliximab, have become the mainstay of treatment in refractory inflammatory bowel diseases (IBD), also in pediatric patients. Currently, there are no clinical, pharmacological, or molecular predictors of response to anti-TNF therapy available for translation in clinical practice. In fact, different response to therapy could be influenced by several factors interacting at different levels.[5]

There is some evidence suggesting that the loss of response in patients treated with infliximab may be in part the result of failure to achieve and maintain adequate drug levels in blood and/or of the formation anti-infliximab antibodies (AIA). Strategies integrating clinical, pharmacokinetic, pharmacodynamics and pharmacogenomic information in pediatric IBD could lead to identification of subsets of patients with a

higher probability of response and to personalization of anti-TNF treatment, resulting in more cost-effective therapies.

In this project, we wanted to evaluate the association between infliximab pharmacokinetics (i.e, concentration of infliximab and AIA) and clinical response to infliximab therapy in pediatric IBD patients by measuring infliximab pharmacokinetics with our NEAs. For this purpose, the biosensor surfaces has been functionalized with TNF-α, based on the method already optimazed for Gliadin Protein Fragment (Chapter 4.1.2), or with infliximab antibodies optimizing a new strategy based on the use of Protein G. Protein G, which is found in the cell wall of Streptococcus human pathogenic strains of the Lancefield group G, binds to the Fc portion of many IgG subclasses, leaving the antigen-specific sites free.[6] In the scheme 4.11, the Fc receptor is the key element for the oriented immobilization of the IgG antibody.

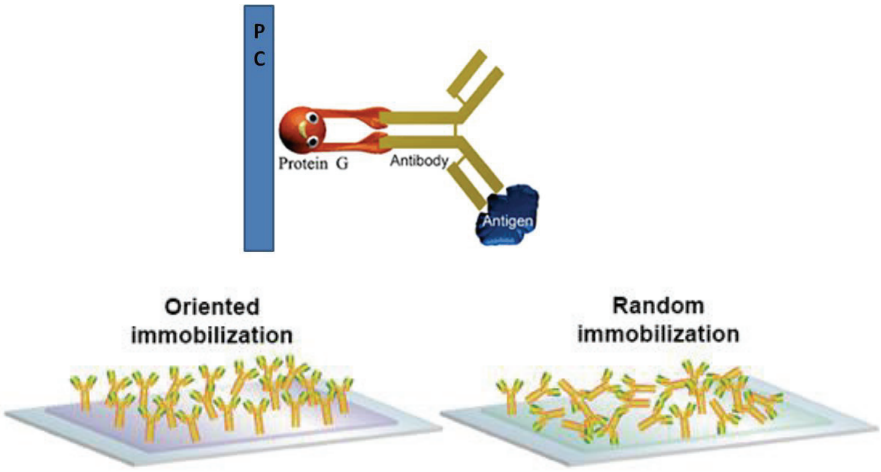

Fig. 4.11: *Protein G binding to antibody and scheme of the different types of immobilization of antibodies: on Protein G layer or without Protein G;*

In figure 4.12 are presented the preliminary results obtained from the functionalization of the PC surfaces of our NEAs with recombinant Human Tumor Necrosis Factor-α (TNF-α) wich is then detected with INFX antibodies labelled with Fluorescein isothiocyanate (FITC). To exclude the presence of aspecific absorption of

INFX-FITC, negative control experiments were performed, using the same protocol of functionalization but without immobilization of TNF-α.

Images Obatined with Nikon inverted confocal microscope TE-2000U equipped with an HBO 103 W/2 Hg short arc lamp as illumination source and reflected light filters for blue to green and red.

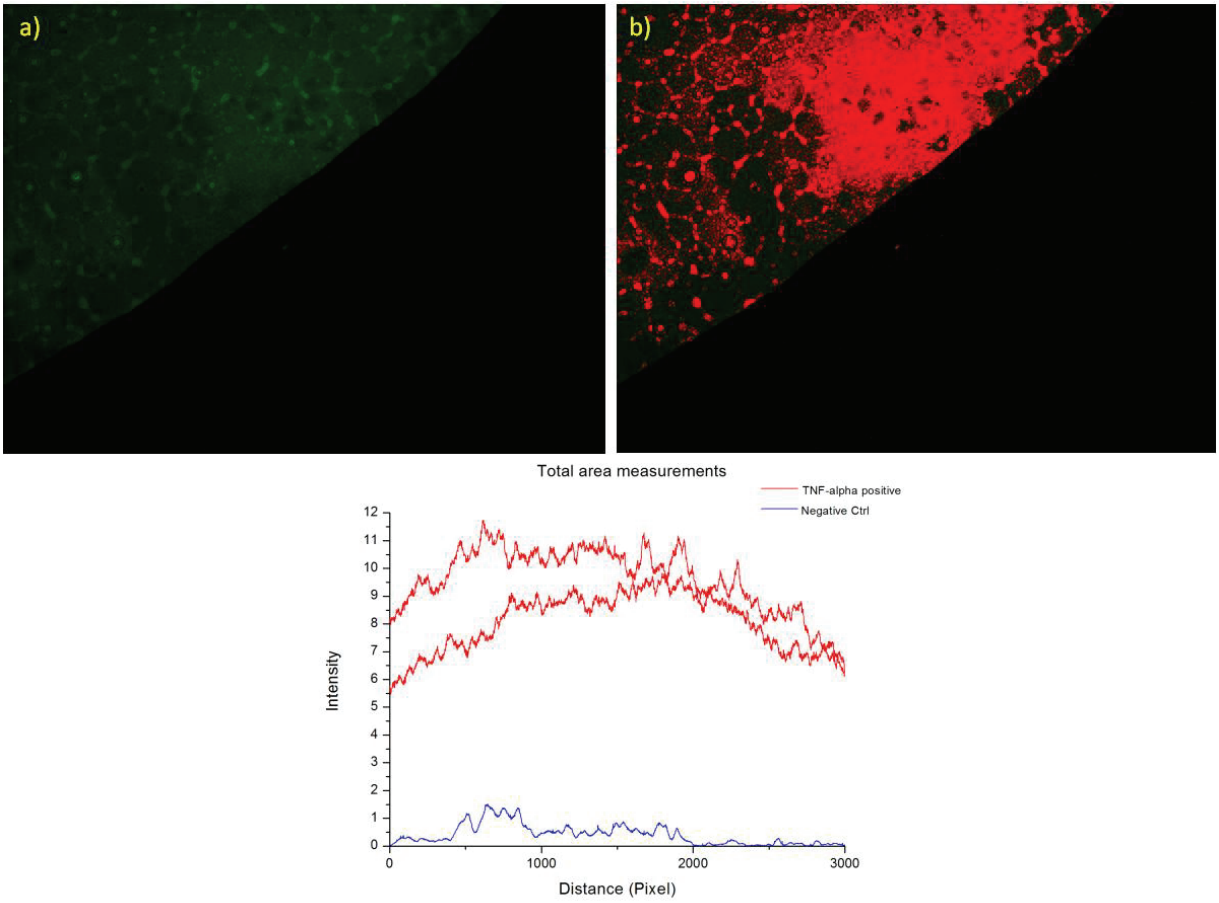

Fig 4.12: *Images of NEAs surfaces functionalized with TNF-α and INFX- FITC* ***a)*** *natural FITC fluorescence and* ***b)*** *red modified intensity by ImageJ. Below, the total area intesity Plot;*

From image 4.12 fluorescence it is easily noticed in correspondence of the active area of the sensor in which TNF molecules were immobilized, while outside the active area no fluorescence is noticed.

The plot shown in figure 4.12 refers to the comparison between the intensity measurements relating to the functionalized area and the negative control. We observe a clear difference in the intensity between the two different samples, indicating that there is not aspecific adsorpion of INFX-FITC on the PC surface of our

NEAs; note that the measurements were carried out in the same portion of the sensors.

As explained above, we took advantage of this project to optimize a strategy to functionalize the polycarbonate surface with antibodies using Protein G. To this aim, protein G has been immobilized on our sensors using the protocol optimized for Gliadin protein fragments and subsequently, 10µl of INFX (10µl/ml in PBS) was poured in the active area of our NEAs. In order to verify the correct immobilization, TNF-α labelled with FITC (10µl/ml in PBS) was dropped in the active area of the sensor. To exclude the presence of aspecific interaction between TNF-α and Protein G or policarbonate surfaces, negative control experiments were performed, using the same protocol of functionalization but without INFX. (Fig. 4.13)

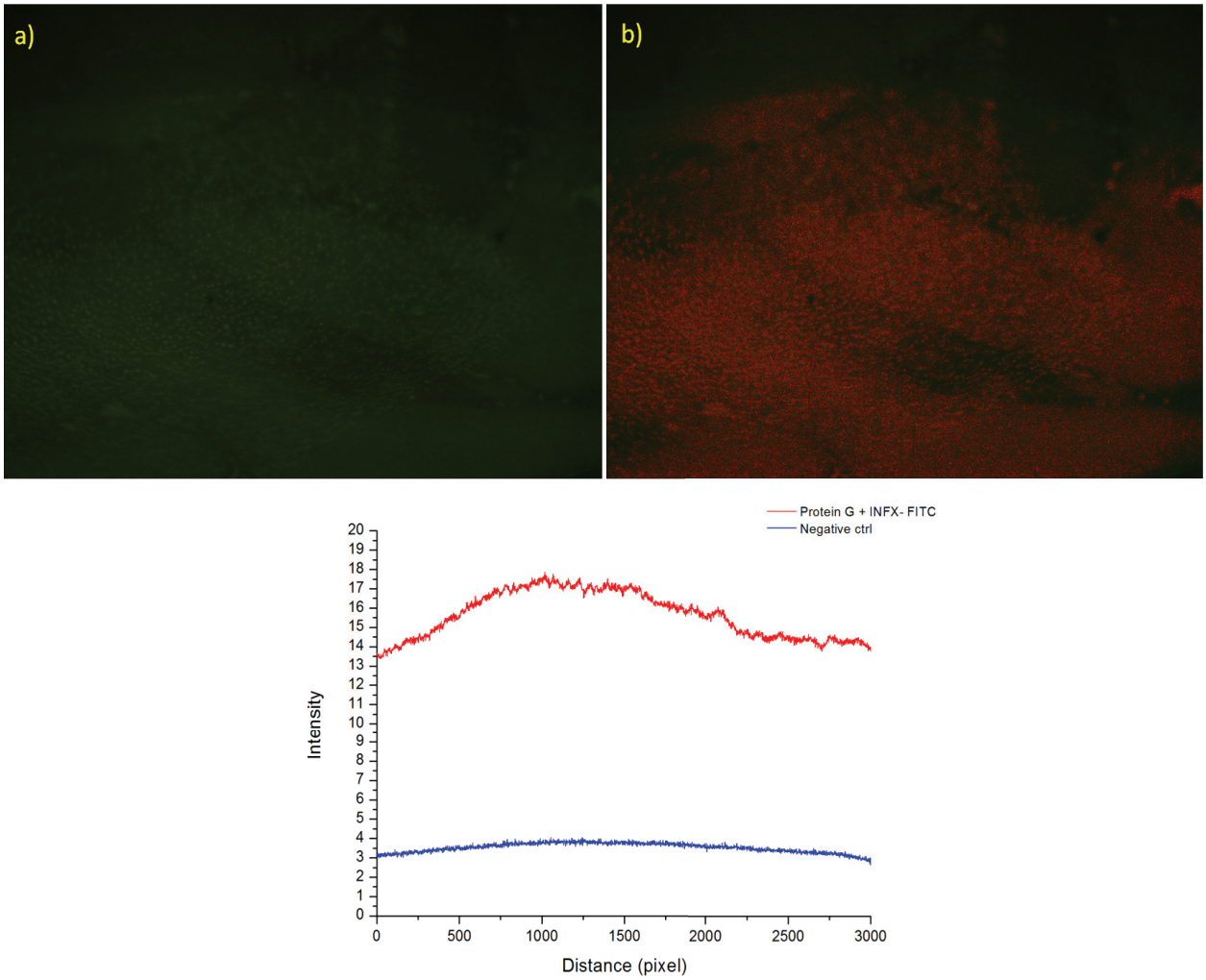

Fig 4.13: *Images of the NEAs surfaces functionalized with Protein G and INFX- FITC* ***a)*** *natural FITC fluorescence and* ***b)*** *red modified intensity by ImageJ. Below, the total area intesity Plot;*

Also in this case, it is still noticed a fluorescence in correspondence of the active area of the sensor functionalized with molecules, while outside the active area no fluorescence is noticed. From the plot it can be seen that in the negative control, a background signal is present, probably due to a non-specific fluorescence emitted by the Protein G. Further experiments will be done in order to clarify this aspect.

To summarize, the problems previously encountered in the hybridization of DNA sequences with complementary sequences produced by PCR were resolved using DNA sequences exactly complementary to the probes. Further investigations will be conducted to optimize the hybridization with sequences produced by PCR. Furthermore, we optimased the protocol and successfully immobilized proteic probes such as Gliadin protein fragment and TNF-α on the PC surface of our NEA and we used both an enzymatic and fluorescent scheme for the detection. In conclusion, we began testing a new strategy for the immobilization of antibodies (INFX) on the surface of our sensors with promising results.

References:

1. Staros, J. V, Wright, R. W. & Swingle, D. M. Enhancement by N-Hydroxysulfosuccinimide of Water-Soluble Carboiimide-Mediated Coupling Reations. *Anal. Biochem.* **156,** 220–222 (1986).
2. Gillison, M. L., Chaturvedi, A. K., Anderson, W. F. & Fakhry, C. Epidemiology of Human Papillomavirus-Positive Head and Neck Squamous Cell Carcinoma. *J. Clin. Oncol.* **33,** 3235–42 (2015).
3. Mitchell RS, Kumar V, Abbas AK, F. N. in *Robbins Basic Pathology 8th Edition* 345 (2007).
4. Hill, I. D. *et al.* Guideline for the Diagnosis and Treatment of Celiac Disease in Children : Recommendations of the North American Society for Pediatric Gastroenterology, Hepatology and Nutrition. *J. Pediatr. Gastroenterol. Nutr.* 1–19 (2005). doi:10.1097/00005176-200501000-00001
5. Wang, S. L. *et al.* Development and validation of a homogeneous mobility shift assay for the measurement of infliximab and antibodies-to-infliximab levels in patient serum. *J. Immunol. Methods* **382,** 177–188 (2012).
6. Lu, B., Smyth, M. R. & O'Kennedy, R. Oriented immobilization of antibodies and its applications in immunoassays and immunosensors. *Analyst* **121,** 29R–32R (1996).

Electrochemiluminescence

5.1 Development of an immunosensor with ECL transduction scheme

The principle of a sensor for molecules detection exploiting ECL signal and based on arrays of nanoelectrodes is presented in figure 5.1. In the specific case of an immunosensor for Gliadin protein Fragment, the capturing agent is adsorbed onto the PC surface of a NEA in such a way to bind with anti-Gliadin antibodies after incubation with the latter. The biorecognition chain is continued by the reaction of a biotinylated secondary antibody with the captured anti-Gliadin. Finally, a streptavidin-$Ru(bpy)_3^{2+}$ derivative (SA-$Ru(bpy)_3^{2+}$) was used as ECL label. The ECL emission is triggered by addition of the co-reactant TPrA. Due to the customized architecture of the biosensor, oxidized TPrA acts both as co-reactant and redox mediator. The oxidized radicals generated at the electrodes, $TPrA^{\bullet+}$ and $TPrA^{\bullet}$, diffuse toward the PC area of the NEA, to provide an ECL signal by reaction with the non-diffusing ruthenium centers.

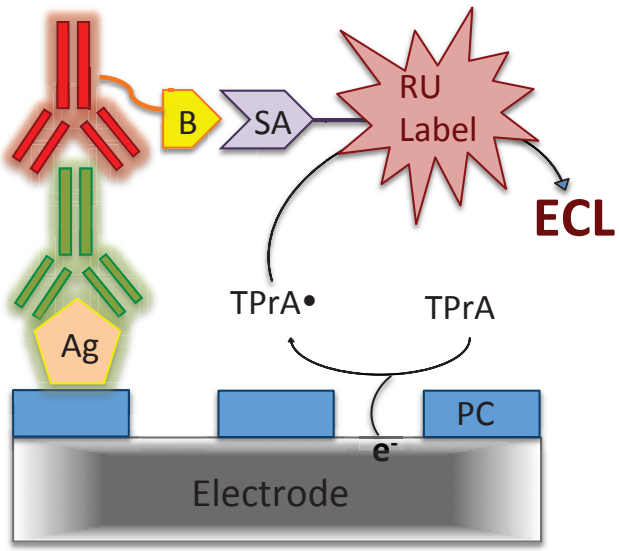

Fig. 5.1: *Scheme of the NEA immunosensor: the PC surface is exploited to immobilize the capture Antigen. The assay is performed by incubating it with a sample containing the target and with a secondary antibody labeled with HRP enzyme;*

5.1.1 Binding streptavidin to $Ru(bpy)_3^{+2}$

The complex streptavidin-$Ru(bpy)_3^{2+}$ (SA-Ru) was obtained as follows. 1 mg of streptavidin was dissolved in 1mL of Milli-Q water. Then 100 µL of this solution was added to 810 µL of water and 90 µL of 1x PBS pH 7.4 and mixed with 1 mg of Bis(2,2-bipyridine)-4-methyl-4-carboxybipyridine-ruthenium N-succinimidyl ester-bis(hexa-fluorophosphate), which was dissolved in 100 µL of dried DMSO. The mixture was kept at 4 °C under continuous stirring for 4h. Finally, it was purified by dialysis in PBS (1x) using Slide-A-Lyzer Dialysis Cassettes 10k molecular weight cut off from Thermo Scientific for about 16 h. The Ru-SA complex was stored at +4°C until used.

5.1.2 Voltammetric and ECL characterization of the immunosensor

All the electrochemical and ECL experiments were performed with an Autolab PGSTAT30 potentiostat, a Hamamatsu photomultiplier tube (PMT) equipped with KEITHLEY 6485 picoammeter and high voltage power supply Hamamatsu Photonics model C9525.

Electrochemical characterization was carried out in 1 mM solution of Ruthenium Hexamine $Ru(NH_3)_6$ dissolved in 0.1M KCl, as reversible redox probe (figure 5.2).

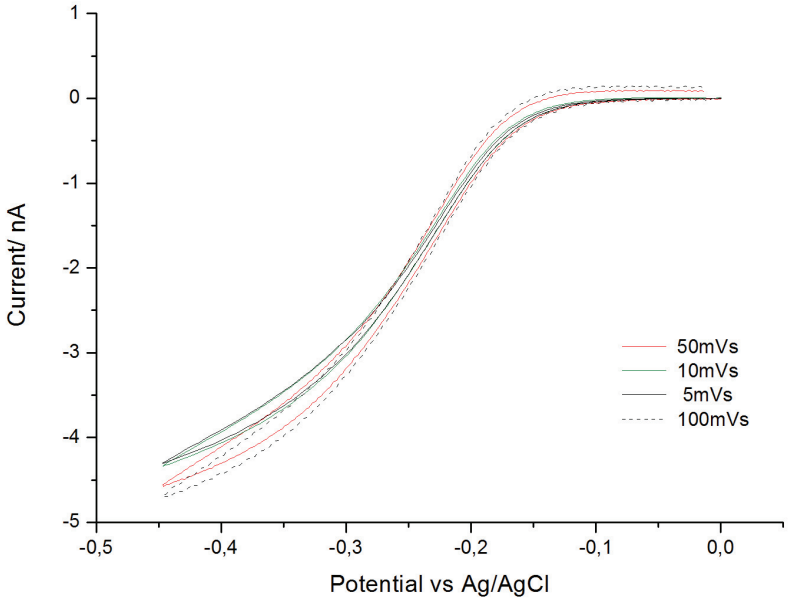

Fig 5.2: *Cyclic voltamograms recorded in 1 mM of $Ru(NH_3)_6$ at different scan rates (5-100 mV/s) with NEAs consisting of dots of 250 nm radius with 120 nm recession depths in a hexagonal array (d-d = 2 µm) on PC film obtained by Nanoimprint lithography.*

Cyclic voltamograms recorded with our NEA are sigmoidally shaped over the entire range of tested scan rates, indicating that they work in non-overlapping hemispherical diffusion regime: in fact, as explained in the section 1.3.1, in case of widely spaced array's elements (i.e. with a large d/r ratio), as in the case of the present NEAs, the volumes of the electrolyte from which the electroactive molecules have the chance to diffuse to the individual electrodes during the voltammetric scan are separated. Therefore, the signals measured by nanoelectrodes are independent from each other, and total current collected by all electrodes in the array is equivalent to that of an equal number of single electrodes connected in parallel.

In the case of partial or total overlapping diffusion spheres, after some time from the beginning of the scan the individual electrodes would start to "compete" for the molecules contained at the intersection of the diffusion spheres (which grow proportionally to the square root of time), leading to a partial reduction of the signal from each single electrode. Clearly, the non-overlap, partial overlap or total overlap regimes depend on both the inter-electrode distance and scan rate.

To evaluate the ability of NEA manufactured in Glassy carbon to properly oxidize the co-reactants used to generate the ECL signals, a set of experiments have been done with a bare NEAs only with 1mM $Ru(bpy)_3^{2+}$ dissolved in TPrA or DBAE co-reactant (Fig 5.3).

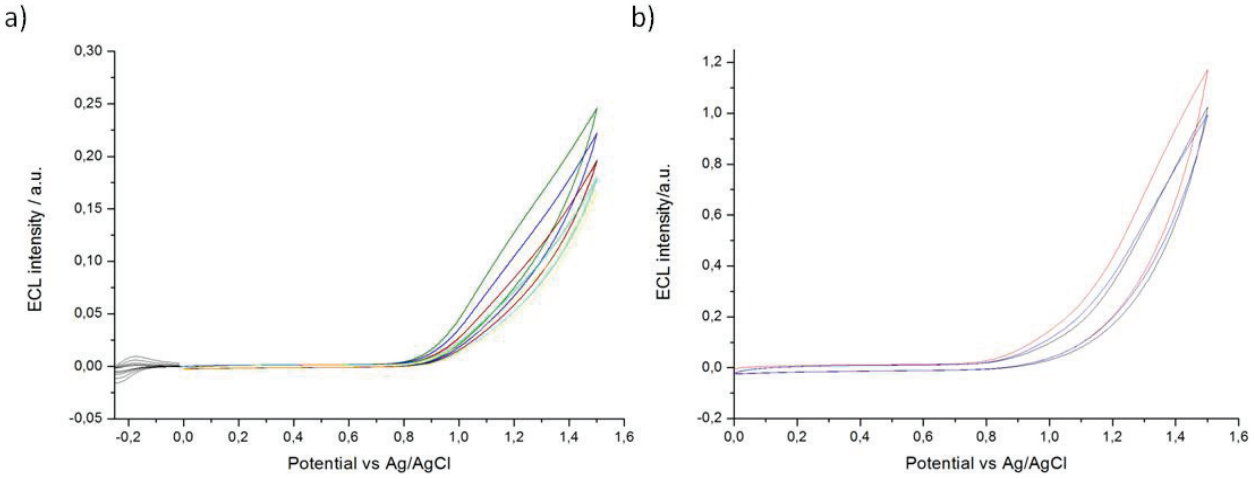

Fig 5.3: *ECL signals of bare NEA recorded in presence of 1mM of $Ru(bpy)_3^{2+}$ dissolved in* ***a)*** *100mM of TPrA and* ***b)*** *20 mM of DBAE. Scan rate 5-100 mV/s.*

Then, NEAs have been functionalized using the strategy described above. Briefly, NEAs were immersed in 5M NaOH aqueous solution for 60 seconds and then rinsed with milliQ water. The surface was spotted with 10 µl of 10 µg/ml Gliadin fragments (Abcam®) in 0.01M Phosphate Buffer (pH 7.2) and incubated for 2 hours at 37°C in order to immobilize the molecules by adsorption on the active area of the sensor. Next, the functionalized NEA was incubated with 10 µL of 10 µg/ml solution of anti-Gliadin in 0.01 PBS (pH 7.2) and subsequently blocked with 1% BSA. The captured primary antibody was then coupled with 10 µL of 10 µg/ml solution of Goat anti-mouse IgG secondary antibody labeled with Biotin.

Finally, the reporter Ru(bpy) complex was incorporated *via* biotin-streptavidin affinity binding for the detection and quantification of the analyte. After addition of TPrA to the electrolyte solution, the ECL response is obtained by scanning the potential between 0 and 1.6 V *vs* Ag/AgCl (scan rate of 100mV/s).

NEAs fabricated using different electrodes (Gold, BDD and GC) by Thermal Nanoimprint Technology, has been tested. Cyclic voltammograms and ECL curves of the different immunosensors are presented in figure 5.4.

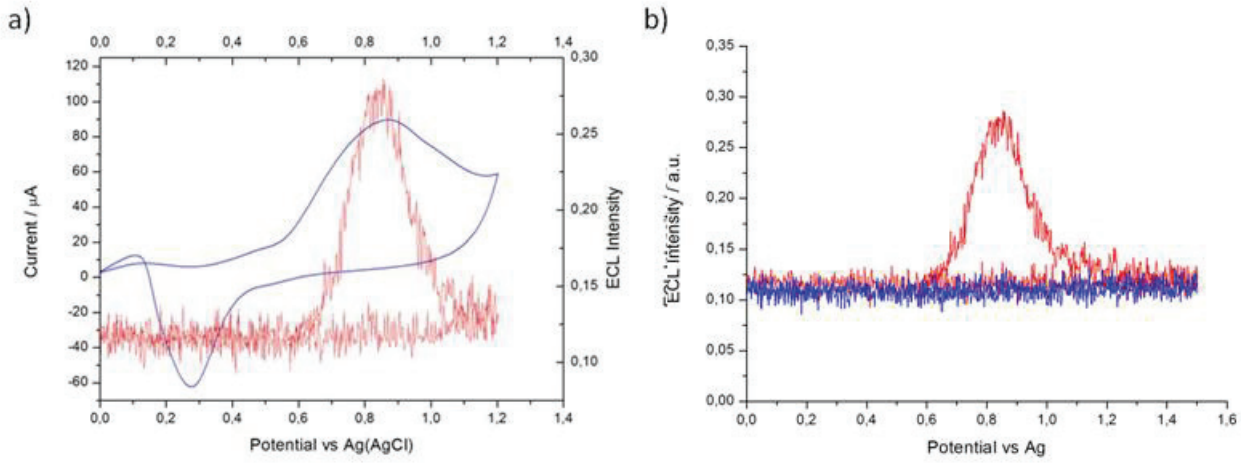

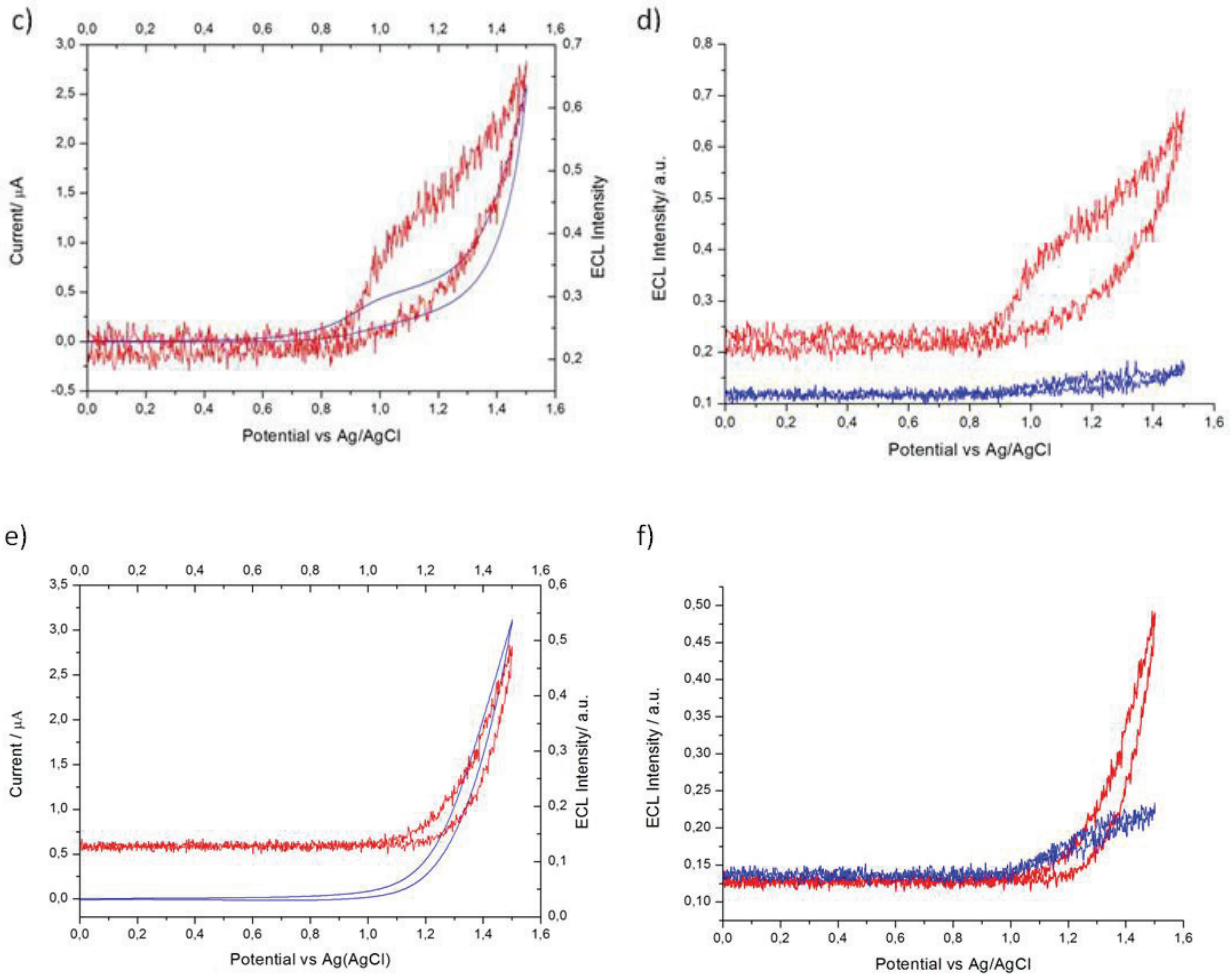

Fig 5.4: a-c-e) *Cyclic voltammogram (blue) at scan rate of 100mV/s and the corresponding ECL signal (red) of the Gliadin NEAs immunosensor fabbricated on Gold, BDD and GC underlying macroelectrodes respectively, in solution of 0.1M PBS pH 7.4 containing 0.1M TPrA;* ***b-d-f)*** *ECL plots of negative control –without Gliadin (blue) and immunosensor with Gliadin (red) in solution as in of 0.1M PBS pH 7.4 containing 0.1M TPrA.*

The ECL curve in figure 5.4a reveals the presence of one intense ECL peak, detected at a potential of +0.87 V *vs* Ag/AgCl during the course of the anodic scan. This ECL signal is emitted at the reported-oxidation potential of TPrA, but well ahead of the oxidation potential of $Ru(bpy)_3^{2+}$.[1] This matches with a well-defined oxidation peak at 0.9 V on the CV curve. For NEAs made in BDD and GC (Fig Xa and Xa respectively) the ECL peak is detected at a potential of +1.5 V *vs* Ag/AgCl, close to the oxidation potential of $Ru(bpy)_3^{2+}$ (+ 1.2 V). The presence of measurable ECL at potential greater than +1.0 V on repeated scans indicates that direct oxidation of Ru(bpy)32+ at the surface of the nanodisks is taking place.

Moreover, the ECL signals of the negative controls (Fig 5.4 b,e,f) carried out on the various NEAs detect an aspecific adsorption of the ruthenium complexes occurring at the polycarbonate or at the electrode surface.

5.2 Tuning of induced luminescence with Ring and Band microelectrodes

Different types of NEAs with precisely controlled geometries, have been reported for electroanalytical applications.[2] As introduced above, NEAs offer significant advantages over larger electrodes, such as enhanced faradaic/capacitive currents ratio (resulting in much lower detection limits), high miniaturization, and thanks to the a partially dielectric-coated surface of the sensor, the possibility for alternative functionalization strategies.[3] Such attractive features, prompted us to examine the characteristics of ECL generated by micro and nanoelectrodes.[4]

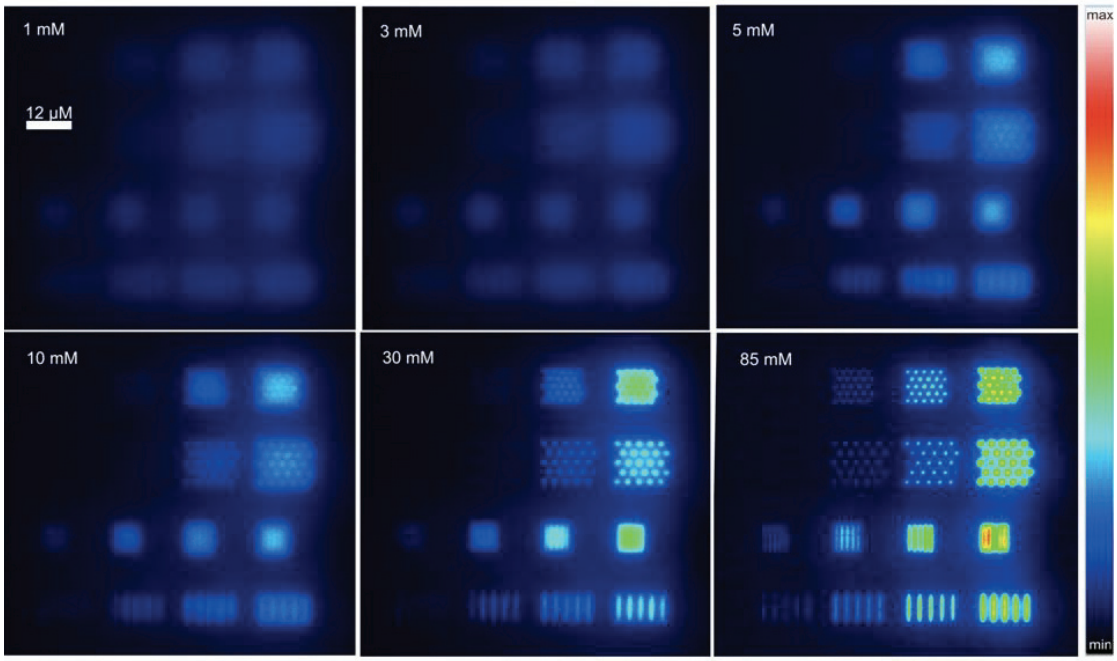

Fig 5.5: *ECL intensity (pseudo-color map) on the MNEA obtained with increasing concentration of TPrA (indicated in top-left corner of each box), during chronoamperometry at 1.2 V vs. Ag/AgCl/KCl; images were acquired with 50X microscope objective at 2 sec. exposure time in normal CCD mode.*

Despite this, no experimental study had ever reported before the use of patterned electrodes at the micrometric scale with well-controlled geometry, such as rings and

bands, to spatially resolve the ECL distribution signal. The promising results obtained with NEAs (fig 5.5) prompted us to examine the characteristics of ECL generated by microelectrodes fabricated with a variety, but well-controlled range of different geometries. To this aim, 5 geometries were fabricated on GC sample-substrate coated with PC (Figure 5.6) providing a platform suitable to capture simultaneously in a single image the ECL emission from the different geometries.

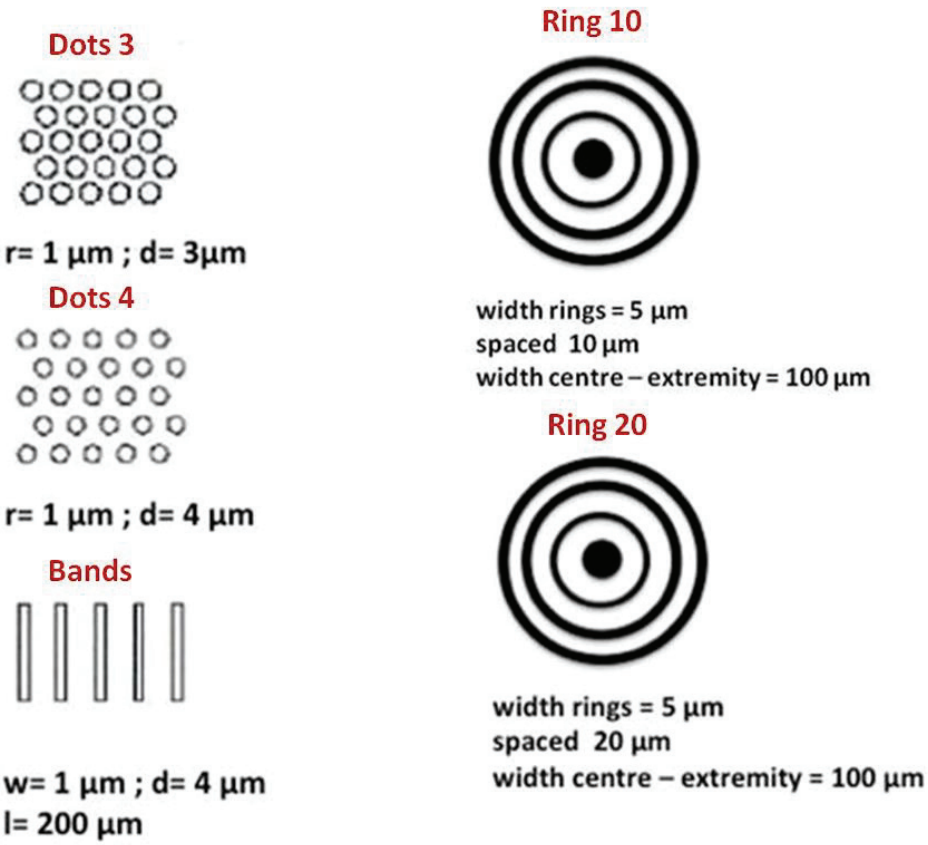

Fig 5.6: *Schematic drawing of geometries of microstructured NEAs fabricated for the spatially resolved ECL experiments: r is the individual disk radius, d the centre-to-centre distance between them; l and w represents the length and the width of each band, respectively;*

Each platform contains only one of the shown geometries. To facilitate identification of each design, especially for arrays of microelectrodes that are hardly visibile, were added larger size markers, not active from an electrochemical point of view, in order not to affect the ECL measurements. Sample of this type were fabricated in order to highlight the changes in the ECL reaction layer as a function of shape and inter-

electrode distance. ECL emission was induced using $Ru(bpy)_3^{2+}$ as the ECL luminophore and TPrA as the co-reactant.

5.2.1 Platform fabrication

The samples were fabricated by the following procedure:

- First, markers were created in order to easily locate the geometries with the microscope. Photo resist S1805 (Shipley) was spin-coated at 2000 rpm on a GC substrate and subsequently annealed on a hot plate at 115 °C for 1 minute. The photoresist was patterned by standard UV-photolithography, using a photomask with the marker pattern (Fig X) for the exposure and then developed in MF-39 developer for 2 minues.

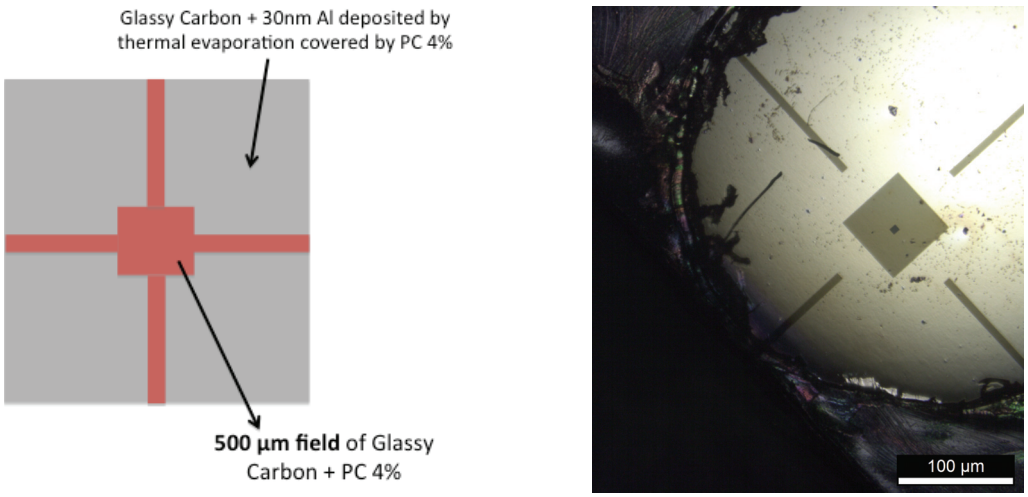

Fig 5.7: *Schematic representation of samples for ECL experiments. Chromium markers, easily visible at the optical microscope and by naked eyes, were made by EBL, metal deposition and lift off. After that, arrays' structures were obtained by lithography on PC film, inside the field delimited by the markers.*

- A layer of PC 4% was deposited on the substrate with markers by spin coating. Structures reported in figure 5.6 were exposed by EBL. Process parameters are reported in Table 5.1.

Resist	PC 4%
Spin speed	2000 rpm
Bake	180°C for 30 minutes
Dose	10000 μC/cm^2
Developer	5M NaOH
Temperature	35°C

Table 5.1: *Conditions used for NEA fabrication described in figure 5.7 exposure.*

- Samples were treated with oxygen plasma by Reactive Ion Etching in an Inductively Coupled Plasma (ICP) system, in order to clean the bottom of the electrodes. O_2 plasma parameters are reported in table 5.2.

ICP parameters	
Process	O_2 strip
O_2	40 sccm
Pressure	4 mT
Coil	200 W
Platen	10 W
Bias	30 V

Table 5.2: *Plasma parameters used for removal of polymer residues from bottom of the electrodes.*

5.2.2 Electrochemical characterization and ECL imaging

The samples prepared as described above were characterized directly by electrochemical measurements without SEM inspection, in order to avoid damaging the PC surface, as this is sensitive to the electron beam.

For the electrochemical experiments, our samples were used as working electrode, while a Pt wire and Ag/AgCl/KCl were the counter and reference electrode, respectively. Figure 5.8 shows the cyclic voltammetry recorded in 1mM (ferrocenylmethyl) trimethylammonium hexafluorophosphate ($FA^+PF_6^-$) (Fig 5.8 a-c) and 1mM Hexaammineruthenium(III) chloride ($Ru(NH_3)_6Cl_3$) (Fig 5.8b-d) dissolved in 0.1M KCl as supporting electrolyte at different scan rate (10-500 mVs) with a potential between 0 and 0.5 V.

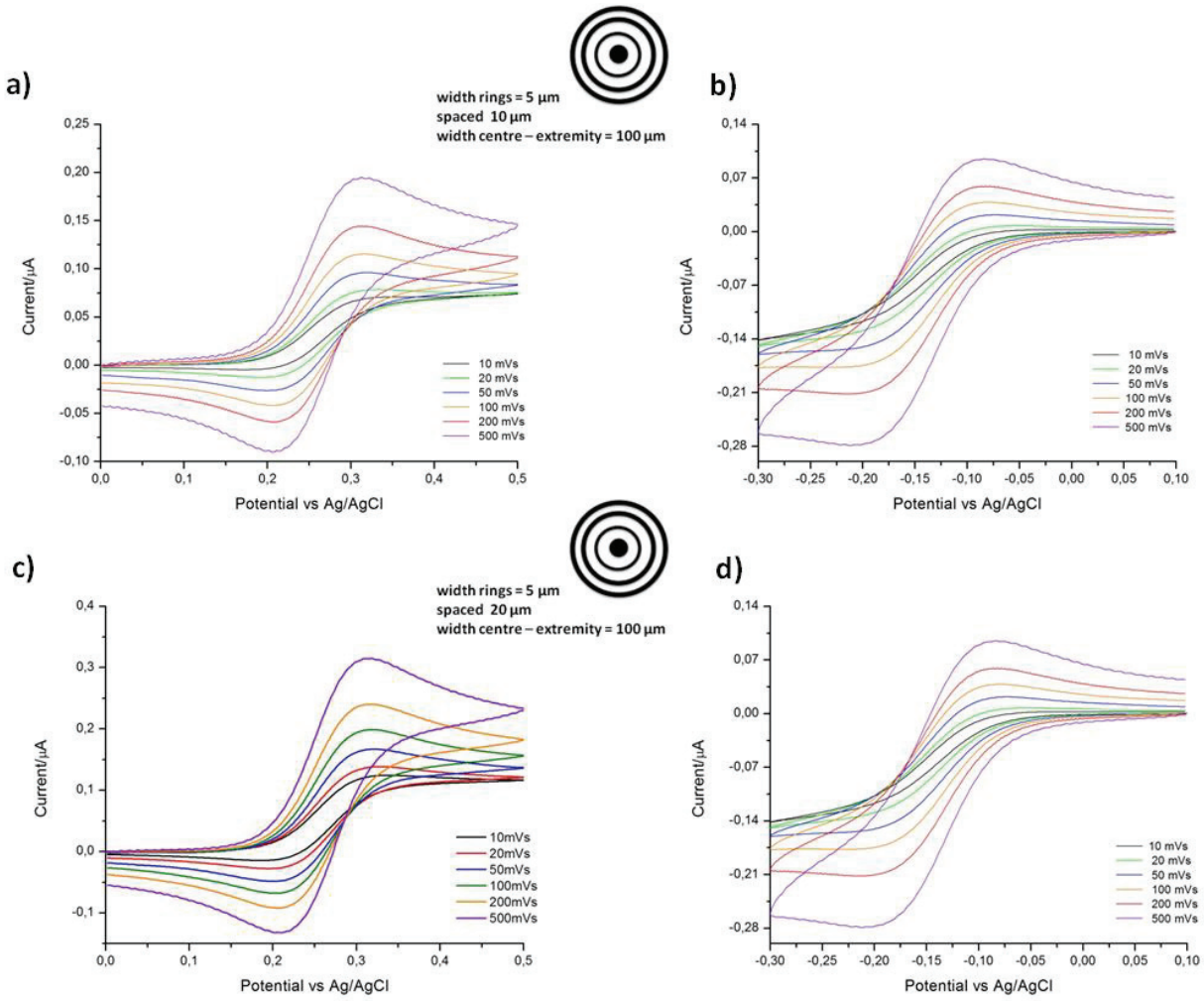

Fig 5.8: *Cyclic voltammograms recorded in* ***(a-c)*** *1mM (ferrocenylmethyl) trimethylammonium hexafluorophosphate (FA^+, PF_6^-) and* ***(b-d)*** *1mM Hexaammineruthenium(III) chloride ($Ru(NH_3)_6Cl_3$), in 0.1M KCl as supporting electrolyte. Scan rate 10-500 mVs.*

The electrochemical measurements carried out show that the patterned electrodes prepared are well conductive and consequently polymer residues on the bottom of the microelectrodes were effectively removed from the bottom of the structures.

Samples patterned with band geometries were not prepared in sufficient number for an adequate electrochemical characterization, and they were saved for the ECL imaging experiments. Electrochemical measurements carried out on dots geometries electrodes did not show well resolved cyclic voltammogramms, probably because of defects in the fabrication process and for this reason they were not used for imaging measurements. For these practical reasons, imaging experiments were carried out only on the geometry Ring10, Ring20 and bands.

Starting from the promising results published by Sentic et al.[4], we wanted to investigate the behavior of ruthenium complex immobilized on the dielectric surface instead of having it in the solution. For this purpose, carboxylic groups present on the PC surface of our sensors, were exploited for the immobilization of $Ru(bpy)_3^{2+}$ amino modified ($Ru\text{-}NH_2$, Sigma Aldrich®) using a carbodiimide/succinimide strategy described in chapter 4 (figure 4.1). Briefly, carboxylic groups were activated with 0.1 M HEPES buffer solution (pH 7.5) containing 2 mM EDC [N-ethyl-N'-(3-dimethylaminopropyl) carbodiimide hydrochloride] and 0.75 mM sulfo-NHS [N-hydroxysulfosuccinimide sodium salt]. The samples were incubated for 1 hour under shaking (at RT) and then the electrodes were dipped into a 0.1 M HEPES buffer solution (pH 7.5) containing 1mM of $Ru\text{-}NH_2$ under stirring for 2 h at 37° C.

For the imaging experiments, a modified epifluorescence microscope (BX-30, Olympus) was used for bright field (BF) and ECL imaging. BF and ECL emission images were collected by a 20X microscope objective and detected by an Electron Multiplying Charge Coupled Device (EM-CCD) Camera. The ECL intensities and ECL profiles were analysed with Image J software. Before each ECL experiment, the focus has been adjusted on the samples surface using bright-field microscopy. Then, the white light was turned off and PL and ECL imaging experiments were performed.

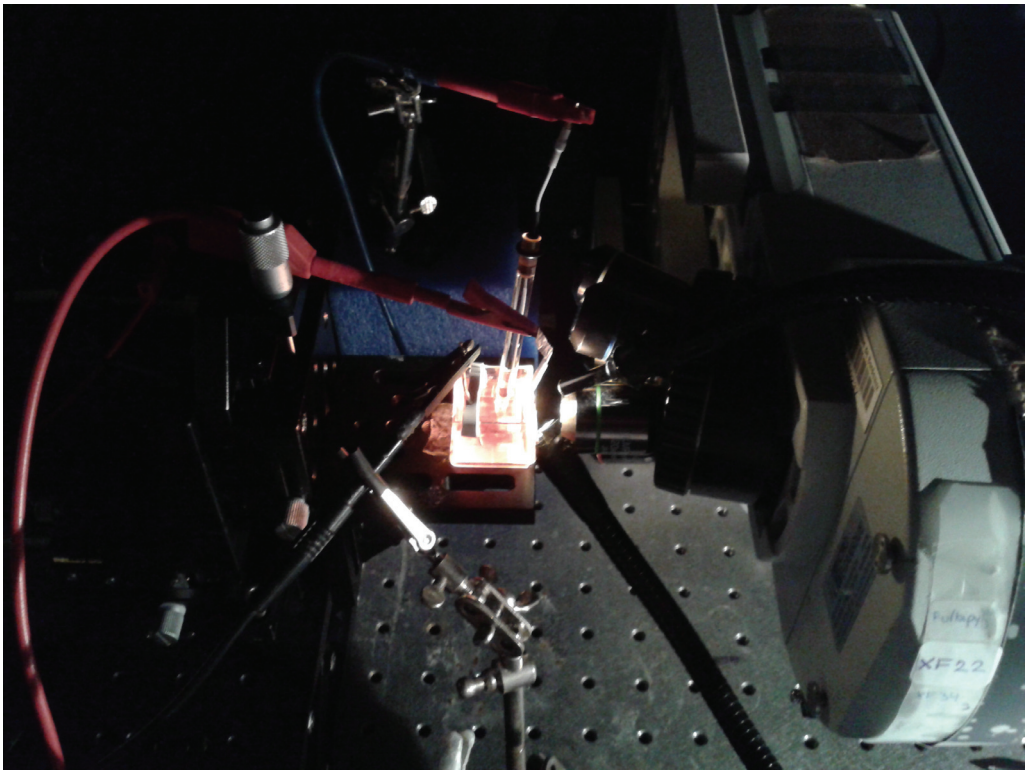

Fig 5.9: Setup for ECL experiments: microscope and electrochemical cell.

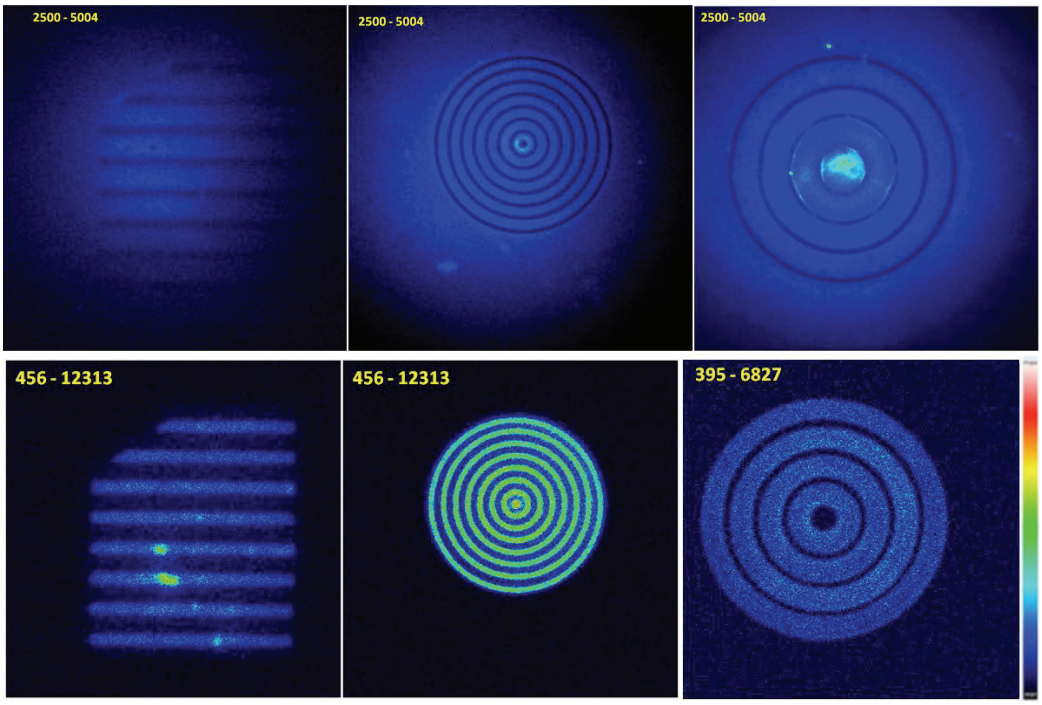

Fig 5.10: *Microscopic photoluminescence (top images) and electrochemiluminescence (bottom images) imaging (false color), of the different geometries, during chronoamperometry at 1.2 V vs. Ag/AgCl/KCl; images were acquired with 20X objective at 2 sec. exposure time in normal CCD mode.*

Figure 5.10 reports preliminary results obtained from the different electrodes functionalized with Ru-NH_2, at +1.2.V in 100 mM TPrA deaerated solution. Emitted ECL patterns are indeed clearly detected. Focusing the attention on the single images below, it can be noted that the emission patterns are particularly bright and well resolved, allowing one to clearly recognize the morphological features typical for these electrodes.

Figure 5.11, shows PL and ECL images of ring and bands electrodes represented with overlaid red lines drawn in correspondence with the position of the areas from which the PC was removed exposing the underlying macroelectrode, in order to estimate approximately the spatial distribution of the ECL signal obtained. Contrarily to what we initially expected, we noted that the ECL is generated in the region of the exposed macroelectrode and also in proximal areas. In fact the black parts between the rings and bands in the ECL images, corresponds to the regions more distant from the electrode, distance that the $TPrA^{\bullet+}$ excited radicals cannot react with the immobilized $Ru(bpy)_3^{2+}$ and generate ECL, before decaying into their ground state radicals because of the limited lifetime.

Moreover, ECL intensity profiles rappresented in figure 5.11 evidence that the peaks are more intense and on the electrode surface than on the surrounding dielectric surface. This indicates that the ECL-emitting region is more confined in the more spaced electrodes (bands and ring20, Fig. 5.11 a,b) with respect to the geometry ring10 (Fig. 5.11c). However, in figure 5.11 one can appreciate more clearly how the ECL intensity is greater at the electrode edges compare to the electroactive center of ring.

This phenomenon could be related to the higher concentration of TPrA radicals in proximity of the electroactive surface, but it also means that Ruthenium complexes are adsorbed on the GC surface.

Further optimizations will be necessary to study in detail the behavior of Ruthenium complexes immobilized on surfaces.

a)

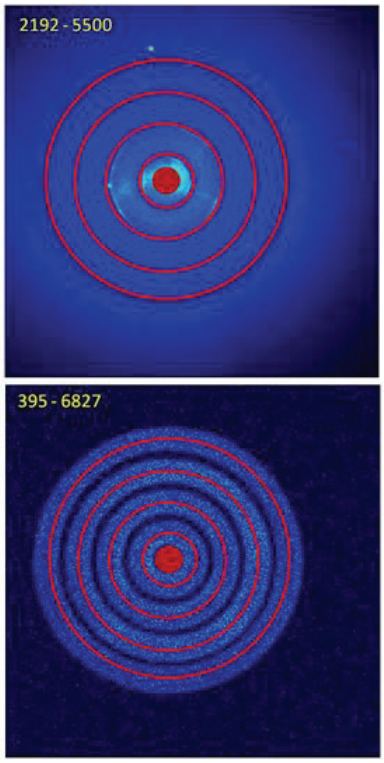
2192 - 5500
395 - 6827

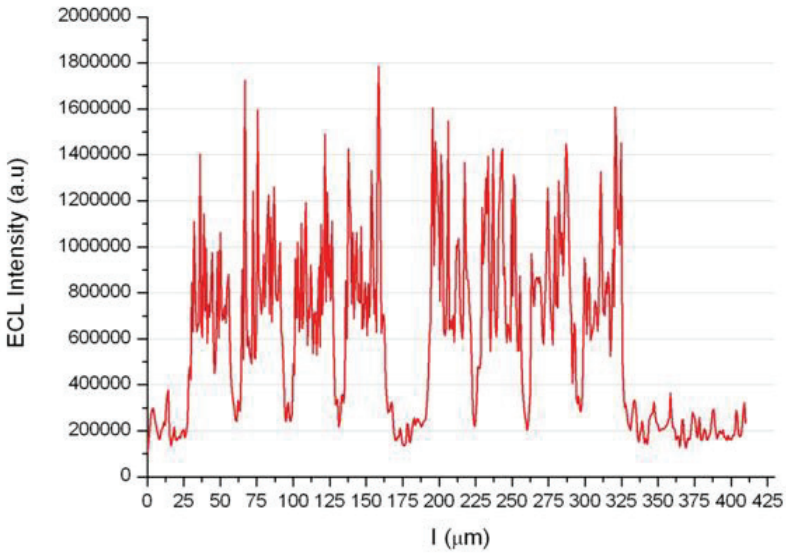
ECL Intensity (a.u)
2000000
1800000
1600000
1400000
1200000
1000000
800000
600000
400000
200000
0
0 25 50 75 100 125 150 175 200 225 250 275 300 325 350 375 400 425
I (μm)

b)

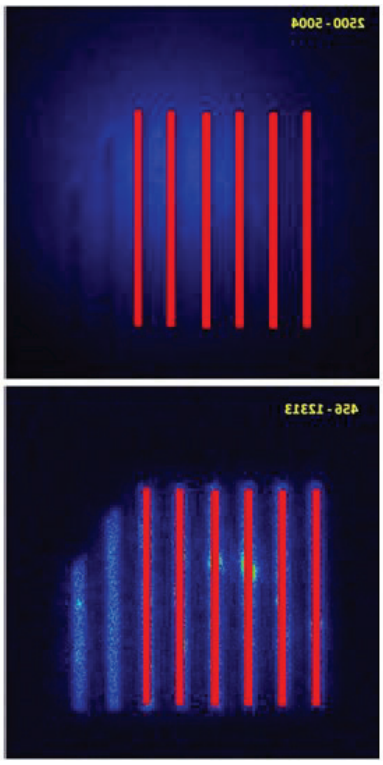

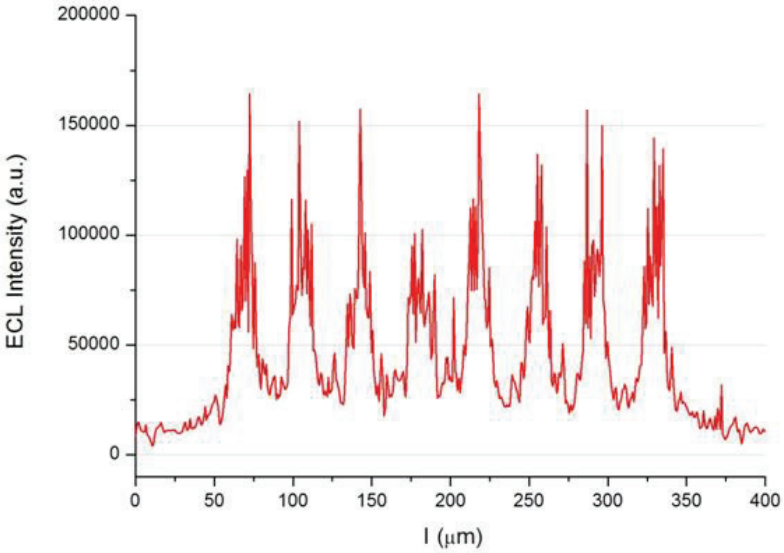
ECL Intensity (a.u.)
200000
150000
100000
50000
0
0 50 100 150 200 250 300 350 400
I (μm)

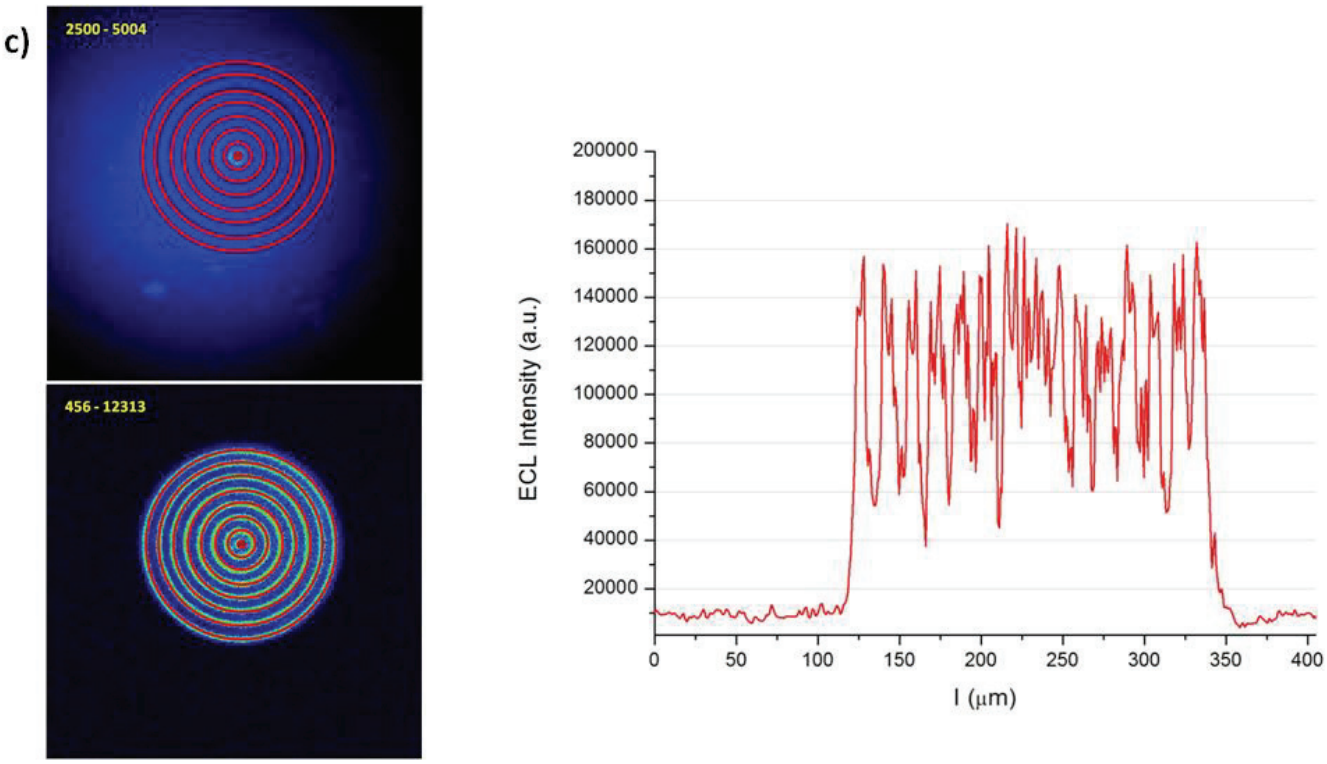

Fig 5.11: *PL and ECL images together with ECL profiles for Ring20* ***(a)****, bands* ***(b)*** *and Ring10* ***(c)****. Plot obtained with Image J.*

References:

1. Miao, W., Choi, J. P. & Bard, A. J. Electrogenerated chemiluminescence 69: The Tris(2,2-bipyridine)ruthenium(II), (Ru(bpy)32+)/tri-n-propylamine (TPrA) system revisited - A new route involving TPrA.+ cation radicals. *J. Am. Chem. Soc.* **124,** 14478–14485 (2002).
2. Virgilio, F., Prasciolu, M., Ugo, P. & Tormen, M. Development of electrochemical biosensors by e-beam lithography for medical diagnostics. *Microelectron. Eng.* **111,** 320–324 (2013).
3. Moretto, L. M., Tormen, M., De Leo, M., Carpentiero, A. & Ugo, P. Polycarbonate-based ordered arrays of electrochemical nanoelectrodes obtained by e-beam lithography. *Nanotechnology* **22,** 185305 (2011).
4. Sentic, M. *et al.* Microscopic imaging and tuning of electrogenerated chemiluminescence with boron-doped diamond nanoelectrode arrays. *Analytical and Bioanalytical Chemistry* 1–10 (2016).

Conclusions

The project involves the development of nanostructured electrochemical and electrochemiluminescence-based sensors for the detection of biomolecules, such as DNA and proteins, with an electrochemiluminescence transduction scheme.

Considering the increasing need for sensing elements that is emerging in different fields and applications, particularly in relation to the Internet of Things, electrochemical and elctrochemiluminescence-based sensors and biosensors, also for their exceptional attributes, such as being easy-to-operate, economical, sensitive, portable, are candidates to become essential pillars in future scenarios and to play a significant role biomedical and environmental monitoring.

Remarkably, recent achievements in nanoscience and nanotechnology, have demonstrated the potential for improving greatly both the sensitivity and selectivity of electrochemical sensors and biosensors. In fact, an electrochemical sensor can be miniaturized to a size less than one micrometer or to small-size arrays of nano-electrodes, offering advantages in terms of increased sensitivity and compactness (NEA). The present work aims at the development of an array of nano-electrodes (NEA) functionalized with a specific "probe" molecule, for diagnostic-type applications.

The fabrication of arrays of nanoelectrodes was performed by deposition of a thin film of polymer (insulating layer) on a layer of conductive material. The polymeric film was then patterned by electron beam lithography, in order to expose underlying conductive areas of controlled shape and size. Afterwards, in order to reduce time and manufacturing costs, the parameters to fabricate the sensors by nanoimprint lithography (NIL) have been optimized. This project has already been initiated, using Boron Doped Diamond (BDD) as the conductive material and polycarbonate (PC) as the polymer-insulating coating. This setup has shown some issues related to the binding of long DNA sequences on the insulating surface, and in addiction BDD is a material quite expensive to assure a proper trade of this system.

For this reasons, alternative materials for the fabrication of the sensors were evaluated by selecting and characterizing the Glassy Carbon (GC) which show to have a potential window and an electrochemical response similar to BDD, proving to be an excellent electrode layer for NEAs. Parameters for producing GC by pyrolysis starting

from common polymeric photoresists, have been optimized. In this way, GC could be rather easily obtained as a thin supported patterned layer, which would be useful for instance for making electrical vias, thus enabling the manufacturing of small-size independent (i.e. multiparametric) sensors at affordable costs.

We demonstrate the possibility to efficiently immobilize biomolecules, on the relatively large surface of the PC of our NEAs in order to develop sensitive electrochemical biosensors. Initially, to understand the nature of the difficulties previously encountered in the binding of DNA, the functionalization of the surface of the PC was carried out using HPV16 (Human Papilloma Virus) sequence as a probe and using as target a synthetic complementary biotinylated sequence, instead of the one provided by the company ABanalitica SRL and obtained by DNA amplification techniques. For the detection the enzyme glucose oxidase (GOX) was used. In this case, hybridization experiments were successful suggesting that the length of the complementary sequence and the purity are crucial in the process of hybridization on the PC surface of NEAs.

Later, we focused on the optimization of the protocol for the detection of proteins by enzyme immuno-assay with the enzyme Horse Radish Peroxidase (HRP), using Gliadin (gliadin Abcam® Fragment) as target. The process of bio-recognition and detection was carried out by cyclic voltammetry.
The development of an electrochemical sensor for Gliadin protein fragment detection is taken as a case study to demonstrate the general applicability of the concept. With the optimized protocol NEAs were successfully functionalized with Gliadin managing to detect a concentration of 0.1 nM for Gliadin fragment and the experiments performed indicate the possibility to further low this limit. It was observed that the functionalized biosensor is stable at least for a week at 8 °C.

Moreover, biosensor surfaces has been functionalized with TNF-α, based on the method already optimazed for Gliadin Protein Fragment, or with infliximab antibodies optimizing a new strategy based on the use of Protein G. Preliminary results shows that the functionalization of the PC surfaces of our NEAs with recombinant Human Tumor Necrosis Factor-α (TNF-α) and detected with INFX antibodies labelled with Fluorescein isothiocyanate (FITC) was successful. Also the

functionalization with Protein G for direct immobilization of INFX antibodies labelled with Fluorescein isothiocyanate (FITC), has shown promising results. However, background signals were observed, probably due to a non-specific fluorescence emitted by the Protein G. Further experiments will be done in order to clarify this aspect.

Nanoelectrode arrays are opening new applicative prospects to the development of highly sensitive, selective and miniaturized biosensing devices. Definitely, nanofabrication techniques such as electron-beam or nanoimprinting lithography, allow the preparation of highly ordered arrays with perfectly controlled geometries. NEAs show dramatically enhanced signal-to-background ratios with respect to any other electrode system, together with the possibility to measure rather easily very fast charge transfer kinetic constant of interest for fundamental studies. Moreover, the high sensitivity of NEAs to the electron transfer kinetics makes their analytical application advantageous mainly for very fast redox couples.

Despite this, we still not have a deep knowledge about the characteristics of diffusion and charge transfer processes at bio-nanostructured surfaces in order to obtain the maximum in biosensing performances from these devices.

From a technical development viewpoint, multiplexed analysis of different analytes will be possible by further developments in the preparation and application of individually addressable arrays of nanoelectrodes. To this aim, the optimization of the parameters for producing glassy carbon from polymeric photoresist could allow to easily create arrays of nanostructured electrodes insulated from each other. These "island of NEA" could be functionalized individually with different probes in order to perform multiple analyzes.

For biosensing purposes, the smart use of the morphological characteristics and the composite structure of our sensor allow to maximize their biorecognition performances. This is the case when the ample area of Polycarbonate interposed between the array, is used to immobilize large amounts of biorecognition molecules.

In fact, PC possesses characteristics that allowed us to fuctionalized it with both DNA (via Carbodiimide Crosslinker Chemistry) and proteic sequences. However, the chemical-physical properties of PC used were not examined in depth, therefore we don’t have a clear idea on the mechanism of functionalization with biomolecules nor

the amount of immobilized molecules on the surface of the PC. Regarding this, further studies should be performed.

Since practical applications for biosensing and diagnostic aims in real samples are growing quickly, it will be essential to evaluate the effect of non-synthetic biological matrices (human blood, saliva, etc.).

In the last part, the electrochemiluminescence properties of NEA for bioanalytical applications were investigate. We exploited the revisited ECL route with TPrA as co-reactant, which enables ECL generation at micrometric distances from the electrode surface at Low Operating Potential (LOP), to study an ECL immunosensor for Gliadin detection. In these sensors the secondary antibody is labbeled with Biotin, that provides a strong interaction with the complex streptavidin- $Ru(bpy)_3^{2+}$. The ECL signal obtained in the presence of the co-reactant tripropylamine (TPrA) was recorded using both a CCD camera and a photomultiplier tube. Using this approach, location of the initial electrochemical step (i.e. oxidation of TPrA) is separated from the biosensing chain and ECL-label, which are immobilized on the non-conductive surface of the NEAs. It therefore minimizes electrical damage on very sensitive biomolecules and oligonucleotide sequences. Also, operating at LOP allows to reduce possible interferences from side reactions dealing with samples of complex matrix like blood; making this method extremely suitable for serological screening.

It was observed that the amount of $Ru(bpy)_3^{2+}$ immobilized on the surface of the sensors is not enough to give a sufficient optical response, while using the photomultiplier tube we obtained results similar to the one observed in cyclic voltammetry. In addition it was found a non-specific adsorption of $Ru(bpy)_3^{2+}$ suggesting the necessity to improve the process of blocking of non-specific binding site on the surface of polycarbonate.

Furthermore, ECL imaging was used for the characterization of ECL generation at Glassy Carbon NEAs. The surface of the PC was patterned by electron beam lithography with different geometries in order to evaluate the diffusion of the electrochemiluminescence signal obtained from $Ru(bpy)_3^{2+}$ immobilized on the surface, in between the different shapes of the electrode.

The $Ru(bpy)_3^{2+}$ was immobilized as previously reported but also in this case it was observed that the amount of $Ru(bpy)_3^{2+}$ immobilized by adsorpion on the surface of the sensors was not enough to give a sufficient optical response. In order to solve this problem, a protocol for the immobilization of the $Ru(bpy)_3^{2+}$ using EDC - NHS crosslink chemistry was optimized exploiting hydroxyl groups naturally present on the surface of the PC.

In the perspective to combine our sensors (NEA or other geometries) with ECL detection and obtain improved biosensors, this study can allow to find the best conditions, regarding shape and size of electrodes, and coreactant nature and concentration, for optimal ECL detection.

Acknowledgments

Acknowledgement

This work has been co-supported by CNR-IOM of Trieste and by European Founds (*Fondo Sociale Europeo, FSE*).

I would like to thank my supervisor Dr. Massimo Tormen for knowledge I gained during these three years, in scientific and quotidian life and for his wide scientific interest and curiosity.
I'd like to thank Dr. Francesca Virgilio who guided me during the first phase of the project, Dr. Alessandro Pozzato e Dr. Alessandro Cian for their precious support, both moral and scientific, and their helpful trainings and suggestions.

I'd like to thank Prof. Neso Sojic and all the group of NanoSystèmes Analytiques of the University of Bordeaux, for the opportunity to expand my knowledge within exciting electrochemiluminescence. In particular, I want to thank Dr. Milica Sentic for her indispensable help during the whole period spent in Bordeaux, for sharing with me his deep scientific knowledge and for the beautiful person she is, I hope that our friendship will continue over time.

I also acknowledge Prof. Giuliana Decorti, Prof. Gabriele Stocco and Dr. Marianna Lucafò from the Pharmacogenomic Group of the University of Trieste, for giving me the opportunity to collaborate with them, especially Marianna for the valuable assistance provided in the fluorescence experiments.

I acknowledge Prof. Paolo Ugo for sharing his Acquaintances on electrochemistry at nano-scale and for his moral support.

Finally, I would like to thank all the stuff of ThunderNIL s.r.l. and all the colleagues (and friends) who have shared with me these three years.